INTEGRAL DESIGN OF A LASER WAKEFIELD ACCELERATOR WITH EXTERNAL BUNCH INJECTION

by

Arie Irman

Samenstelling van de promotiecommissie:

Voorzitter & secretaris:

prof.dr. J.L. Herek	University of Twente, The Netherlands

Promotor:

prof.dr. K.-J. Boller	University of Twente, The Netherlands

Assistent-promotor:

dr.ir. F.A. van Goor	University of Twente, The Netherlands
dr. A.G. Khachatryan	University of Twente, The Netherlands

Leden:

prof.dr.ir. H.J.W. Zandvliet	University of Twente, The Netherlands
prof.dr. V. Subramaniam	University of Twente, The Netherlands
prof.dr. W.J. van der Zande	Radboud University Nijmegen, The Netherlands

The work described in this thesis is a part of the research program of the "Stichting voor Fundamenteel Onderzoek der Materie" (FOM), which is financially supported by the "Nederlandse Organisatie voor Wetenschappelijk Onderzoek" (NWO).

The research presented in this thesis was carried out at the Laser Physics and Non-Linear Optics Group, Department of Science and Technology, MESA+ Institute for Nanotechnology, University of Twente P.O. Box 217, 7500 AE Enschede, The Netherlands.

ISBN: 978-90-365-2806-1

Printed by Print Partners Ipskamp, Enschede, The Netherlands

INTEGRAL DESIGN OF A LASER WAKEFIELD ACCELERATOR
WITH EXTERNAL BUNCH INJECTION

PROEFSCHRIFT

ter verkrijging van
de graad van doctor aan de Universiteit Twente,
op gezag van de rector magnificus,
prof.dr. H. Brinksma,
volgens besluit van het College voor Promoties
in het openbaar te verdedigen
op donderdag 2 april 2009 om 15.00 uur

door

Arie Irman

geboren op 7 april 1980
te Padang, Indonesië

Dit proefschrift is goedgekeurd door:

De promotor:	prof.dr. K.-J. Boller
De assistent-promotor:	dr.ir. F.A. van Goor dr. A.G. Khachatryan

This thesis is dedicated
to my mother and father
and my beloved wife and son.

Contents

1 Introduction

1.1 Laser wakefield acceleration: overview and state-of-the-art

Conventional particle accelerators are capable of generating bunches of charged particles with their speeds approaching the speed of light. These highly relativistic (highly-energetic) bunches are of scientific interest in the investigation of the fundamental structure of matter and energy. In addition, particle acceleration is a key to provide advanced research tools in many other fields, such as: material science, biology and chemistry. Examples are synchrotrons and free-electron lasers (FELs) which provide bright radiation at extremely short wavelengths, aiming on microscopy with atomic resolution and on ultra-short (femtosecond to attosecond) time scales. However, there are severe drawbacks and limits associated with conventional particle accelerators. One main limit is the large size of such accelerators which requires enormous financial efforts to be made, usually extending beyond the capabilities of single country. Typically, state-of-the-art super-structure accelerator facilities cost billions of euros, both for their installation and operation. The most prominent example of these is the world's largest and most powerful particle accelerator, the Large Hadron Collider (LHC) at the Centre Européenne de Rescherches Nucléaires (CERN). The LHC has a length of no less than 27 km and stretches over two countries (Switzerland and France). The Stanford Linear Accelerator Center (SLAC) in Menlo Park, California, measures 3.8 km and the largest storage ring of the Deutches Elektronen-Synchrotron (DESY) in Hamburg is about 7 km. The large size and costs of such facilities bring about their main disadvantage, namely, these facilities have to be shared among researchers world wide. This

has the effect of slowing and narrowing scientific and technological progress as the access of scientists to advanced accelerators is often inconvenient and rather exclusive. Therefore it is of fundamental importance that novel concepts are pursued for particle acceleration that can provide relativistic particle energies using facilities of significantly reduced size.

To identify suitable novel concepts it is instructive to recall what the physical working principles and limitations are in standard accelerators. These are based on chains of cavities (resonators) in which high-power microwaves generate electric fields that are as high as possible in order to minimize the acceleration length required for a given kinetic energy. However, the fundamental problem is that the maximum electric field strength inside such cavities is limited by vacuum breakdown to values of at most 100 MV/m, and in practice the effective accelerating field has to be set at much lower values (in the order of 10 MV/m). This means that, to design an accelerator for electron energy of 1 GeV, the length of the accelerator would have to be on the order of 100 m. Indeed, the 1 GeV accelerator for FLASH (at DESY), which is currently the leading free-electron laser, is approximately 200 m long. The conclusion that can be drawn is that any new approach needs to provide electric fields orders of magnitudes higher and maintain these along a sufficiently long acceleration distance.

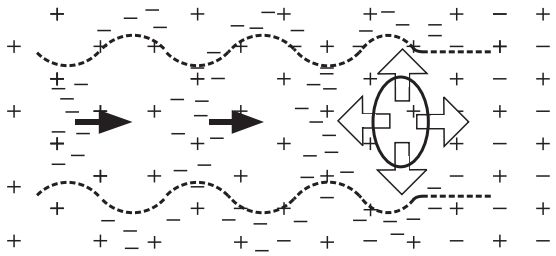

Figure 1.1: Illustration of plasma electron oscillations (dashed line) as excited by a laser pulse (oval region). The ponderomotive forces (big arrows) push electrons away from the pulse leaving heavier ions immobile. The displacement of the plasma electrons induces a strong accelerating field (the black arrows) which can be used to accelerate electrons.

In 1979 Tajima and Dawson [1] proposed a novel concept for particle acceleration which, theoretically, would provide much higher fields. They proposed to accelerate charged particles using the strong electric fields generated by collective electron oscillations in a plasma, in the form of a plasma wave as is indicated in Fig. 1.1. The plasma wave would be driven by an intense and ultra-short laser pulse that propagates through a plasma with a pulse length matching the plasma wavelength. At sufficiently high laser intensity, the ponderomotive force associated with the intensity gradient of the pulse would expel a significant amount of plasma electrons away from the path of the pulse, whereas the ions would remain close to their original positions due to their much higher mass. As a result, the laser pulse provides

a charge separation, i.e., it generates a spatial region of net positive charge located directly behind the laser pulse. The Coulomb forces generated by the charge separation tend to restore the neutrality of the plasma and thus push the electrons back towards their original equilibrium position. Due to the inertia of the electrons, equilibrium is reached in collective charge density oscillations. In this way a plasma (charge separation) wave is generated behind the laser pulse, and this, so-called, wake wave follows the laser pulse velocity which is near the speed of light in vacuum. Similarly, the Coulomb field distribution associated with the wake wave also travels through the plasma as well driven by the laser pulse, therefore called the laser wakefield.

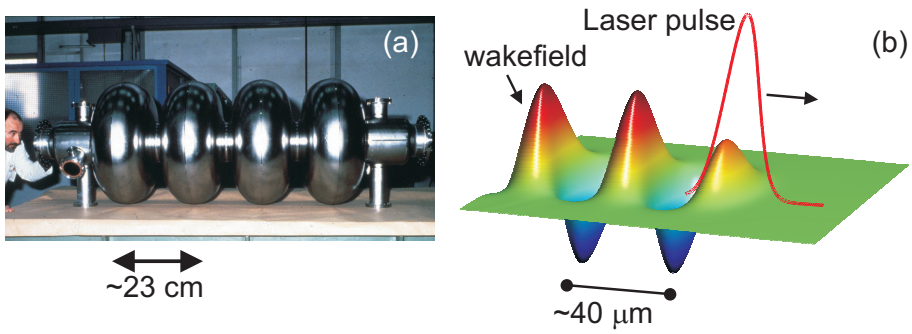

Figure 1.2: (a) A conventional accelerator cavity structure designed for operation with a microwave drive field at a standard frequency of 1.3 GHz [2]. The wavelength of the microwave field is about 23 cm and the accelerating field is limited to well below 100 MV/m. (b) On the contrary, in a laser wakefield accelerator, the typical wake wavelength is about 40 μm and the accelerating field of wakefield can reach values as high as 100 GV/m, leading to a much shorter acceleration distance for a given kinetic energy.

The attractiveness of this wakefield for particle acceleration becomes apparent when looking at the numbers involved. The charge separation in plasma can generate huge electric fields with amplitudes as large as 100 GV/m. This is three to four orders of magnitude higher than can be achieved in conventional accelerators. Furthermore, the described mechanism of ponderomotive driven charge separation provides that, in the spatial range directly behind the laser pulse, the wakefield is oriented such that electrons are accelerated along the laser pulse propagation direction. It can be expected that, when an electron bunch is properly injected into the accelerating region of the wakefield, the bunch will co-propagate with the laser wakefield and be accelerated to ultra-relativistic energies within a short distance. This scheme is called laser wakefield acceleration (LWFA). Its promise lies in the circumstance that three to four orders of magnitude higher electric fields in LWFA could be employed to reduce the size of particle accelerators, bringing km-sized

acceleration lengths down to the order of one meter or less.

The potential of LWFA is pictured schematically in Fig. 1.2. The conventional accelerator structure shown comprises of four microwave cavities over a length of about 1 m, and it would be suitable for accelerating electrons to a typical kinetic energy of 10 MeV. In comparison, the shown laser wakefield, which we calculated for a realization of acceleration methods as described in this thesis, might enable to approach the GeV level of energies within just a few centimeters of acceleration length.

The fundamental advantages that LWFA can offer have been described. However, as can be seen in the original work of Tajima and Dawson, to excite a laser wakefield to a sufficiently large amplitude, it is necessary to provide laser pulses with extremely high intensities and ultra-short pulse duration (about half of a period of the plasma wave). For typical electron densities in the plasma in the range of 10^{17}-10^{19} cm^{-3}, the corresponding pulse durations (full width at half maximum) are in the range of 15 to 150 fs. Hence, the main problem at the time of their publication was that no suitable laser was available to use as the driver and it seemed unlikely that light pulses with the necessary properties would ever be realized.

This situation changed gradually while laser technology matured. A leap towards much higher intensities was made with the invention of the chirped pulse amplification (CPA) in 1985. This technique allowed researchers to take advantage of the large energy-storage capabilities of Nd-glass lasers to generate sub-picosecond pulses, with several terawatt peak power [3, 4]. Since then, much experimental progress has been made towards the demonstration and investigation of laser wakefield acceleration in a number of laboratories around the world [5–10]. Although these experiments have successfully proved the basic working of the laser wakefield acceleration concept; the energy spread of the accelerated electrons has remained extremely broad, with the spread typically as large as the average energy itself (100% spread). Such results are particularly undesirable because most applications of accelerated particles, as will be described at the end of the introduction, require a rather narrow energy spread (in the order of one percent or less).

The large spread can be traced back to a complete lack of control over the injection of electrons (from the plasma) into the wakefield. The spreads obtained actually indicated that electrons were injected into all accelerating phases of the wakefield. More precisely, injection occurred across a volume as large as the wavelength of the plasma wave, and distributed temporally over an interval as large as a period of the plasma wave. In order to obtain narrow energy spectra, electrons must be injected into a much smaller volume, which is a small fraction of the plasma wavelength, and within a much shorter time interval, being a small fraction of the plasma wave period. To better illustrate what the requirements are, to gain the desired control over electron injection, let us look at the corresponding numbers. With a typical plasma wavelength of 40 μm and a plasma period of 130 fs one would have to inject an electron bunch with a size of the order of (1 μm)^3, with a spatial precision of about 1 μm, and with a duration of only a few fs. The problem with these numbers is that they are far beyond the capabilities of current technology. Furthermore, such injection would be extremely hard to align when no

special measures are taken to visualize the wakefield before injection. Note that the experimental visualization of the structure of a laser wakefield: its location, timing and wave front curvatures, became possible only recently, due to work in 2006 by a group at the University of Texas at Austin [11]. The precise injection of suitable electron bunches is currently the central problem in laser wakefield acceleration.

It has taken about 20 years for laser wakefield acceleration to develop to the point where some clear success in narrowing the energy spread of accelerated electron bunches has been achieved. In 2004 groups from Imperial College [12], Lawrence Berkeley National Laboratory (LBNL) [13], and Laboratoire d'Opique Appliquée (LOA) [14], produced quasi-monoenergetic electron bunches with energies of the order of 100 MeV with a relative energy spread of a few percent. Here, the plasma was created by ionizing a gas with a high intensity drive laser pulse. These experiments were the first to utilize increased laser intensities in combination with high plasma densities thus providing a strongly non-linear laser-plasma interaction. An important feature in this interaction is that the drive laser pulses experience self-focusing and self-steepening during propagation in the plasma, leading to a rapid increase of the laser intensity. This way the drive laser can provide the highest intensity gradients with the strongest ponderomotive forces, which expel plasma electrons completely from its path. The laser thereby generates a void, called a bubble, in the electron distribution where only ions are present. The expelled plasma electrons then form a sheath around the bubble and collect at the trailing end of the bubble upon further propagation. When the electron density increases there beyond a critical value, electrons are expelled, in the form of a small bunch, back into the bubble which can also be seen as the first accelerating phase of the wakefield. The bubble-based injection process depends in a strongly non-linear manner on the plasma density and laser pulse parameters and can be termed a wave-breaking process, similar to the breaking of ocean waves. This regime of laser wakefield injection and acceleration is often called the bubble regime and was proposed by Pukhov and Meyer-Ter-Vehn in 2002 [15], based on extensive numerical modeling. More recent experiments in the bubble regime were performed in the LBNL [16] by channeling a 40 TW peak power, 40 fs laser pulse in a 3.3-cm-long capillary discharge waveguide. These experiments showed an unprecedented 1 GeV bunch energy and some of the recorded acceleration events showed a reasonably low energy spread of 2.5 %. These results clearly emphasize the large potential of LWFA, however, the reported shot-to-shot reproducibility was still poor. This can be attributed to the complicated non-linear laser-plasma interaction on which the bubble regime relies. On the one hand, high intensities and plasma densities are required to obtain injection via the strongly non-linear bubble dynamics. On the other hand, it is precisely these non-linearities which makes the scheme extremely sensitive to small fluctuations of experimental parameters, such as shot-to-shot fluctuations in the laser and plasma parameters. Many attempts have been made to improve the stability of bubble-based laser wakefield acceleration by an improved control of the laser and plasma parameters. One promising idea is to impose a reasonably reproducible plasma density profile on a gas jet several mm in length via laser ionization [17] and with special jet designs to achieve a very stable

gas flow [18]. However, it remains clear that instabilities are an inherent problem when working in such a highly non-linear regime.

A considerable improvement in the stability of laser wakefield acceleration was demonstrated by the LOA group [19] in 2006. These experiments made use of two counter-propagating laser pulses with the same wavelength and polarization. The first, stronger, laser pulse was used to create a wakefield in a 2 mm thick supersonic helium gas-jet. The second, weaker, pulse injected some plasma electrons into the wakefield at the appropriate time. The injection timing is controlled by the interference between the two laser pulses. When the two pulses meet (collide) in the plasma, their interference creates a standing wave with tiny (wavelength-size) intensity fringes, which is associated with a correspondingly strong intensity gradient. The resulting ponderomotive force then locally pre-accelerates some plasma electrons in a range of directions, and to a range of energies. Electrons with an appropriate momentum and sufficient energy can then be trapped in the wakefield and accelerated further to relativistic energies. This scheme is known as the colliding-pulse regime. The laser wakefield used in this experiment operates in a linear or a weakly non-linear regime and the kinetic energy of the output bunches showed reduced fluctuations compared to the bubble regime. The kinetic energy of the output bunches could also be scaled over a range by displacing the location of the pulse collision with regard to the exit face of the gas jet, thereby changing the acceleration length. Nevertheless, there remains a significant lack of scalability and control because the injected electrons were pre-accelerated from the plasma background in a weakly defined manner that resembles a rapid thermal (laser-heating) process.

In 2008, an injection scheme, which could potentially assist in solving the injection problem and has better stability and reduced relative energy spread, was demonstrated experimentally by the LBNL group [20] using a gas-jet. For their so-called density-gradient injection scheme, they used the sharp edge of the gas-jet to pre-form a steep plasma density gradient (down-step) so that the wakefield experiences a rapid decrease in the plasma density as the laser pulse propagates through the gradient. The phase velocity of the plasma wave reduces at the gradient in a step-like fashion. For properly chosen laser and gas-jet parameters, the maximum velocity of the plasma electrons oscillating in the wakefield exceeds the phase velocity of the wakefield. This results in local wave breaking, consequently, plasma electrons become trapped and accelerated by the wakefield. In the 2008 experiment, a trapped bunch showed a more than ten-fold lower momentum spread, with better stability compared to previous experiments. The measured average bunch energy was still rather low, e.g., below an MeV. This means that, to reach ultra-relativistic energies, the bunch still needs to be injected into a following laser wakefield acceleration stage.

Our approach

To describe our own approach for solving the injection problem, this thesis presents a unique design and experimental setup which aims to externally inject electron bunches from a standard microwave-driven linear accelerator (linac). This may

sound surprising because, as described above, the size of the bunches from such accelerators is much larger than the plasma wavelength. Also the duration of the bunches is much longer than the plasma wave period. Thus, it was believed that standard accelerators would be of no advantage as only a small fraction of the injected bunches would be accelerated due to insufficient spatial overlap. Also, the relative energy spread would be in the order of 100% because electrons are injected randomly into all phases of the accelerating wakefield. However, it was recently shown by one of our team that, theoretically, the injection of such long and wide bunches into the laser wakefield can lead to the generation of an ultra-relativistic electron bunch and to a surprisingly low energy spread with a high fraction of the injected electrons being accelerated [21–23]. If this could be demonstrated experimentally, it would be the first experimental demonstration of laser wakefield acceleration with fully controlled injection. Full control, in particular the timing and spatial alignment, but also the scaling of the output energy is expected in this scheme as here the production and injection of electrons are fully separated from the laser wakefield acceleration process. This injection method is known as 'the external injection scheme', and this thesis describes the most important experimental steps towards its demonstration. The steps included in this thesis are: the complete (front-to-end) simulation, and the design and construction of a corresponding experimental setup. There are only a few research groups worldwide capable of performing similar experiments. This is due to the fact that these experiments need a rather unique expertise and infrastructure covering state-of the-art laser physics and technology at TW-power levels and, simultaneously, state-of-the-art experience and technology regarding standard particle accelerators.

In our unique approach, sub-picosecond electron bunches with an energy of a few MeV from a photo-cathode rf-linac will be injected into a plasma channel, just before the arrival of a high intensity drive laser pulse [21–23]. Inside the channel, the bunch will be overtaken by the laser pulse. The wakefield following the pulse should trap and strongly compress the bunches in both the longitudinal and transverse directions. The design and construction of the experimental setup presented here has been chosen so that acceleration towards ultra-relativistic energies of several hundred MeV can be expected, with low energy spreads and stable operation.

1.2 Challenges and the applied approach

As discussed in the previous section, it is of particular importance for progress with laser wakefield acceleration that the quality of the accelerated bunches is improved, that full controllability is achieved, that shot-to-shot reproducibility is gained and that scaling to higher energies becomes possible. In this thesis, we address all of those challenges by a careful front-to-end modeling of the entire laser wakefield accelerator and by turning the findings from modeling into an experimental design which is feasible in our laser laboratory. The model comprises of: generating an electron bunch from a photo-cathode, bunch propagation and pre-acceleration in a microwave driven accelerator (linac), temporal bunch compression and focusing with magnetic fields and, finally, the injection, trapping and acceleration of

this bunch in a laser wakefield that is generated by a multi-TW laser in a plasma capillary through which the laser pulses are guided [21–25]. Our modeling of the experiment with the chosen and experimentally implemented design parameters suggests that the laser wake field accelerator can indeed be operated in the almost linear (only weakly non-linear) regime, where the accelerating wake field structure is more regular and robust. This is similar to the accelerating field in a radio-frequency linear accelerator. Following the physical working and properties of our approach, as is described in details in section 2.3.1, the design and construction, assembly and synchronization included all of the following instrumentation and steps:

Bunch generation and injection
Electron bunches with a typical charge of tens of pico-Coulomb are generated and pre-accelerated to approximately 3 MeV kinetic energy by a conventional photo-cathode linear accelerator. The bunches then enter a transportation line, and their direction of flight is magnetically bent towards the entrance of a discharge-based plasma channel. The bending magnets are designed to also provide a temporal compression of the bunches to a duration of a few hundreds of femtosecond. Quadrupole magnets are designed to focus the bunch upon injection into the plasma channel.

TW laser system
A TW laser system is designed based on the chirped pulse amplification (CPA) technique. This uses a femtosecond Ti:sapphire laser oscillator, a regenerative amplifier and several power amplifiers to obtain a peak power currently in the range of 10 TW. This laser is currently the most powerful laser source in the Netherlands.

Laser focusing, waveguiding and timing
The temporally compressed laser pulses are focused to a spot size of a few tens of micrometers at the entrance of the plasma channel, where the near-parabolic profile of the capillary plasma density distribution serves for waveguiding of the focused pulse. An electronic timer is developed and installed that locks the laser's pulse emission to the microwave oscillation of the rf-linac with a precision of a few picoseconds.

Trapping of bunches, compression and acceleration
The design and construction of the laser, the plasma density and the kinetic energy of the injected bunches are chosen such that the laser pulse and its wakefield overtakes the bunch within the plasma channel. The injected bunch duration is chosen to enable the working of the novel bunch trapping and compression scheme, such that within approximately 1.8 cm propagation distance the bunches are compressed towards the region of maximum accelerating wakefield and also compressed to the optimum accelerating phase. The modeling of the laser wakefield acceleration then predicts a maximum bunch energy of around 750 MeV, with a relative energy spread of about 1 %, which is feasible within a 5 cm long plasma

channel.

1.3 Potential applications

The aim of the experimental setup realized within the course of this thesis, and the tests and synchronization of the essential sub-units, is to perform the first demonstration of laser wakefield acceleration with controlled injection. Based on the current state of the experimental apparatus we intend to achieve this demonstration within the present year (2009), after having completed this thesis. However, a sole working demonstration is not the end goal, but a means to open the way for a number of subsequent research steps at the forefront of relativistic light-matter interactions. Namely, previous experiments as well as supporting numerical modeling show that the generated bunches posses unique properties. This allows for novel experiments which are much less attractive to do with standard bunches from conventional accelerators.

As a first example, it can be expected that controlled laser wakefield acceleration would enable the generation of GeV-level bunches with an energy spread of 1 % or less and highest peak-currents in the range of hundreds of kilo-Amperes, due to the extreme small duration of the bunches. The availability of such peak currents is highly attractive for the generation of femtosecond X-ray pulses. One prominent approach employs free-electron lasers, where high currents are required to reach the pump threshold, particularly when short wavelengths are to be generated. In such a scheme, the bunches are injected into an arrangement of magnets with a spatially alternating transverse magnetic field, the so-called undulator [26]. Recently, at the Friedrich-Schiller-University of Jena, bunches from a laser wakefield accelerator were injected into an undulator for the first time [27]. The low kinetic energies (between 55 to 75 MeV) and low peak currents available are reasons why only spontaneous emission in the visible range of frequencies has been observed so far. However, with controlled and scalable laser wakefield acceleration (such as with the near 1 GeV expected), and with 1 nC charge per bunch it should be possible to obtain stimulated emission (powerful laser radiation) at wavelengths as short as 0.25 nm by propagation along an undulator of 5 m length [28]. In comparison, the most advanced free-electron laser to date, designed for emission with wavelengths as short as 6.5nm (FLASH, Freie-Elektronen Laser in Hamburg) requires a rather long undulator of 30 meters, despite the longer wavelength. This comparison indicates the particular potential of ultra-high peak-current from bunches generated by laser wakefield acceleration.

Another important scheme to generate bright, tunable, femtosecond X-rays with bunches from a laser wakefield accelerator is to employ Thomson scattering. In this scheme, a relativistic bunch of electrons collides with a counter-propagating laser pulse in either a head-on collision (also called Thomson back-scattering) or a collision including a small angle. In both cases electrons are oscillating following the cycles of the laser field and thus re-emit collimated radiation, similar that which occurs when a laser beam is reflected from a metallic mirror that moves with a high velocity. At high bunch velocities, there appears to be a strong Doppler up-

shift of the laser frequency, as experienced by the electrons, and another up-shift takes place when observing the re-emitted frequency in the laboratory frame. As a result, 1 GeV bunches from a laser wakefield accelerator would generate an X-ray pulse during head-on collision with a standard infra-red laser pulse. The first experimental demonstration of Thomson back-scattering by colliding a bunch from laser wakefield acceleration with an infrared laser pulse was performed at the Friedrich-Schiller-University of Jena [29]. Due to the relatively low output energy of the electrons in that experiment the measured photon energy (0.4-2keV) only reached the XUV range. However, calculations show that the collision between a 1 GeV electron bunch from an improved laser wakefield accelerator and an infra-red laser pulse would produce a very high photon energy of up to 1 MeV, with the re-emitted pulse duration about the electron bunch duration, typically a few femtoseconds.

Finally, we name an example of femtosecond X-ray generation which is particularly attractive due to its simple approach as it does not require an undulator or an additional laser. When bunches generated and transversely confined by laser wakefield acceleration travel through plasma, the electrons are performing oscillations around the propagation axis, so-called betatron oscillations and thereby generate radiation [30–33]. The resulting X-ray emission would be temporally incoherent, but Phuoc, *et.al.*, [31] have observed that the output would be tightly collimated, in the form of a laser beam, with a small divergence in the mrad-range, with an ultrashort pulse duration in the femtosecond range (based on calculations) and with a small effective size of the source of 1 μm.

The distinct properties of the X-ray pulse that might be generated based on laser wakefield acceleration as described here, would provide researchers with a unique tool for a deeper understanding of ultra-fast dynamics in numerous physical, chemical and biological systems. A wide review of other applications, such as radiotherapy, medicine, material science, is given in reference [34].

1.4 Outline of the thesis

This thesis is organized as follows. In chapter 2, we give an overview of the basic theory that describes the excitation of a wakefield in plasma using a laser, and of the acceleration of electrons in a laser wakefield. The wakefield is described using a fluid model, and studied analytically for a one-dimensional geometry, before a numerical model is used for the description in three dimensions. In the three-dimensional case, the excitation of a laser wakefield is considered to take place inside a plasma channel that provides a parabolic density profile, which is used to obtain a waveguiding of the drive laser pulse. External bunch injection, trapping and acceleration conditions are investigated.

In chapter 3, we study the dynamics of a femtosecond energetic electron bunch when it propagates in free-space (vacuum). This is of interest if one considers the transportation of such a bunch to a target or to an experimental area. We describe as an outlook a possible scheme to increase the energy that can be obtained with laser wakefield acceleration by a, so-called, staging laser wakefield accelerator. Particularly, we investigate the bunch dynamics during the second acceleration stage.

In chapter 4, we investigate numerically the transverse and longitudinal dynamics of an electron bunch starting from its generation at the photo-cathode, and propagating through the rf-linac employed here for pre-acceleration. The modeling extends further, describing propagation along the in-house designed electron beam transportation system, which also includes a temporal bunch compression and spatial focusing sections, to calculate the properties of the bunches as they are injected into the laser wakefield. The modeling is completed with calculating the injection, trapping, compression and acceleration in the laser wakefield for particular design parameters that we decided to use for an implementation in a corresponding experimental setup.

In chapter 5, we describe the experimental setup. The TW-laser, which we designed and realized, is based on chirped pulse amplification (CPA) using Ti:sapphire as the active medium. The laser output is, temporally compressed and spatially focused in vacuum and, is directed into the interaction chamber. The rf-linac, which provides electron bunches with energies in the range of about 2 to 6 MeV is described, followed by a description of the bunch transportation line. The plasma channel, chosen to allow the drive laser pulses to be guided through the plasma is based on a pulsed discharge in a hydrogen-filled capillary made of alumina with a length of 3-5 cm and an inner diameter of 306 μm. We report on essential tests of the experimental setup, including the successful waveguiding of the TW laser pulses by the discharge based plasma channel, and the spatial, temporal and spectral monitoring of the waveguiding. Particular issues are the maximization of the overall transmission in the fundamental mode with a matched spot size of the incoming beam, and identification of a suitable time window where ionization induced spectral shifts are minimized. Further, we describe the timing and synchronization scheme of the experiment. In order to produce stable electron bunches from the linac, the drive laser and the rf field inside the linac need to be synchronized to an accuracy in the order of a few ps. We have devised such synchronization by a phase-locking the 16^{th} harmonic of the laser oscillator repetition rate to the microwave master oscillator of the rf-linac. Other essential issues of synchronization involving optical delay lines and electronic schemes will be presented.

Finally, in chapter 6, the main conclusions and achievements are discussed. This includes a brief discussion of some final issues that will become important during the subsequent demonstration experiments. This is experimental techniques to verify a proper timing of the bunch injection and the verification of a proper spatial alignment of the electron beam with the optical beam along the axis of the plasma channel.

2

Theory of laser wakefield generation and electron acceleration

A high intensity ultrashort laser pulse propagating through a plasma can excite a large-amplitude plasma wave which is called laser wakefield. This is a result of collective electron oscillations through an action of the ponderomotive force associated with the intensity gradient of the pulse. The accelerating field can be as large as a few hundreds of gigavolts per meter which is of great interest for particle acceleration. Here, we present the potential of laser wakefield acceleration to generate relativistic electron bunches with unique properties, and with the advantage of enabling a highly compact design of particle accelerators. Particularly, we describe our novel injection method where an electron bunch provided by an external source is injected into a plasma channel shortly before the arrival of the drive laser pulse. In the channel, the bunch will be overtaken by the laser pulse. Subsequently, the laser wakefield following the laser pulse traps, compresses and accelerates the bunch to ultrarelativistic energies. With this approach, a better control over the relevant parameters of the laser wakefield acceleration process seems possible. Our calculations show that high-quality and extremely short relativistic electron bunches can be obtained over a very short acceleration distance. This can not be realized with conventional accelerators.

2.1 Introduction

The invention of the chirped pulse amplification (CPA) technique in the mid 1980s [3, 4] boosted the maximum light intensity available from pulsed lasers to values well above 10^{18} W/cm^2. One important application of such CPA laser systems is

laser wakefield acceleration. In a laser wakefield acceleration scheme, a high intensity laser pulse with an ultra-short duration (typically in the order of the plasma period) propagating inside a plasma excites a large-amplitude plasma wave [1]. The resulting, extremely large, accelerating field makes the laser wakefield very attractive for the development of a new generation of particle accelerators.

Many experiments investigating the possibilities for laser wakefield acceleration in different regimes have been previously performed [6–10, 35]. These previous experiments have successfully confirmed the basic viability of the concept of laser wakefield acceleration. However, the quality of the accelerated electron bunches was poor which meant that the relative energy spread could not be controlled and remained large, in the order of 100 %. This renders such particle beams unattractive for many of the envisioned applications. In 2002, it was predicted that certain narrow and unexplored ranges of the laser and plasma parameters (where strongly non-linear dynamics leads to wave-breaking) might yield ultrashort electron bunches with a much narrower energy spread [15]. In this regime, also known as the bubble regime, it would not be required to inject externally formed electron bunches, but electrons from the background plasma would be trapped in the accelerating phase of the plasma wave. Later, in 2004, groups from the Imperial College [12], Lawrence Berkeley National Laboratory (LBNL) [13], and Laboratoire d'Opique Appliquée (LOA) [14], demonstrated the generation of quasi-monoenergetic electron beams with energies in the order of 100 MeV as supporting evidence for the buble regime. Unfortunately, the reported shot-to-shot reproducibilty was poor and scaling to other parameters was not possible. This can be attributed to highly non-linear plasma and laser pulse dynamics. Recently, an important step was taken by the LBNL group [16] who showed the generation of electron bunches in the bubble regime with an unprecedented energy of 1 GeV, by channelling a 40 TW peak-power laser pulse in a 3.3-cm-long capillary discharge waveguide. A significant improvement of the shot-to-shot reproducibility was demonstrated by the LOA group [19], at the end of 2006, by using a second, counter-propagating laser pulse. In this latest experiment carried out by the LOA group, the first laser pulse excites the plasma wave in a 2 mm supersonic helium gas-jet and the second laser pulse injects plasma electrons in the acceleration phase of the wakefield.

Besides the development of the laser wakefield accelerator described earlier, a well-controlled, i.e., shot-to-shot reproducible laser wakefield acceleration yielding ultrashort and quasi-monoenergetic bunches with GeV-level energies, remains a big challenge and an important issue for many future applications [28, 36]. Better control could be expected if it were possible to separate the production and injection of electron bunches from the actual acceleration process, similar to the process used in standard accelerators. Furthermore, it is generally expected that control of laser wakefield acceleration requires the laser wakefield dynamics to be kept near the linear regime where the accelerating field distribution is regular and easier to predict. However, even when these conditions could be fulfilled, it seemed impossible to obtain a low energy spread from laser wakefield acceleration due to the limits of the available technology. There appeared to be no physically viable method to externally generate electron bunches much smaller than a plasma wavelength, and

inject them with a temporal precision much shorter than a plasma wave period. This is commonly referred to as the injection problem in laser wakefield acceleration.

Recently, it was theoretically shown that the injection problem might be overcome by injecting electron bunches from conventional rf-linacs although it seemed that such bunches would be far too long (much longer than the plasma wavelength) [21–24, 37–42]. In order to prepare a corresponding demonstration experiment at the University of Twente, we carried out a more detailed theoretical investigation of a novel bunch injection method. More specifically, we modeled the injection of long (sub-picosecond) electron bunches with an energy of a few MeVs into a plasma channel, where a high intensity ultrashort laser pulse generates a wakefield with amplitudes near the upper end of the linear regime. The key feature in this approach is to employ a counterintuitive injection sequence where the electron bunch is injected in front of the laser pulse [21–23]. In this case the bunch will be overtaken by the pulse in the plasma and trapped by the wakefield. This leads to the key to controlled injection: a dramatic compression of the bunch both in the longitudinal and transversal directions, before the same wakefield accelerates the bunch. Theoretically, this should result in a femtosecond micron-sized ultrarelativistic electron bunch with a low energy spread.

In this chapter, to arrive at an experimental setup that allows the execution of a corresponding demonstration experiment, we start by recalling the basic theory of laser wakefield acceleration in two steps. In the first step, we describe how a wakefield is generated by a laser pulse and we calculate the spatial structure of a wakefield. In the second step, we describe the acceleration of electrons for which we use the wakefield structure given in the first step. To model the first step, we describe the interaction of a laser pulse with plasma using a fluid model (section 2.2). This model is relevant to our approach when we are considering laser-plasma interactions that are limited to the linear and weakly non-linear regimes where no highly non-linear processes such as wave-breaking occurs. In the next section 2.2.2, we discuss the requirements for providing a concave spatial density profile of the plasma through which the drive laser travels, a so-called plasma channel. The channel aims to optically guide the drive laser pulse and thus maintain a high drive intensity over many Rayleigh lengths. This is necessary for extending the laser-plasma interaction (acceleration) length and for increasing the energy of the accelerated electrons. In a one-dimensional geometry, the basic concept of laser wakefield excitation can be illustrated analytically as described in section 2.2.3. However, a more realistic description is required for predicting wakefield generation for an experimental approach. Therefore we model wakefield generation also in a three-dimensional geometry as discussed in section 2.2.4. In our case, where a waveguiding plasma channel is employed, the wakefield shows an axially-symmetric profile. For such a profile, we numerically model the novel bunch injection scheme where an electron bunch generated from an external source is injected in front of the drive laser pulse as discussed in section 2.3.1. These calculations determine the particular conditions and parameter settings needed to be realized in an experimental setup to achieve an optimum trapping, compression and acceler-

ation of the injected bunches.

2.2 Fluid description of laser wakefield

In this section, we present basic equations which describe the interaction between a laser pulse and a plasma. These equations are derived by using a fluid model. In the model, the plasma is considered to be initially neutral and fully ionized. At the time-scale of laser wakefield acceleration, the ions can be considered as immobile because of the large mass-difference between electrons and ions. Furthermore, the density of the unperturbed plasma electrons (n_e) is assumed to be much less than the so-called critical plasma density $n_{cr} = \omega_0^2 m_e / 4\pi e^2$ [43], i.e., $n_e << n_{cr}$, where ω_0 is the carrier frequency of an incoming electromagnetic wave, m_e and e are the rest mass and the absolute charge of electron. Such plasma is also called an under-dense plasma which is optically almost transparent, and in which a laser pulse propagates with a velocity close to the speed of light in a vacuum c. In the opposite case of a so-called over-dense plasma where $n_e >> n_{cr}$, the plasma would reflect an incoming electromagnetic wave, just like a metallic mirror. The unperturbed plasma electron density, n_e, may vary as in the case of a plasma channel. Because the laser pulse and the wakefield velocities are much larger than the thermal velocity of plasma electrons, the thermal effects are small [43], i.e., the plasma is treated as a cold fluid. Furthermore, there are no external magnetic fields applied to the plasma (unmagnetized plasma).

With these assumptions, the motion of plasma electrons under the influence of an electromagnetic field can be described by the Lorentz equation:

$$\frac{\partial \mathbf{p}}{\partial t} + (\mathbf{v}\cdot\nabla)\mathbf{p} = -e\Big[\mathbf{E} + (\frac{\mathbf{v}}{c}\times\mathbf{B})\Big], \tag{2.1}$$

where $\mathbf{p}$ and $\mathbf{v}$ denote the momentum and velocity of plasma electrons. They are related according to $\mathbf{p} = m_e\gamma\mathbf{v}$, where $\gamma = 1/\sqrt{1-\mathbf{v}^2/c^2}$ is the relativistic Lorentz factor.

The electromagnetic field is governed by the Maxwell's equations:

$$\nabla\cdot\mathbf{B} = 0, \tag{2.2}$$

$$\nabla\times\mathbf{E} = -\frac{1}{c}\frac{\partial \mathbf{B}}{\partial t}, \tag{2.3}$$

$$\nabla\cdot\mathbf{E} = 4\pi\rho, \tag{2.4}$$

$$\nabla\times\mathbf{B} = \frac{1}{c}(4\pi\mathbf{j} + \frac{\partial \mathbf{E}}{\partial t}). \tag{2.5}$$

Here ρ and $\mathbf{j}$ denote the charge density and the current density of the plasma electrons, which are given by $\rho = -e(n - n_e)$ and $\mathbf{j} = -en\mathbf{v}$. The electron concentration ($n = n(\mathbf{r}, t)$) follows the continuity equation,

$$\frac{\partial n}{\partial t} + \nabla\cdot(n\mathbf{v}) = 0. \tag{2.6}$$

Then, to enable a more convenient description, the vector potential $\mathbf{A}(\mathbf{r},t)$ and the scalar potential $\varphi(\mathbf{r},t)$ are introduced to replace the electric and magnetic fields,

$$\mathbf{E} = -\nabla\varphi - \frac{1}{c}\frac{\partial \mathbf{A}}{\partial t}, \tag{2.7}$$

$$\mathbf{B} = \nabla \times \mathbf{A}. \tag{2.8}$$

In what follows, we choose the vector potential which satisfies the Coulomb gauge definition, i.e., $\nabla \cdot \mathbf{A} = 0$, which implies $\mathbf{A}_{\parallel} = 0$. This means that the vector potential lies in the transverse plane.

By using the identity [43],

$$m_e c^2 \nabla\gamma = (\mathbf{v}\cdot\nabla)\mathbf{p} + \mathbf{v}\times\nabla\times\mathbf{p}, \tag{2.9}$$

and definition of the vector and scalar potentials, the Lorentz equation (2.1) can be rewritten as

$$\frac{\partial}{\partial t}(\mathbf{p} - \frac{e}{c}\mathbf{A}) = \nabla(e\varphi - m_e c^2\gamma) + \mathbf{v}\times\nabla\times(\mathbf{p} - \frac{e}{c}\mathbf{A}). \tag{2.10}$$

Taking the curl of this equation gives [44]

$$\frac{\partial \Omega}{\partial t} = \nabla \times (\mathbf{v}\times\Omega). \tag{2.11}$$

where $\Omega = \nabla\times(\mathbf{p} - e\mathbf{A}/c)$ is called the generalized vorticity. For the case of an unmagnetized plasma, Ω is defined as zero at $t = 0$ and remains zero for $t > 0$. This gives $\nabla\times(\mathbf{p} - e\mathbf{A}/c) = 0$. Thus, we rewrite the equation (2.10) as follows

$$\frac{\partial}{\partial t}(\mathbf{p} - \frac{e}{c}\mathbf{A}) = \nabla(e\varphi - m_e c^2\gamma). \tag{2.12}$$

The first and the second term at the right hand-side of eq.(2.12) are the space-charge force and the non-linear ponderomotive force, respectively [43].

The wave equation propagating through a plasma can be obtained by substituting eq. (2.7) and eq. (2.8) into eq. (2.5). This yields

$$\nabla^2\mathbf{A} - \frac{1}{c^2}\frac{\partial^2}{\partial t^2}\mathbf{A} = \frac{1}{c}\frac{\partial}{\partial t}\nabla\varphi + \frac{4}{c}\pi e n\mathbf{v}. \tag{2.13}$$

Furthermore, by substituting equation (2.7) into equation (2.4) Poisson's equation can be obtained

$$\nabla^2\varphi = 4\pi e(n - n_e). \tag{2.14}$$

The momentum and continuity equation, eq.(2.12) and eq.(2.6), together with the wave equation, eq.(2.13), and the Poisson's equation, eq.(2.14), are the basic equations describing the laser-plasma interaction. In the following, to provide a more compact notation we will use the normalized scalar potential ($\phi = e\varphi/m_e c^2$) and vector potential ($\mathbf{a} = e\mathbf{A}/m_e c^2$).

2.2.1 Ponderomotive force and plasma oscillations

In this section, we discuss qualitatively the origin of the laser wakefield. As described by the Lorentz equation, see eq. (2.1), in the presence of an electromagnetic field, the plasma electrons are oscillating following the cycle of the electric field. This motion is called the quiver motion. It can be shown that the quiver momentum **p** of the plasma electrons relates to the normalized vector potential **a** via [45]

$$\mathbf{a} = \frac{\mathbf{p}}{m_e c}. \tag{2.15}$$

In a non-relativistic case ($\mathbf{v}/c << 1$), such as driving the plasma with a laser pulse of low intensity, this motion is predominantly transverse to the direction of light propagation, that is, the electron trajectory lies in the polarization plane. As the motion of electrons enters the relativistic regime ($\mathbf{v}/c \sim 1$), such as driven by laser pulse with high intensity, the Lorentz force which points along the laser propagation direction, becomes comparable to the electric force. This leads to a motion of the electrons which has components in the transverse as well as in the longitudinal direction.

In the case of an electromagnetic wave with spatially homogeneous and temporally constant amplitude, the electrons will return to their original position after each quiver cycle. Thus, the cycle-averaged (time-averaged) force exerted by the field on the electrons is zero. However, for an electromagnetic field with a spatial dependence, e.g., a short laser pulse with a Gaussian longitudinal profile or focused in the transverse direction, the cycle-averaged force is no longer zero. In this case, the quivering electrons move to regions with lower laser intensity as is indicated in Fig. 2.1. The cycle-averaged force that can be addressed to this movement is called the ponderomotive force. For a laser pulse with amplitude $E_0(\mathbf{r})$, it can be shown that the ponderomotive force equals [46],

$$\mathbf{F}_p = -\frac{e^2}{4\gamma m_e \omega_0^2} \nabla E_0(\mathbf{r})^2. \tag{2.16}$$

Due to the ponderomotive force, a pulsed laser beam propagating through plasma will push the electrons aways from regions of higher laser intensity. This means that, the plasma density is decreased in the region behind the pulse. However, this is only a transient perturbation. Because the ions are immobile, the electron displacement creates a charge separation. The charge separation generates a Coulomb force field distribution which tends to restore the perturbed density distribution when the laser pulse has passed. Furthermore, electrons accelerated back towards the depleted regions by the restoring force overshoot the equilibrium (neutral density) position, due to their inertia. As a result, after the laser pulse has passed, the plasma density will restore in an oscillatory manner. The characteristic frequency is known as the plasma frequency ω_p and depends on both the initial charge density and the electrons (relativistic) mass,

$$\omega_p = \sqrt{\frac{4\pi n_e e^2}{m_e \gamma}}, \tag{2.17}$$

where γ is the relativistic factor averaged over the laser oscillations.

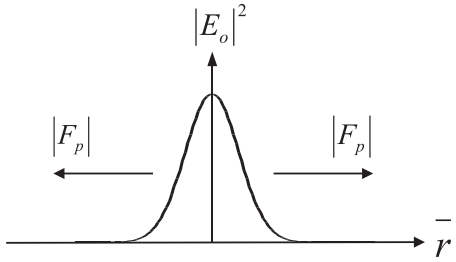

Figure 2.1: Schematic of the ponderomotive force for a laser pulse with a Gaussian intensity profile $|E_0(\mathbf{r})|^2$

These oscillations create a charge separation wave (plasma wave) that follows the laser pulse in the form of a wake with a wavelength of $\lambda_p = 2\pi v_p/\omega_p$, where v_p is the phase velocity of the plasma wave. This phase velocity is equal to the group velocity of the laser pulse in the plasma. The spatio-temporal Coulomb field distribution associated with the plasma wake wave is called the laser wakefield. In section 2.2.3, we will give a quantitative description of such laser wakefield generation. As a coarse estimate, the strength of the wakefield can be obtained via $E_0[V/cm] \approx \sqrt{n_e[cm^{-3}]}$ [45] of which the component of the wakefield oriented parallel with the propagation of the laser pulse is of interest for accelerating charged particles. For a typical plasma electron concentration n_e of 10^{18} cm^{-3}, the expression yields a wakefield strength of $E_0 \approx 100$ GV/m. Note that this approximately three to four orders of magnitude larger than that found in conventional accelerators.

2.2.2 Optical guiding of high intensity laser pulse

To push the plasma electrons and excite a large amplitude wakefield, a laser pulse with a high peak intensity is required. The required intensity may be reached in a straightforward manner by tightly focusing of a laser pulse generated with a terawatt laser system down to a spot size in the order of ten micrometers. However, the intensity obtained thereby can not be maintained for a longer propagation distance. The reason is that freely propagating light beams diffract after a characteristic distance determined by the Rayleigh length $z_R = \pi\sigma_r^2/\lambda_0$, in which σ_r is the laser pulse radius and λ_0 is the laser wavelength. This situation is indicated in figure 2.2 as the dashed lines. As an example, for a laser pulse generated by a titanium:sapphire laser system, with a central wavelength of 800 nm, focused down to a spot size of 30 μm, the Rayleigh length is about 3.5 mm. Correspondingly, at such distance behind the focus, the laser intensity would drop by a factor of approximately 100, due to diffraction in both transverse dimensions. When operating close to the linear regime, the wakefield would drop by the same factor which essentially

terminates the particle acceleration. For comparison, when the peak intensity in the laser focus can be maintained during propagation, the maximum possible acceleration length is given by the, so-called, dephasing length $L_d \approx \lambda_p^3/\lambda_0^2$ [43] where λ_p is the plasma wavelength. For example, with a plasma density of 10^{18} cm^{-3} (λ_p=33.4μm) the maximum acceleration length amounts to about 5.8 cm or 16.5z_R. It is obvious that, when using freely propagating drive laser beams, diffraction limits the acceleration length and thus the maximum energy of the electrons that can be obtained with laser wakefield acceleration. Therefore, it is essential that the laser pulse is optically guided as is schematically shown in figure 2.2 as the solid lines.

There are several methods available to overcome the diffraction, for example: relativistic self-guiding [45, 47, 48] and index guiding in a preformed plasma channel [13, 49–55]. When using the relativistic self-guiding method, the mass of the electrons increases if the quiver motion of the electrons becomes relativistic in regions with higher laser intensity, such as on the propagation axis of the drive laser pulse. This results in a decrease in the plasma frequency, $\omega_p \sim (\gamma m_e)^{-1/2}$. Since the phase velocity of the laser ($v_\phi = c/\eta$) is proportional to the inverse of the plasma's refractive index ($\eta = \sqrt{1-(\omega_p/\omega_0)^2}$), which increases for smaller ω_p, the laser's phase velocity will decrease in regions of higher laser intensity. For a laser pulse with a spatial Gaussian profile, this process will lead to focusing of the pulse which counteracts the diffractive defocusing. The relativistic self-guiding can only be achieved when the laser power is sufficiently high; the power threshold is given by [45]

$$P_{cr}[GW] \approx 17\left(\frac{\omega_0}{\omega_p}\right)^2. \tag{2.18}$$

The main problem with relativistic self-guiding is that it does not work with laser pulses as short as those required ($l_{laser} < \lambda_p$) to near-resonantly drive a wakefield to high amplitudes. This is because the refractive index of the plasma changes on a slow time-scale, $\sim \omega_p^{-1}$ [56]. In the opposite case for longer pulses ($l_{laser} > \lambda_p$), laser-plasma instabilities start to play a role, i.e., self-modulation, which leads to generation of large plasma waves and can trap and accelerate background plasma electrons. These dynamics terminate relativistic waveguiding while the accelerated electron bunches are of low quality, due to their large (about 100%) energy spread [43, 45]. A general disadvantage of relativistic self-guiding is that guiding is intensity dependent, while the effect which must be compensated for (diffraction) is not depending on the intensity. As a result the compensation is limited to a particular intensity dependent on the beam size which would be difficult to maintain over a longer propagation distance.

A very attractive method to guide high intensity laser pulses is to propagate through a preformed plasma channel. In this type of guiding, the density of the plasma is tailored such that it yields a maximum refractive index on the axis, and a decreasing index with increasing distance from the axis. As a result, the laser phase velocity attains a minimum on the propagation axis and grows with the distance from the axis. This leads to a focusing of the laser pulse. When this focusing compensates for the diffraction, the laser pulse will be guided.

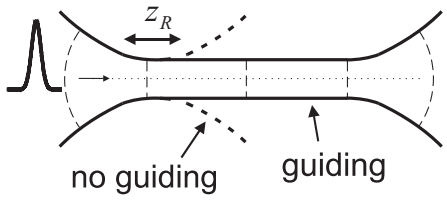

Figure 2.2: Schematic drawing of the propagation of a laser pulse without waveguiding (dashed line) and with guiding (solid line)

A plasma channel preformed to the described shape can be produced by a number of techniques. The first is the, so-called, igniter-heater technique [13, 51] based on two laser pulses delivered consecutively. The first pulse (called igniter pulse) is a short pulse (<100 fs) of lower energy but sufficiently high intensity to partly ionize a neutral gas of low Z-number, e.g., Hydrogen or Helium. The second pulse (heater) is a longer (~100 ps) and more energetic laser pulse. This pulse excites a quiver motion of the electrons that were ionized by the igniter pulse, and collisions of quivering electrons lead to a rapid heating and full ionization of the gas. The heater pulse thereby generates a radial shockwave along its path, which decreases plasma density on axis and provides the desired plasma channel. The igniter-heater technique is a technologically attractive technique because generating the high-energy (heater) pulse is straightforward and only relatively long (picosecond to nanosecond) pulse durations are required. However, it has the disadvantage that comparatively high gas densities are required for the heater pulse to work efficiently. The high gas densities yield electrons densities that are undesirably high (typically larger than 10^{19} cm^{-3}) for subsequent laser wakefield acceleration. This is due to the fact that such high values of the plasma density lead to a relatively short dephasing length causing a reduction of the maximum acceleration, which decreases the final energy gain of accelerated bunches.

Another technique employed to form a plasma channel uses weakly diffracting laser beams, such as Bessel beams, generated by axicon lenses. These beams ionize a neutral gas and heat it over a longer and narrower range along the beam axis, which is, again, followed by a radially expanding shockwave [52–54]. However, this technique employs high-Z gases, such as Xe, Ar, N_2, which become ionized to only a limited degree. This is a disadvantage because when the drive laser for laser wakefield acceleration is guided through an only partly ionized plasma channel, the pulse experiences strong losses and defocusing through ionizing remaining neutral gas atoms.

A third method is to form a plasma channel by implosion in a fast capillary discharge [55]. The strong azimuthal magnetic field induced by the discharge current (~4.5 kV) compresses the plasma toward the axis creating a plasma density profile for optical guiding. Unfortunately, the desired transverse density profile in such channels exists only for a few nanoseconds, which makes the injection time of the

drive laser pulse into the channel critical.

The most important technique, currently being used in a number of experiments, to form waveguiding plasma channels is attractive due to its overall simplicity and proved working. Here, a plasma channel is produced in a slow capillary discharge where, near thermodynamic equilibrium, heating by the discharge current and cooling of the plasma at the walls of the capillary generates the desired hollow plasma profile [49, 50]. A channel created in this way has several advantages in comparison with the techniques previously described. First, as with all pre-formed channels, the guiding does not have a threshold intensity (unlike the relativistic self-guiding). This allows the generation of wakefields in the linear and weakly non-linear regime where the spatio-temporal structure of the wakefield is regular and ideal for a controlled accelerator (see section 2.2.4 for details). Secondly, lower values of the plasma density can be used, in a range of 10^{17} to 10^{18} cm^{-3}. These lower densities imply a longer dephasing length, electrons can be accelerated over longer distances and, thus, gain more energies. Thirdly, gases with a low-Z number can be used, in particular Hydrogen, which can be fully ionized. This significantly reduces absorption and defocusing losses compared to the use of high-Z gases. Finally, the relatively slow dynamics, due to operation near equilibrium, provides a relatively long temporal window of about $\sim$100 ns duration for low-loss waveguiding. This relaxes the timing constraints between the initiation of the discharge and the injection of the drive laser pulse and the electron bunch into the plasma channel. Which, in turn, allows for greater tolerance of jitter.

Motivated by these advantages we have selected the slow capillary discharge technique to be realized and tested in our experiments. Experimental details regarding this plasma channel will be presented in chapter 5. Here, to provide a more quantitative basis for the setting of the experimental parameters, we will briefly recall the main scaling laws for waveguiding in such a capillary discharge. In a capillary discharge waveguide, it is possible to realize a plasma channel with an approximately parabolic increase of the electron density profile as described by [49, 57]

$$n_p(r) = n_0 + \Delta\left(\frac{r}{r_{ch}}\right)^2, \tag{2.19}$$

where $n_p(r)$ is the plasma electron concentration, n_0 is the on-axis density, $n_0 = n_p(0)$, r is the distance to the axis, and r_{ch} is the channel radius. The laser pulse spot size, σ_r, relates to Δ via $\sigma_r = [r_{ch}^2/(\pi r_e \Delta)]^{1/4}$ in which r_e is the classical electron radius. For a laser beam with a Gaussian-shaped radial intensity profile, the best guiding (with the beam maintaining a constant cross section during propagation) occurs if the laser spot size matches the channel radius, i.e., when $\sigma_r = r_{ch}$. If the laser spot size does not match the channel radius, $\sigma_r \neq r_{ch}$, then the laser beam cross section will oscillate in size during the propagation with a characteristic wavelength of z_R [45]. These undesired oscillations are due to the formation of a beat-wave by different modes propagating in the channel [53].

2.2.3 One-dimensional model of laser wakefield

To also provide a quantitative description, required for performing corresponding experiments, of the underlying physics involved in the excitation of a laser wakefield, we start with a simple one-dimensional model. This has the advantage that analytical expressions can be derived and typical numbers are quickly obtained. This allows for a better physical insight and enables a first view on the typical absolute size of the parameters when starting the design of a corresponding experiment.

For the drive laser pulse we consider a Gaussian longitudinal profile laser pulse which propagates along the z-axis inside a plasma. The laser pulse is assumed to be linearly polarized in the y direction. The normalized vector potential can then be expressed by

$$\mathbf{a}(z,t) = a_0 \exp\left\{-((z-ct)/\sigma_z)^2\right\} \hat{y} \exp\left\{-i(k_0 z - \omega_0 t)\right\}, \tag{2.20}$$

where $k_0 = 2\pi/\lambda_0$ is the wavenumber of the carrier wave of the light pulse, σ_z relates to the full width at half maximum of intensity (τ_0) via $\sigma_z = c\tau_0/\sqrt{2\ln 2}$ and λ_0 is the central wavelength of the pulse. As we chose to restrict our model to a single dimension (the z-dimension), the laser field is assumed to be uniform in the transverse directions. Due to its normalization, a_0 expresses the interaction strength of light with electrons, and relates to the laser peak intensity I_0 of a linearly polarized laser pulse via

$$a_0 = \frac{p_{y0}}{m_e c} = \sqrt{\frac{2e^2\lambda_0^2}{m_e^2 c^5 \pi} I_0}, \tag{2.21}$$

where p_{y0} is the amplitude of the transverse momentum of electrons. For a typical laser wavelength $\lambda_0 = 0.8$ μm, $a_0 = 1$ corresponds to an intensity of 2.1×10^{18} W/cm^2. This intensity can be reached, for instance, by focusing a laser pulse with 1.3 joule energy and 40 fs duration to a spot size of 30 μm. If $a_0 \geq 1$, the electrons motion becomes relativistic. In this case, the magnetic force in the Lorentz equation becomes comparable to the electric force. This can lead to a considerable longitudinal momentum of plasma electrons.

For convenience, further studies will be executed in a moving frame coordinate (ξ, τ), which co-propagates with a speed equal to the group velocity of the laser pulse. Here ξ is defined as $\xi = k_p(z - c\beta_g t)$ and $\tau = t\omega_p$ with $k_p = 2\pi/\lambda_p$ and $\beta_g = v_g/c$ is the normalized group velocity of the laser pulse. By using transformation derivatives $\partial/\partial z = k_p \partial/\partial\xi$ and $\partial/\partial t = \omega_p \partial/\partial\tau - k_p c\beta_g \partial/\partial\xi$, the momentum-, the continuity-, the wave- and the Poisson's equation can be rewritten in the one-

dimensional geometry as follows:

$$k_p \frac{\partial}{\partial \xi}\Big[\gamma(1-\beta_g\beta_z)-\phi\Big] = -\frac{\omega_p}{c}\frac{\partial}{\partial \tau}\gamma\beta_z, \quad (2.22)$$

$$k_p \frac{\partial}{\partial \xi}\Big[n(\beta_g-\beta_z)\Big] = \frac{\omega_p}{c}\frac{\partial}{\partial \tau}n, \quad (2.23)$$

$$\Big[k_p^2(1-\beta_g^2)\frac{\partial^2}{\partial \xi^2}+2k_p\omega_p\frac{\beta_g}{c}\frac{\partial^2}{\partial \xi\partial \tau}-\frac{\omega_p^2}{c^2}\frac{\partial^2}{\partial \tau^2}\Big]a = k_p^2\frac{n}{n_e}\frac{a}{\gamma}, \quad (2.24)$$

$$\frac{\partial^2}{\partial \xi^2}\phi = \frac{n}{n_e}-1, \quad (2.25)$$

with $\gamma=\sqrt{(1+a^2/2)/(1-\beta_z^2)}$, $a=a(\xi,\tau)$, $\phi=\phi(\xi,\tau)$ and $n=n(\xi,\tau)$. We define that, in the (ξ,τ) frame, the light field is non-zero only in the region where $\xi\leq 0$ while at $\xi>0$, i.e., in front of the laser pulse, we have $a=0$, $n=n_e$, $\beta_z=0$ and $\gamma=1$.

Equations (2.22)-(2.25) can be simplified by using the quasi-static approximation [58, 59]. This approximation is valid for the macroscopic plasma quantities, i.e., n, β_z and γ. The quasi-static approximation assumes that the evolution of the laser pulse in the considered coordinate frame (moving with nearly the speed of light) is much slower than the plasma response. This means that the laser pulse envelope does not significantly evolve during the transit time of plasma electrons through the laser pulse. This requires that the duration of the laser pulse, τ_0, is much shorter than the laser pulse evolution time τ_E ($\tau_E\sim 2\gamma(n_e/n)(\omega_0/\omega_p)/\omega_p$), which is typically on the order of the laser diffraction time τ_d ($\tau_d=z_R/c$). These conditions are satisfied as long as $\omega_p << \omega_0$ meaning that an under-dense plasma is used, as will be the case in the experiments we will perform. By applying the quasi-static approximation, we can neglect $\partial/\partial\tau$ in the momentum equation (eq. (2.22)) and the continuity equation (eq. (2.23)). However, $\partial/\partial\tau$ in the wave equation (eq. (2.24)) is to be maintained since it describes the evolution of the laser pulse during its propagation through the plasma. The one-dimensional laser wakefield equation for a linearly polarized laser pulse can be obtained from eq. (2.22), (2.23) and (2.25) [43]. With the help of the quasi-static approximation, we find

$$\frac{d^2\Phi}{d\xi^2}=\beta_g^2\gamma_g^2\left(\beta_g\frac{1}{\sqrt{1-\frac{1}{\gamma_g^2}\frac{1+a^2/2}{\Phi^2}}}-1\right), \quad (2.26)$$

where $\Phi=1+\phi$ and $\gamma_g^2=1/(1-\beta_g^2)$ is the gamma factor of the driver laser pulse. The electric field of the excited wakefield, normalized to the non-relativistic wave-breaking field $E_0=m_e v_g\omega_p/e$ [43], can be found from the equation:

$$E_z=-\frac{1}{\beta_g^2}\frac{d\Phi}{d\xi}. \quad (2.27)$$

In figure 2.3(a), we show the calculated wakefield (dashed curve) obtained with the Gaussian laser pulse (solid line) set to an energy of 1.3 J and a duration of 40

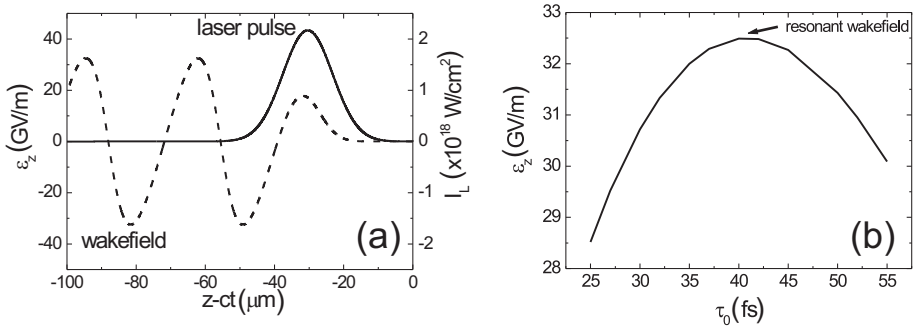

Figure 2.3: In part (a), the intensity of the drive laser (solid curve with peak centered at -30 μm) and the excited wakefield (dashed line) are plotted. The plasma density is chosen as 1.1×10^{18} cm^{-3}. The laser peak intensity is 2.1×10^{18} W/cm^2, which corresponds to $a_0 = 1$. In the chosen frame both the laser pulse and the wakefield stand still, but in the lab frame they propagate along the z-axis. In part (b) shows how the calculated wakefield can be maximize via adjusting the laser pulse duration with a constant plasma density and peak intensity (same as in (a)). The parameter ϵ_z is the actual field which is defined as $\epsilon_z = E_z \cdot E_0$.

fs. Such laser parameters can be realized with powerful CPA laser systems. For the shown results we have taken a plasma electron density that is 1.1×10^{18} cm^{-3} which corresponds to a plasma wavelength of 32 μm. This can be realized by fully ionizing Hydrogen with a pressure of about 46 mbar in a discharge capillary. In the normalized units, those parameters are equivalent to $a_0 = 1$, $k_p\sigma_z = 2$, and $\omega_0/\omega_p = 40$. The laser wakefield reaches a maximum value of 32.5 GV/m, which is three orders of magnitude higher in comparison to that achieved in conventional accelerators. Note that, in the phase of the wakefield immediately following the laser pulse, the electric field values are negative while both the laser pulse and the wakefield travel into the positive z-direction. This corresponds to an electric field pointing opposite to the propagation direction of the wakefield. However, when considering the negative charge of electrons to be accelerated, it is this phase (region) with a negative field that provide the desired (accelerating) force along the propagation direction.

As was explained in section 2.2.1, the ponderomotive force displaces plasma electrons from the path of the laser pulse while the electron dynamics (due to restoring Coulomb forces and inertia) shows a resonant frequency, the plasma frequency. As with any driven system exposing a resonance, there should be a maximum amplitude of the wakefield, here, this occurs when the pulse length of the drive laser is of the order of the plasma wavelength. This can be inspected in Fig. 2.3(b), which displays the maximum value of the calculated wakefield amplitude as a function of the pulse duration. It can be clearly seen that the wakefield amplitude shows a maximum value for a certain pulse duration, when $k_p\sigma_z = 2$ is fulfilled. In the shown example the pulse duration τ_0 (FWHM of the intensity) is 40 fs when the amplitude

of the electric field is at the maximum. The wakefield in this case is called the resonant wakefield. For the design of an experiment, in order to excite a wakefield with highest amplitude for acceleration to a maximum bunch energy, it is important to mutually match the plasma density (which depends on the gas pressure) and the pulse duration of the laser (which depends on the construction and alignment of the laser system).

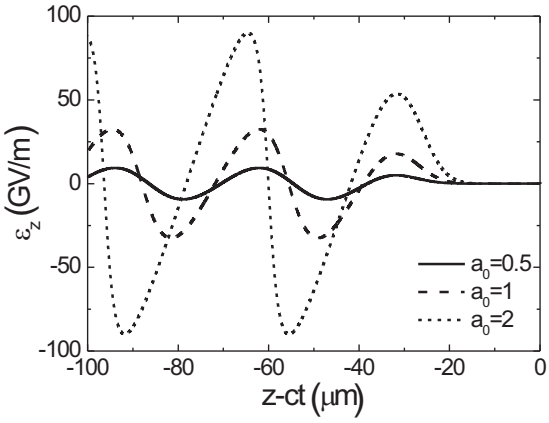

Figure 2.4: The laser wakefield calculated for three different laser peak intensities (the laser pulse is not shown but is centered as in Fig. 2.3). For a peak intensity of 5.5×10^{17} W/cm^2 ($a_0 = 0.5$) the wakefield is linear (solid line), for 2.1×10^{18} W/cm^2 ($a_0 = 1$) the wakefield is weakly non-linear (dashed line) and for 8.5×10^{18} W/cm^2 ($a_0 = 2$) the wakefield is non-linear (dotted line). Other parameters are kept the same as in Fig. 2.3(a). The parameter ϵ_z is the actual field which is defined as $\epsilon_z = E_z \cdot E_0$.

If the intensity of the drive laser increases, the wakefield exhibits various shapes. This can can be seen in figure 2.4. At sufficiently low drive laser amplitudes, i.e., $a_0 < 1$ (such as with $a_0 = 0.5$, the solid trace), the wakefield exhibits a shape that is very close to sinusoidal. This is called the linear regime. In the shown case, the wakefield amplitude is 9.4 GV/m and the plasma wavelength is $\lambda_p = 32\mu$m. When the drive laser amplitude and thus the wakefield amplitude increases (see $a_0 = 1$, the dashed trace), the wakefield amplitude raises and begins to show some smaller deviations from a purely sinusoidal shape. This regime is called the weakly non-linear regime because the essential properties of the wakefield, in particular its peak amplitude and wavelength, start to deviate slightly from a linear dependence of the drive laser intensity. Here, the wakefield grows to 32.5 GV/m, which is slightly less than the four-fold increase from $a_0^2 = 0.25$ to $a_0^2 = 1$. Also the wavelength of the wakefield starts to change and becomes $1.02\lambda_p$. When the drive laser amplitude is further increased into the regime with $a_0 > 1$ (see $a_0 = 2$, the dotted trace), a clear steepening of the wakefield can be seen. In this situation, the motion of the plasma electrons becomes relativistic. This can also be seen as a clearly in-

creased wavelength of the wakefield $1.14\lambda_p$, due to a relativistically increased mass of the plasma electrons when performing their restoring oscillation. The wakefield amplitude grows, but the growth is only to a value of 89.9 GV/m which is much less than the four-fold increase from $a_0^2 = 1$ to $a_0^2 = 4$.

In this one-dimensional model, we have considered a laser pulse in the form of a plane wave profile in the transverse directions. This model has illustrated the typical dynamics of the laser wakefield in the linear regime, and also what type of deviations occur when entering the weakly non-linear and the non-linear regime. The basic features discussed, such as the spatio-temporal shape of the wakefield and deviations in the wakefield wavelength are quite instructive in gaining a better understanding of more complex situations. Specifically, in an experimental approach, the drive laser pulse possesess a certain transverse profile which is determined by the focusing and waveguiding conditions as was explained above (see section 2.2.2). It can be expected that these properties are reflected in a correspondingly modified wakefield structure, which contains coupled longitudinal and transverse components, when considering the full (three-dimensional) character of the wakefield. In the next section, we will use a three-dimensional model to include the more realistic profiles of the drive laser pulse to calculate the shape and strength of laser wakefields that might better resemble the experimental situation.

2.2.4 Three-dimensional model of laser wakefield

In the previous section, we neglected the transverse variation of the drive laser field in order to enable an easier description of discussion. Therefore, that analysis only applies for plasma electrons which are close to the laser pulse propagation axis. Here, in order to include the three-dimensional character of the laser pulse and laser wakefield, a three-dimensional model needs to be employed. In this three-dimensional model, we considered that the laser pulse is an axially-symmetrical, which is the case in an experiment with standard (non-astigmatic) laser beams. Under this condition, the electric field can be described as $\mathbf{E} = (E_r, 0, E_z)$ in cylindrical coordinates, where E_r and E_z are the radial and longitudinal components of the electric field, respectively. The magnetic field is $\mathbf{H} = (0, H_\theta, 0)$, where H_θ is the azimuthal component. A linearly polarized laser pulse in the cylindrical coordinates is described as follows:

$$a(\xi, r) = a_0 e^{-(\xi-\xi_c)^2/(k_p\sigma_z)^2} e^{-r^2/(k_p\sigma_r)^2}. \tag{2.28}$$

For a more compact description, we introduce normalized parameters $\nabla \to \nabla/k_p$, $\mathbf{r} \to k_p\mathbf{r}$, $\mathbf{p} \to \mathbf{p}/m_e c$, $\tau \to t\omega_p$, $\phi \to e\varphi/m_e c^2$, $\mathbf{a} \to e\mathbf{A}/m_e c^2$, $\mathbf{E} \to \mathbf{E}/E_0$, $\mathbf{H} \to \mathbf{H}/E_0$, $N \to n(\xi, r)/n_p(r=0)$ for plasma electron concentration and $N_p \to n_p(r)/n_p(r=0)$ for unperturbed plasma electron concentration. Here $E_0 = m_e\omega_p v_g/e$ is called the non-relativistic wave-breaking field. Furthermore, we again neglect the evolution of the laser pulse during propagation in plasma, and assume an under-dense plasma of high transparency. The three-dimensional laser wakefield, expressed in cylindrical coordinates, can then be obtained by solving numerically the following

set of equations [60]:

$$\frac{\partial p_r}{\partial \xi} - \frac{\partial p_z}{\partial r} - \beta_g^2 H_\theta = 0, \tag{2.29}$$

$$\beta_g \frac{\partial p_r}{\partial \xi} - \frac{\partial \gamma}{\partial r} - \beta_g^2 E_r = 0, \tag{2.30}$$

$$\beta_g \frac{\partial p_z}{\partial \xi} - \frac{\partial \gamma}{\partial \xi} - \beta_g^2 E_z = 0, \tag{2.31}$$

$$-\frac{\partial H_\theta}{\partial \xi} + \beta_g \frac{\partial E_r}{\partial \xi} + \beta_r N = 0, \tag{2.32}$$

$$\nabla_\perp H_\theta + \beta_g \frac{\partial E_z}{\partial \xi} + \beta_z N = 0, \tag{2.33}$$

$$\nabla_\perp E_r + \frac{\partial E_z}{\partial \xi} + (N - N_p) = 0, \tag{2.34}$$

$$\beta_g \frac{\partial H_\theta}{\partial \xi} + \frac{\partial E_z}{\partial r} - \frac{\partial E_r}{\partial \xi} = 0, \tag{2.35}$$

where $\gamma = (1 + p_z^2 + p_r^2 + a^2/2)^{1/2}$. Equation (2.29) is derived from the generalized vorticity equation ($\Omega = \nabla \times (\mathbf{p} - e\mathbf{A}/c)$=0). The r- and z-components of the Lorentz equation are presented in equation (2.30) and equation (2.31), respectively. Equation (2.32) and equation (2.33) are derived from the Ampère's law in the Maxwell's equations. Finally, equation (2.34) and equation (2.35) are Gauss's law and the θ-component of the Faraday's law, respectively.

To explore the typical wakefield dynamics and its properties in both the linear and the weakly non-linear regime, we calculated the normalized electric field distribution (E_z) and the transverse force distribution ($F_r = \beta_g H_\theta - E_r$) of the laser wakefield excited in a plasma channel at two different laser intensities. The results are shown on Figs. 2.5 (a) and (b), where a peak intensity of 5.5×10^{17} W/cm^2 ($a_0 = 0.5$) and of 2.1×10^{18} W/cm^2 ($a_0 = 1$) are assumed, respectively. The laser pulse is centered at $\xi = -6$, as is indicated by the elliptical traces, and propagates along the ξ-axis, i.e., from left to the right. The transverse profile of the plasma density follows equation (2.19) with an on-axis electron density of 1.1×10^{18} cm^{-3}. The channel radius was set to match a laser spot size of 30 μm. In the electric field distribution, the field is accelerating in the blue areas (in the red regions the field is decelerating). A new feature of the wakefield in the three-dimensional geometry when compared to the one-dimensional case previously discussed, is the appearance of a transverse force fields. It can be seen that there are regions of focusing force (shown in red) which would accelerate electrons towards the propagation axis and that, importantly, these regions partly overlap with the forward accelerating regions. The advantage of this overlap is that it prevents off-axis electrons from leaving the forward acceleration process. The defocusing force, shown as blue areas, scatter electrons out of the wakefield in such a way that these electrons would not be accelerated further. Another feature of the three-dimensional wakefield is that a pronounced curvature of the wakefield wave front is observed. The curvature is present because we consider acceleration in a plasma channel where the

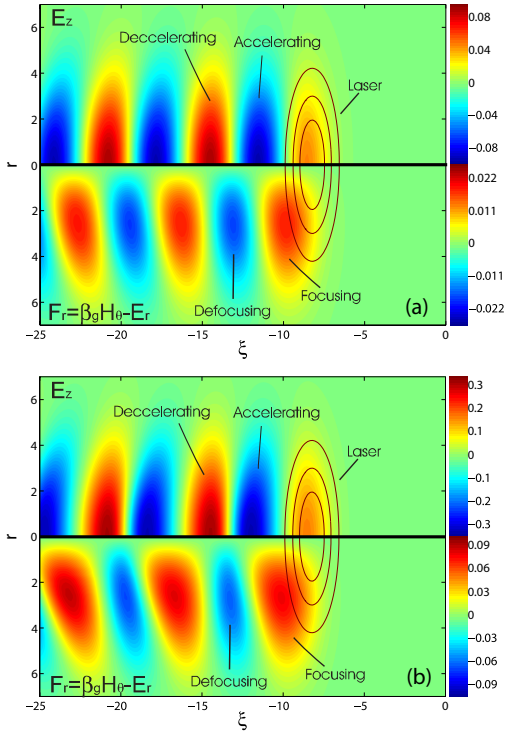

Figure 2.5: The normalized electric field distribution (E_z) and the focusing force distribution ($F_r = \beta_g H_\theta - E_r$) of the laser wakefield generated in a plasma channel are plotted. The laser pulse is centered at $\xi = -6$ as indicated by the elliptical traces. The wakefield in Fig. 2.5(a) and in Fig. 2.5(b) is excited by a Gaussian laser pulse with a peak intensity of 5.5×10^{17} W/cm^2 ($a_0 = 0.5$) and 2.1×10^{18} W/cm^2 ($a_0 = 1$), respectively, $\xi = k_p(z - c\beta_g t)$ and r is normalized to $1/k_p$.

initial plasma is not homogeneous but where the plasma density radially increases, yielding a longer plasma wavelength on the axis. It can also be seen that, when the wakefield amplitude enters the weakly non-linear regime as in Fig 2.5(b), the curvature of the wave fronts becomes even stronger. This can be addressed to the onset of a relativistic increase of the plasma wavelength, as was discussed already with the one-dimensional model.

For the purposes of electron acceleration it is very important that the overlap between the accelerating field and the focusing force is as large as possible. Electrons in this overlap region can be accelerated over a long distance while remaining close to the propagation axis, where the accelerating field is at its maximum. This serves also for a low energy spread in the accelerated bunch because the accelerating field amplitude decreases with the distance from the axis; electrons situated

relatively far from the axis would gain less energy compared to the on-axis electrons. Finally, in the external bunch injection scheme considered here, described in section 2.3.1, a large overlap between regions of focusing force and regions of acceleration, particularly with the first accelerating region following the laser pulse, is an essential requirement to trap (and accelerate) electrons that are injected from an external source. Here it is shown to be advantageous to consider laser wakefield acceleration in a plasma channel because the overlap area is larger than in a homogeneous plasma [22, 23, 45, 61].

2.3 Electron acceleration

The longitudinal electric field of a laser wakefield as described in the previous sections for one- and three-dimensional geometry can be used to trap and accelerate electrons, provided that these are injected under certain physical conditions. These conditions are: a suitable position and timing with regard to the wakefield structure, and a certain initial velocity as will be described in the following. During acceleration the electron velocity will increase and approach the speed of light. Since the wakefield phase velocity (given by the drive laser group velocity) is less than the speed of light, $v_p < c$, the electrons will slip forward with regard to the wakefield, outrun the accelerating region and eventually enter a region where the wakefield is decelerating. The distance, which is needed for electrons to travel and to gain energy before they enter the decelerating phase of the wakefield is called the dephasing length. The dephasing length in the linear wakefield can be approximated by $L_d \approx \gamma_g^2 \lambda_p$ [1]. The dephasing limits the energy gain of the accelerated electrons. For an optimum acceleration, the length of the accelerator should match the dephasing length.

In order to obtain, with laser wakefield acceleration, an electron bunch with high energy and a low relative energy spread, an electron bunch is to be injected in a very small volume with a narrow distribution of the accelerating phase. It was long believed that this could only be achieved when the dimensions of the injected bunch were as small as a tiny fraction of the plasma wavelength. However, since the plasma wavelength is in the order of tens of micron, injected bunches would have to have extremely short lengths in the order of a few microns, which corresponds to a duration of a few femtoseconds. Similarly, it was also believed that the width of the injected bunch would have to be much less than the transverse size of the wakefield, comparable to the spot size of the driver laser pulse. This indicates that the transverse bunch size would have to be in the order of a few micrometers. Moreover, one would expect that timing of the injection would require precise control, on a femtosecond scale. These requirements, summarized in the term "controlled injection" are beyond standard accelerator technology. Therefore, it was expected that the injection of electron bunches, e.g. from a standard linac, into a laser wakefield would render accelerated bunches with an intolerably wide energy spread of near 100%. For this reason, the controlled injection of electrons has remained the central issue in realizing laser wakefield acceleration that yields high quality bunches as described above.

To illustrate the nature of this injection problem in more detail, and to identify a possible solution, two methods of injection need to be considered. These methods are called internal and external electron injection. In an internal electron injection scheme, electrons from the background plasma can be injected into the wakefield via a wave-breaking mechanism [12–15, 62], colliding of laser pulses [19, 63, 64], tunneling ionization [65] or by employing a sharp plasma density gradient [20, 66–68]. If the trapping of these electrons is successful, the electrons will be accelerated by the wakefield. As previously stated, much progress has recently been achieved with such methods, however, the reliance of such methods on non-linear dynamics has remained a severe obstacle for a stable and scalable acceleration to high energies with a low energy spread. In an external injection scheme [38, 69], electron bunches are generated with an independent source outside the plasma, the goal being to realize a better control. However, due to the technological limits previously discussed, the bunches will be relatively long (typically several plasma wavelengths). Thus, when injecting such bunches following the standard and intuitive manner, i.e., directly into the wakefield structure behind the drive laser pulse, there is a narrow parameter range where the resulted energy spread might be a few percents. To our knowledge this approach is well investigated through modeling but a corresponding experiment has not been reported yet. A closer investigation shows that such an experiment might encounter additional problems. For example, if the injected bunches comprised a length of several plasma wavelengths, they would be sliced into several sub-bunches trapped in several accelerating regions behind the laser pulse. The next problem with injection behind the laser pulse is that the injected bunch would become scattered by the drive laser pulse (in the vacuum region in front of the plasma) [42] if high drive intensities are used. The scattering is caused by the ponderomotive force associated with the intensity gradient of the drive laser pulse and it can significantly reduce the fraction of the injected electrons trapped in the wakefield. Finally, bunch injection behind the laser pulse can suffer from a disturbed trapping and acceleration due to the smooth density transition between vacuum and plasma [70]. In this transition region, as seen in the frame moving with drive pulse, the plasma wavelength quickly increases during trapping, which disturbs the desired dynamics. In conclusion, external injection seems to remain rather difficult unless alternative methods are explored.

In the following we will present a novel approach to externally inject electron bunches into a laser wakefield. Although very similar to the intuitive approach discussed so far, it shows that only slight modifications might yield dramatic improvements and lead to a solution of the injection problem in laser wakefield acceleration.

2.3.1 External bunch injection in front of the drive laser

The main idea of how external injection of long bunches from standard accelerators can enable control laser wakefield acceleration is schematically shown in Fig. 2.6 [22, 23]. There are two main differences to the approach of injection behind the laser pulse. The first is that the bunch is injected first, i.e., in front of the laser

pulse (1). This injection appears counterintuitive because the bunch is injected into a region where no wakefield is present. The second difference is to raise the drive laser intensity into the weakly non-linear regime. For a more detailed discussion we shall proceed with typical parameters that may also be relevant in a first experimental demonstration of this scheme. After injection, the bunch travels through the plasma with a relatively low-energy (a few MeVs) and possessing an appreciable duration, such as several hundreds of femtoseconds. The velocity of the bunch, v_b, is then relatively small when compared to the group velocity of the terawatt laser pulse, v_g, which is injected later (2). The laser pulse generates a wakefield (3) which propagates with a phase velocity that is equal to the group velocity of the laser pulse. Since the laser pulse and the wakefield travel faster than the bunch, $v_b < v_g$, the bunch will be overtaken by the laser and the wakefield after some propagation distance which we call the trapping distance L_{tr}. It can be shown that $L_{tr} \approx 2\gamma_0^2 l_0$ [23], where $\gamma_0 = [1-(v_b/c)^2]^{-1/2}$ is the Lorentz factor of the injected bunch with a length of l_0. When the laser wakefield is sufficiently strong, the injected electrons are trapped and accelerated in a small region within the first accelerating region in the wakefield.

To illustrate the underlying physics in this external bunch injection scheme, we consider how a single, injected 'test' electron is driven by a one-dimensional laser wakefield. As with standard accelerators, trapping, acceleration and dephasing can be studied by examining the electron orbit in the (γ,ξ) phase space, as is shown in Fig. 2.7. An important characteristic of the phase space is the so-called separatrix $\gamma_s(\xi)$ shown as the solid trace. It separates phase space regions where electrons perform closed orbits after injection (and are thus trapped) from open orbit (no trapping after injection). It can be seen that there are three phase space regions, namely, the central region of closed orbits inside the separatrix, and the lower and upper regions of open orbits, below and above the separatrix. The three regions are mainly separated by the kinetic energy of the electron which is displayed in relative and logarithmic units on the vertical scale. If the electron is injected with a low initial energy in front of the wakefield, indicated by the lower dashed trace which begins at $\xi_0 = 0$, the electron will follow a phase space trace in the lower region of open orbits. In this case the spatial coordinate will become increasingly negative, accompanied by only smaller and quasi-periodic changes in kinetic energy. This means that the (periodic) wakefield overtakes the electron but does not trap it, so that the electron just slips backwards with regard to the wakefield. For the upper phase space region the injected electron is already faster than the plasma wave. An electron injected at some negative space coordinate is not caught either (not decelerated in this case) and will outrun the wave. However, when the electron is injected in front of the wakefield with a certain minimum energy, such as indicated as point (A), the space coordinate will not decrease below a certain value which means that the electron is trapped and pulled along with the wakefield, thus gaining velocity. The correspondingly increasing energy be seen as the phase space trace moving upwards (points (B) and (C)). Thus, in order to trap and accelerate electrons, the initial injection energy needs to be high enough to enter a closed orbit in the phase space.

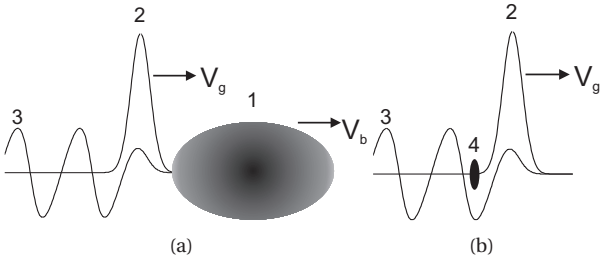

Figure 2.6: Schematic description of laser wakefield accelerator scheme that would solve the injection problem. A relatively long and slow electron bunch from a standard accelerator (1) is injected ahead of the laser pulse (2). After traveling some distance, the wakefield (3) behind the laser traps, compresses and accelerates the electrons to an ultra-relativistic energy (4).

In the (ξ,τ) frame, the motion of a test electron inside the one-dimensional laser wakefield can be quantitatively investigated by solving the following set of equations [22]

$$\frac{dp_e}{d\tau} = -\frac{1}{4\beta_g\gamma_e}\frac{da^2}{d\xi} - \beta_g E_z \tag{2.36}$$

$$\frac{d\xi}{d\tau} = \left(\frac{\beta_e}{\beta_g}\right) - 1 \tag{2.37}$$

where γ_e is the relativistic factor of the test electron $\gamma_e = \sqrt{1+p_e^2+a^2/2}$, β_g is the normalized group velocity of the driver laser, $\beta_e = \sqrt{\gamma_e^2 - 1 - a^2/2}/\gamma_e$ is the normalized velocity of the test electron, $\tau = \omega_p t$, and $\xi = k_p(z - v_g t)$. The first term on the right hand side of equation (2.36) describes the force exerted by the laser pulse on the electron, the ponderomotive force. This force is usually not considered in another case (bunch injection behind the pulse). In our scheme it is important to include this force because electrons injected in front of the laser pulse, will encounter this ponderomotive force as the laser pulse overtakes the electrons.

For a better understanding of the special features of this novel injection scheme, it is instructive to inspect Fig. 2.6 more carefully. It can be seen that, the growth of the ponderomotive force on the injected electrons (which would push electrons forwards) is occurring simultaneously with the growth of wakefield to positive field values (which decelerates electrons). It turns out that these forces approximately cancel each other out and the electrons just pass the laser region without much distraction. These arguments remain valid when inspecting three-dimensional laser intensity and wakefield distribution such as in Fig. 2.5. Only electrons with very high energy $\gamma_e \cong \gamma_g$ can be trapped inside the region of high laser intensity [23].

In order to describe the trapping mechanism, we consider the initial injection energy and trapping position of the test electron. By using the integral of motion

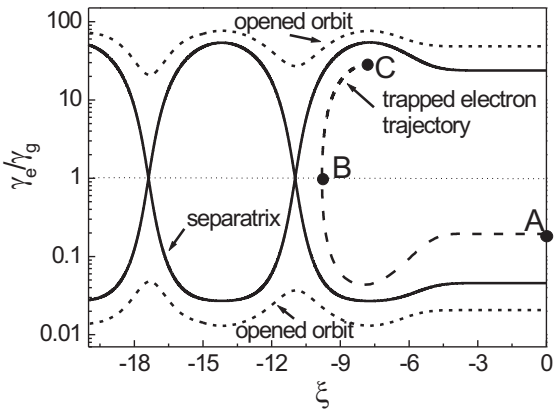

Figure 2.7: The trajectory for an electron injected in front of the laser pulse (at A) is plotted as the thicker dashed line. Electrons injected with insufficient energy or too high energy for being trapped are shown as open orbits (dotted lines). The drive laser pulse has $a_0 = 1$, $\sigma_z = 2/k_p$, $\omega_0/\omega_p = 40$ and a center at $\xi_c = -6$ as presented in Fig. 2.3(a). The plasma density is 1.1×10^{18} cm^{-3}. The initial energy of the injected electron is 3.45 MeV ($\gamma_0 = 6.76$) at $\xi_0 = 0$ and is increased by approximately two orders of magnitude (to several hundreds of MeV) when the electron reaches point C. The solid line is the separatrix calculated for the named laser and plasma parameters.

(Hamiltonian), i.e., $\gamma_e(1-\beta_e\beta_g)-\phi = constant$ [22], a relation between the initial electron energy $\gamma_{e,0}$ and the trapping position of the test electron can be found

$$\gamma_{e,0} = \gamma_g^2\left[S - \beta_g\sqrt{S^2-\gamma_g^{-2}}\right] \tag{2.38}$$

where $S = \gamma_g^{-1} - \phi(\xi_{tr})$ and $\phi(\xi_{tr})$ is the potential at the trapping position.

The calculated relation between the minimum injection energy and the trapping position for an injected test electron is plotted in Fig. 2.8(a). The parameters for the laser pulse and plasma are identical to the previous case, figure 2.3(a). For injection with an energy of 0.93 MeV, the electron is trapped at a position z, where $E_z = 0$. As the injection energy increases, the trapping position shifts to larger values of the wakefield. The region in which electrons can be trapped lies between the two dashed lines, i.e., $E_z(z) = 0 \le E_z(z_{tr}) \le E_z(z) = -E_{z,max}$. By increasing the strength of the drive laser, the wakefield becomes steep, thus the length of the trapping region will reduce, although the wakefield wavelength increases. Another important result of the calculations is that the required minimum injection energy can be decreased by increasing the strength of the drive laser, because this results

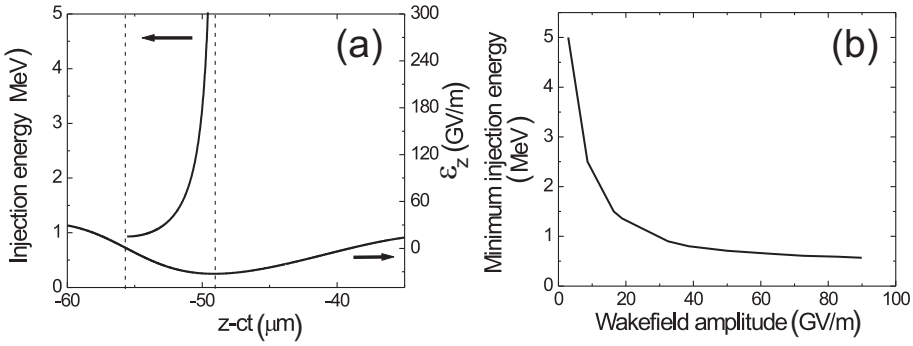

Figure 2.8: The theoretical relation between the minimum injection energy and the trapping position is plotted in part (a) for $a_0 = 1$. The trapping region lies between the two dashed lines. The calculated relation between the minimum injection energy for trapping at $E_z = 0$ versus the wakefield amplitude is presented in part (b). The input parameters for the calculations are: $\sigma_z = 2/k_p$, $\omega_0/\omega_p = 40$.

in a larger wakefield (see Fig. 2.8(b)). It can also be said that trapping electrons in a weaker wakefield (such as in the linear regime) requires a higher injection energy.

More detailed information on the described dynamics, particularly in the three-dimensional case, was obtained by solving the Lorentz equations for electrons injected in numerically calculated wakefields, such as shown in Fig. 2.5. To study the dynamics of an entire bunch of electrons with a realistic size and energy spread, it is possible to slightly vary the injection parameters accordingly. However, we order to be able to safely neglect perturbing effects resulting from Coulomb repulsion within the injected bunch and a distortion of the wakefield by the injected bunch (sometimes term beam loading). This description is limited to bunches with a sufficiently low charge. Our estimates yield that bunches with a charge of the order of tens of pC can be safely described this way.

A typical example of the results from such calculations in three-dimensional geometry, showing: trapping, bunch compression and acceleration, is shown in Fig. 2.9. This figure shows the dynamics of a relatively large electron bunch of lower kinetic energy, obtained from a standard rf-linac, in the form of snapshots taken at increasing times and at an increasing space coordinate (Δz) in the plasma. For a better comparison, the snapshots are again taken in the frame moving with the group velocity of the laser towards the positive z-direction. Therefore, the associated laser wakefield, appears as stationary (frozen) while the injected electron bunch (moving slower than the frame) initially appears as propagating to the left. In this frame, when the wakefield overtakes the electron bunch, the electron bunch moves to the left until it approaches the the wakefield. In the shown example, we use parameters for the drive laser, the plasma channel and the bunch similar to those of the experimental specifications of our setup. These specifications will be presented in

detail in section 4.5 as derived by optimization in chapter 4 and as implemented in the design and experimental setup in chapter 5. These are a laser pulse duration of 35 fs (FWHM), a peak intensity of 2×10^{18} W/cm^2, a wavelength of 800 nm and a Gaussian beam radius in the waist of 30 μm. The on-axis density of the plasma channel is selected 8.6×10^{17} cm^{-3}, which corresponds to a plasma wavelength of about 36 μm. The injected bunch is chosen to possess a kinetic energy of 2.88 MeV ($\gamma_0 = 6.7$) and a duration of 250 fs (which is about 7 plasma wavelengths). Initially, after injection, the bunch is travelling in front of the laser pulse as can be seen in the first frame (a) in Fig. 2.9. After some propagation distance (indicated as Δz above each frame), the electron bunch starts to encounter the wakefield forces and, then, is trapped once it reaches the trapping position. The focusing region of the wakefield focuses electrons toward the axis and this force helps to increase the number of trapped electrons, see Fig. 2.9(b). However, the electrons which were injected too far from the axis will not experience a sufficiently strong attraction to the axis, and scatter away from the wakefield as depicted in Fig. 2.9(c). After the trapping process is completed, and the injected bunch has interacted over its entire length with the wakefield, the trapped electrons will accumulate in a very small space in the laser wakefield. Thus all of the trapped electrons experience approximately the same accelerating field, particularly, because the focusing force keeps them near the axis, see Fig. 2.9(d). As a result, the relative energy spread of the bunch decreases monotonously during the acceleration. In the shown example, the transverse size of the bunch after the acceleration shrinks to 1.7 μm in the x-direction and to 1.3 μm in the y-direction while the bunch length reduces to 1.8 μm, corresponding to a duration of 6 fs. The residual ellipticity in the transverse directions is due to an elliptical injected bunch. This case will be discussed in details in chapter 4.

In Fig. 2.10, we plot snapshots of the evolution of the electron energy during the described process, using the same conditions as used for calculating the data in Fig. 2.9. Again, the frames are set to be moving with the laser group velocity. Initially, the injected bunch has a kinetic energy of about 2.88 MeV, see Fig. 2.10(a). When the electrons interact with the accelerating field of the wakefield, a certain fraction of them (the ones being sufficiently close to axis) become trapped and gain some energy, which is depicted in Fig. 2.10(b). During this trapping and acceleration process the electron energy shows a relatively large energy spread, as can be seen in Fig. 2.10(c), as distribution which is widely extending in the direction of the vertical axis. This is due to the large size of the injected bunch which causes that a part of the electrons is already trapped and gains high energy, while another part still enters the accelerating phase and is still at a lower energy. However, after the trapping process has been completed, all the trapped electrons gain energy and are accelerated along the acceleration length. As can be seen in Fig. 2.10(d), although the initial bunch was seemingly too long and thus not useful for external injection, one can see that a highly relativistic average energy of about 744 MeV is predicted and a rather low relative energy of approximately 1%.

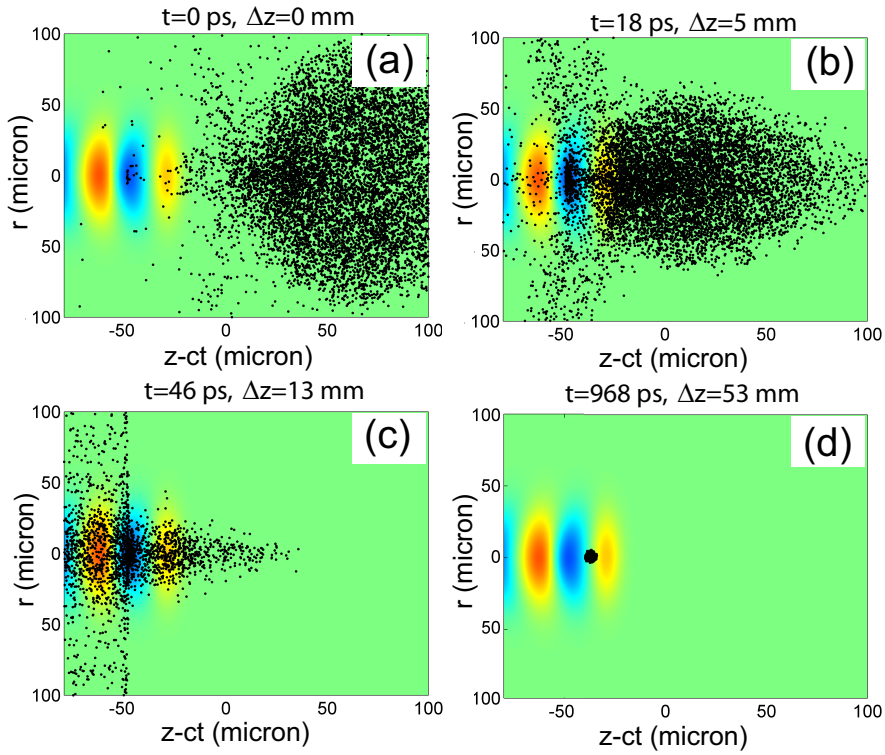

Figure 2.9: Snapshots of numerical modeling of a novel bunch injection scheme for laser wakefield acceleration. These calculations demonstrate the trapping, compression and acceleration of a relatively long bunch with low energy, as can be generated by a standard accelerator, after injection in front of the drive laser pulse. The shown coordinate frame is moving with speed of the laser group velocity towards the positive z-direction, such that the wakefield structure appears as standing still. The injected electrons which move slower than the frame appear to move to the left until, if trapping finishes, they slowly move forward riding the wakefield. The snapshots show the electron bunch at four times (t), at propagation distances in the plasma channel of Δz= 0 mm, 5 mm, 13 mm and 53 mm.

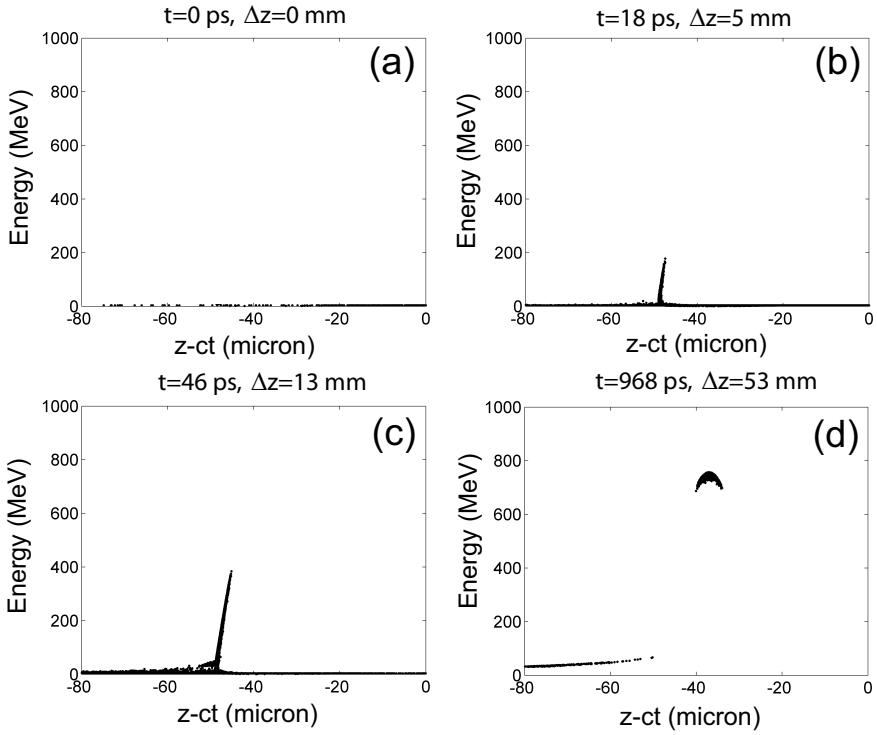

Figure 2.10: Calculation of the trajectories of electrons in phase space in a moving frame. The snapshots demonstrate the evolution of position and energy of electrons injected in the form of a relatively long and wide bunch of low energy during trapping, compression and acceleration process as presented in Fig. 2.9.

2.4 Conclusions

In this chapter we have shown the possibility of generating highly relativistic electron bunches with a few femtoseconds duration and a few microns beam size in a novel external injection scheme for laser wakefield acceleration. In this scheme the initial bunch is injected in front of the drive laser pulse. The great promise of this scheme is that, although high-quality, highly relativistic bunches are obtained, the scheme works even with rather long bunches (many plasma wavelengths, a few hundreds of microns), which can be provided by a conventional linear accelerator. This opens up the possibility that laser wakefield acceleration may be controlled via external injection and with existing technology, while the linearity of the scheme promises scalability and shot-to-shot stability.

3

Femtosecond bunch dynamics in vacuum and laser wakefield

Recent advances in laser wakefield acceleration have demonstrated the generation of extremely short relativistic electron bunches with low relative energy spread. We study the dynamics of such bunches during propagation in free-space (vacuum) and acceleration inside channel-guided laser wakefields. Our results show that strong bunch dynamics occur already within millimeter scale propagation distance, both in plasma and in vacuum. When the bunch propagates in vacuum, the transverse size and the normalized transverse emittance grows considerably, which deteriorates the focusability of the bunch. For propagation in a channel-guided laser wakefield, it is found that fast longitudinal betatron phase mixing occurs in the bunch as it propagates along the wakefield axis. When the bunch propagates off-axis, fast emittance degradation due to the finite bunch length was observed. [This chapter is based on the article A. G. Khachatryan, A. Irman, F. A. van Goor, K.-J. Boller, Phys. Rev. ST Accel. Beams, 10, 121301(2007)]

3.1 Introduction

A plasma wave excited by a high intensity laser pulse with an ultra-short duration can be used to accelerate electron bunches to relativistic energies. This acceleration scheme is named laser wakefield acceleration. Measurements and supporting numerical simulations show that these relativistic bunches have unique properties, which differ from those produced by standard accelerators, namely, a duration of a few femtoseconds, a transverse size of a few microns, a charge of tens of pC, and energy of tens to hundreds of MeVs, a relative energy spread of a few percent and

a normalized transverse emittance on the order of 1 μm [12–14, 16, 19, 71]. These parameters make such electron bunches a qualitatively new object and also new tool in physical research [27, 28].

For applications, such relativistic bunches, after leaving the accelerating plasma, are to be transported, e.g., to a target or to an experimental area. Since these bunches have the unique properties described earlier, it is important to investigate their propagation in free-space (vacuum). Based on such study, one may design a correspondingly suitable beam transportation system. In our case, this knowledge is necessary for transporting the accelerated bunch to an electron diagnostic system. In our experimental setup, the bunch is to be propagated in a vacuum beam line across a distance of about 50 cm before it enters an electron spectrometer. Details about our diagnostic system are described in chapter 5.

In the first approach, we present an analytical expression for the bunch radius as a function of propagation distance. Here, one can see a straightforward relationship between bunch radius at a certain position and the initial bunch parameters, namely: energy, normalized emittance, and bunch radius. In the second approach, we employ numerical calculations provided by the General Particle Tracer (GPT) code [72], which is capable of tracking the trajectory of each electron in the bunch while also including the Coulomb force between electrons. This modeling aims to simulate the bunch dynamics to more detail as expected from experiments. Furthermore, we extend our study to a possible scheme which may boost the energy of laser wakefield accelerated bunches to reach even higher-energies, so-called multi-stage laser wakefield acceleration. In this scenario, a number of laser wakefield accelerators are positioned behind each other, so that the output from first wakefield accelerator is injected into the second-stage and so forth, just as in conventional accelerators. Particularly, as a prototype example of such staging, we study the bunch dynamics of a femtosecond bunch during acceleration from the first into the second-stage of a laser wakefield accelerator. With the described propagation studies, this chapter aims to give a qualitative outlook on the type of physics that one will encounter with bunches from laser wakefield acceleration, while more details and mathematical derivations can be found in the reference [73] on which this chapter is based.

3.2 Bunch dynamics in vacuum

In this section, we study the dynamics of a femtosecond energetic electron bunch generated from a laser wakefield accelerator during propagation in free-space (vacuum). This is important when one considers staging of laser wakefield accelerator [74–77] with drift regions between the stages, or when the bunch is to be transported to a target.

As a bunch exits from the accelerating plasma, the strong focusing fields of the laser wakefield which keep the electrons close to the propagation axis, cease to act on the bunch. As a result, the bunch radius will grow due to the transverse momentum of electrons within the bunch. The growth of the bunch radius depends on its initial energy, the initial bunch radius and the normalized transverse emittance,

and can be estimated via

$$\sigma = \sigma_0 \left[1 + (z - z_*)^2 / Z_b^2\right]^{1/2}. \tag{3.1}$$

Here σ is the rms[1] bunch radius after propagation over a distance z. The parameter Z_b is the characteristic distance over which the bunch radius grows by a factor of $\sqrt{2}$ and is defined as $Z_b = \gamma\sigma_0^2/\epsilon^N$, where γ and ϵ^N are the relativistic factor of the bunch and the normalized transverse emittance. In light-optics, Z_b can be considered as the analogy of the Rayleigh length. The parameter z_* is the position with regard to the exit of plasma where the bunch radius possesses its minimum value, σ_0. This parameter z_* is introduced because during acceleration inside laser wakefield, the bunch radius is performing oscillations due to so-called betatron phase-mixing. Details about this betatron phase-mixing will be described in the next section. The value of z_* depends on the bunch parameters at the exit of plasma, namely, the bunch radius (σ_p) and its derivative with regard to the propagation axis (σ'_p), the normalized transverse emittance and the bunch energy, via $z_* = -\sigma'_p\sigma_p/h$ where h is defined as $h = (\sigma'_p)^2 + \epsilon^N/\gamma^2\sigma_p^2$. In figure 3.1 we schematically illustrate how the bunch radius evolves as it propagates in vacuum. If $z_* > 0$, a minimum bunch radius is reached at a distance z_* outside the plasma as shown in Fig. 3.1(a). This means that at the time when the bunch exits the plasma it is still converging before the minimum bunch radius is reached. In the other case, i.e., $z_* < 0$, the bunch radius outside the plasma grows monotonically as depicted in Fig. 3.1(b).

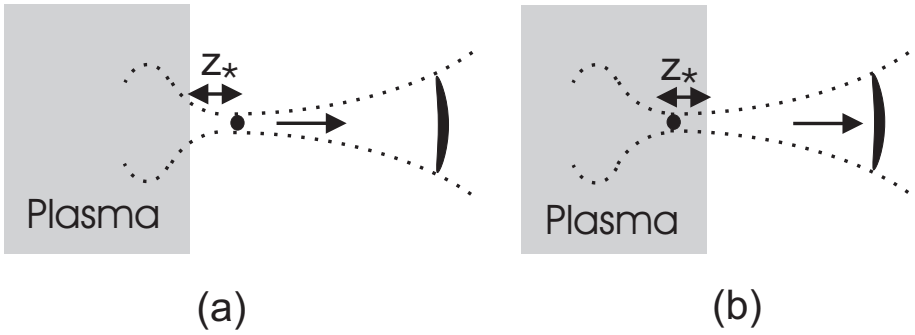

Figure 3.1: Illustration of electron bunch propagating out of the laser wakefield (in plasma) into vacuum. In part (a), the bunch still tends to focus when it leaves the plasma. The minimum bunch radius is reached at a distance z_* behind the plasma before the radius grows monotonically. In part (b), the position of the minimum bunch radius is located inside the plasma. In this case, the bunch radius directly enlarges once it is in vacuum.

By using equation (3.1), it is possible to quickly estimate the bunch radius at a

[1] The rms (root-mean-square) value is defined as $\sigma_{rms} = \sqrt{\frac{1}{N}\sum_{i=1}^{N}(r_i - \langle r\rangle)^2}$, where $\langle r\rangle = \frac{1}{N}\sum_{i=1}^{N} r_i$ and r_i is the position of a single electron.

certain propagation distance for a given set of initial bunch parameters. As an example, we calculate the bunch radius at a propagation distance of 50 cm from the exit of plasma, i.e., about the entrance of our electron spectrometer. As the initial bunch parameters, we consider to use, as an example, typical numbers obtained after laser wakefield acceleration, namely, a normalized transverse emittance of 0.95 μm, a relativistic factor of 400 (corresponding to 204.4 MeV), a minimum bunch size of 1.91 μm, and an energy spread of 2%. With this, we obtain Z_b as 1.54 mm and a size of the bunch of 620 μm after propagation over 50 cm. This indicates that the bunch radius grows very rapidly during free propagation in vacuum, to more than 300 times of its original size of about 2 μm in 50 cm distance. One might consider focusing in order to obtain small (micrometer-scale) bunches again. However, further calculations presented shortly, show that the normalized transverse emittance of the bunch also grows considerably as a function of propagation distance. This means that the focusability of the bunch also degrades considerably, because the minimum bunch radius depends on the normalized transverse emittance via $\sigma_0 = \epsilon^N/\gamma h^{1/2}$. These results suggest that, in order to preserve the unique properties of laser wakefield accelerated bunch, one should use the bunch as closely as possible to the exit of the accelerating plasma.

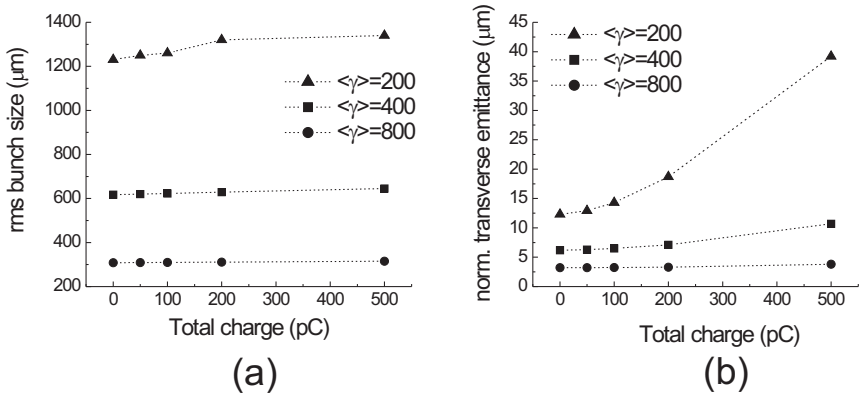

Figure 3.2: Calculated transverse bunch size, $\sigma_{x,y}$, in part (a) and normalized transverse emittance, $\epsilon^N_{x,y}$, in part (b) of the femtosecond electron bunch, after 50 cm propagation in vacuum, depending on the average energy, $\langle\gamma\rangle$, and the total charge of the bunch.

To improve our estimation of bunch parameters at a particular distance, we have simulated the bunch dynamics by using the particle tracking (GPT) code. Here the approach is numerical, but one can analyze more comprehensive bunch dynamics, meaning: the normalized transverse emittance, the bunch radius and also the bunch duration. Moreover, the 3D space-charge model was implemented into the GPT to calculate the Coulomb force effect on the bunch during propagation [78, 79]. In these calculations, we varied the total charge and the relativistic factor while

keeping the other parameters identical to those used in the previous case. In figure 3.2 we plot the rms bunch size and the normalized transverse emittance as a function of the total charge and the average relativistic factor for a propagation distance of 50 cm. For a relativistic factor of 400, we found an rms bunch radius of 617 μm for a zero charge (meaning that the space-charge effect was set deliberately to zero as a test). This result gives a good agreement with our analytical estimation described earlier. As the charge increases, the rms bunch radius also increases. This indicates that the space-charge can contribute noticeably to the growth of the bunch radius depending on the relativistic factor, as shown in Fig. 3.2(a). Another important result in these numerical calculations is that the normalized emittance tends to grow during propagation. The growth is found to be approximately a factor of 6.5 for a zero charge and of 11.2 for 500 pC. The increase of the normalized emittance can be attributed to the initial energy spread of the bunch. When the energy spread is not zero, faster particles travel a longer distance compared to slower particles. Furthermore, particles propagating under an angle with regard to the propagation axis end up with a larger transverse position and a smaller z compared to on-axis particles. This causes a redistribution of electrons in the bunch after some propagation distance and, thus, the normalized transverse emittance increases. This emittance growth does not violate Liouville's theorem (Appendix A) because the growth is seen only in the projected emittance, i.e., phase-plane (x, p_x) in this example, while the six-dimensional phase space volume, (x, p_x, y, p_y, z, p_z), remains conserved [80].

The effect of the space-charge can be identified by comparing the bunch parameters using different charges and relativistic factors. It can be seen from these results that the space-charge has a small effect on the bunch parameters for higher $\langle\gamma\rangle$ as expected. For lower $\langle\gamma\rangle$ the space charge considerably reduces the bunch quality, particularly for bunches with total charge larger than 100 pC. The bunch length after propagation does not depend much on the bunch charge; we found an rms bunch length of 3.2, 1.2 and 0.98 microns, compared with the initial value of 0.95 μm, for $\langle\gamma\rangle$ = 200, 400 and 800, respectively. This means that the bunch length can be preserved quite well despite increasing transverse bunch parameters during propagation in vacuum.

Our estimations, numerical calculations and examples have shown that the bunch propagation dynamics has to be taken into account when designing a suitable beam transportation line for a particular purpose. However, if the bunch energy is very high, similar to the value that we hope to achieve experimentally (an energy of $\approx$750 MeV which corresponds to the relativistic factor of $\approx$1468), then the bunch quality would remain high for a long propagation distance, even for a large charge.

3.3 Two-stage laser wakefield acceleration

In this section, we describe a possible scheme to increase the energy obtained with laser wakefield acceleration using, so-called, staging. Particularly, we study the bunch dynamics during acceleration in a second-stage laser wakefield accelerator. The scheme that we consider is drawn schematically in figure 3.3. As the first accelerator we consider a gas-jet illuminated by an intense ultra-short laser pulse

(laser 1) to generate an electron bunch of moderate kinetic energy. For such an accelerator, we consider a typical bunch generated in the bubble regime, assuming an average energy of about 200 MeV, a FWHM length of 2.25 μm (corresponding to a duration of 7.5 fs), a bunch radius of 2.87 μm, a relative energy spread of 2% and a normalized transverse emittance of 0.95 μm. The bunch from the first accelerator is injected into the channel-guided laser wakefield driven by a second laser pulse (laser 2). The distance between the accelerating stages is kept as short as possible to maintain the bunch quality while propagating in vacuum, i.e., in the order of a few millimeters, following the considerations outlined in the previous section. Due to the use of two separately focusable laser pulses, the scheme shows an important advantage. When the first laser is tightly focused, it will diverge quickly so that it has only a small effect on the wakefield in the channel. The bunch from the first accelerating stage is further accelerated in the channel-guided laser wakefield where the plasma wavelength is chosen to be considerably longer via chosing a plasma of a lower density compared to that in the gas-jet. Another advantage is that it is rather straightforward to realize in an experiment.

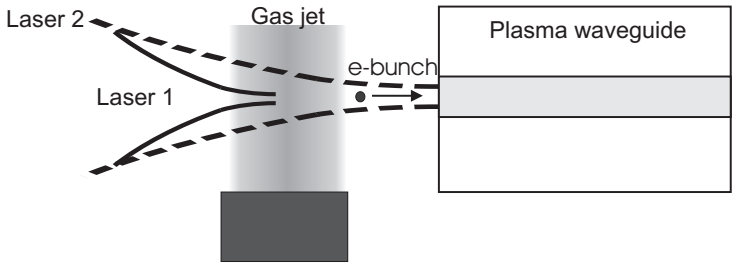

Figure 3.3: Scheme of a two-stage laser wakefield accelerator with a short distance between the stages

For this study we calculated the wakefield in the plasma channel with our fluid-Maxwell code as described in section 2.2.4. Typical results are depicted in figure 3.4. Further, to describe the motion of electrons in such a wakefield, we consider the equation of motion [22]:

$$\frac{d\boldsymbol{p_e}}{d\tau} = -\beta_g(\mathbf{E} + \boldsymbol{\beta_e} \times \mathbf{B}) - \frac{1}{4\beta_g\gamma}\nabla a^2, \tag{3.2}$$

where $\boldsymbol{p_e} = \boldsymbol{\beta_e}\gamma$ and $\boldsymbol{\beta_e} = \boldsymbol{v_e}/c$ are the normalized momentum and velocity of the electron, respectively. The normalized time, τ, is defined as $\tau = \omega_p t$. The vectors **E** and **B** are the electric and magnetic fields of the excited wakefield structure normalized to the non-relativistic wavebreaking field defined as $E_0 = m_e\omega_p v_g/e$. The parameters $\beta_g = v_g/c$ and $\gamma = (1 + \boldsymbol{p_e}^2 + a^2/2)^{1/2}$ are the normalized laser group velocity and the Lorentz factor of the electron, respectively. We divide this study in two cases, namely, when the bunch is injected on-axis into the second accelerator and the case for off-axis injection.

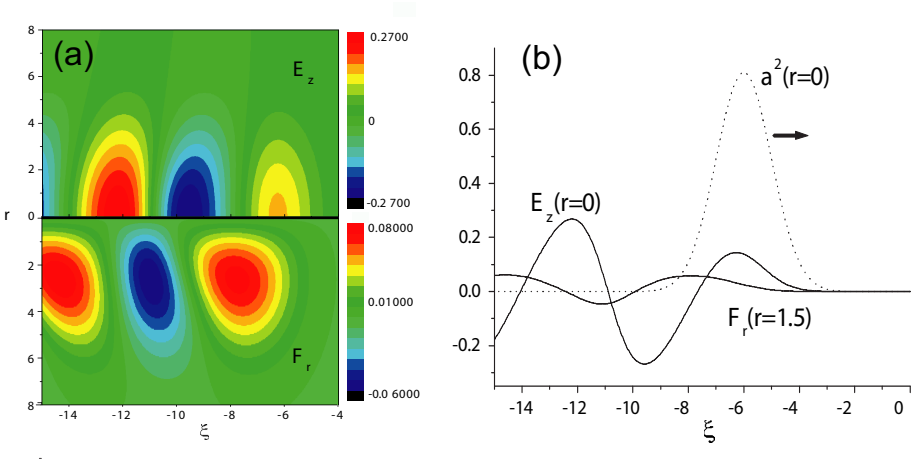

Figure 3.4: The calculated normalized longitudinal (E_z) and transverse (F_r) components of the channel-guided laser wakefield are plotted in part (a). The laser pulse (not shown) has a Gaussian transverse and longitudinal profile, is centered at $\xi = -6$ and travels to the right. In part (b), the accelerating and focusing fields of the laser wakefield presented in part (a) are plotted. For this study, we used the following laser parameters: $k_p\sigma_z = 2$, $k_p\sigma_r = 5$, $a_0 = 0.9$ and $\gamma_g = 70$. The on-axis plasma density was chosen as 3×10^{17} cm^{-3} which corresponds to a plasma wavelength of 60 μm.

3.3.1 On-axis bunch injection

In this case, the bunch is considered to enter the second accelerator stage precisely on-axis at a longitudinal position where the accelerating field has a maximum amplitude, i.e., at ξ_0=-9.5. Because the speed of the injected bunch (γ=400) is already higher than the phase velocity of the wakefield (γ_g=70), the bunch will be directly accelerated and slip forwards with regard to the wakefield. However, because the bunch has a finite length and radius, the individual electrons in the bunch experience slightly different accelerating and focusing fields depending on their position in the wakefield. Moreover, the initial transverse momentum of electrons tends to expand the bunch while the focusing field of the wakefield counteracts this motion. The resulting dynamics are referred to as betatron oscillations about the propagation axis. We have determined the betatron frequency as $\omega_B = \omega_p(f/\gamma)^{1/2}$ [81, 82], where ω_p is the plasma frequency and $f = \partial F_r/\partial r$ is the gradient of the focusing field in the radial direction. Further, the amplitude of the betatron oscillation is proportional to $(\gamma_0/\gamma)^{1/4}$, where γ_0 is the initial relativistic factor of the bunch. One can see that the betatron frequency and amplitude decrease as the bunch energy increase during acceleration. As a result, individual electrons in the bunch will per-

form different betatron motions due to their different initial position in the wakefield.

We have numerically simulated this situation and results are presented in figure 3.5. After some acceleration distance, about 5 cm in this case, we found that the bunch radius does not remain constant along the bunch while the bunch energy increases to about ≈880 MeV. Moreover, the calculated normalized transverse emittance grows to by 50% in this case indicating that the bunch quality degrades.

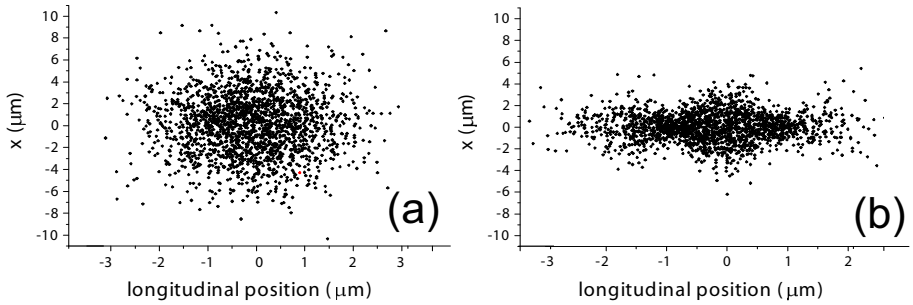

Figure 3.5: In part (a), the calculated longitudinal cross-section of the injected bunch is shown. The bunch is considered to enter the wakefield precisely on-axis. In part (b), the calculated longitudinal cross-section of the bunch after acceleration in a 5 cm plasma channel is presented. The bunch radius does not remain constant due to the betatron phase mixing.

To preserve the bunch quality in the second stage laser wakefield accelerator, one needs to avoid these betatron oscillations. This may be achieved by using a longer plasma wavelength, so that the electrons in the bunch experience the same accelerating field, and a large transverse size of the wakefield, which can reduce the focusing gradient of the wakefield.

3.3.2 Off-axis bunch injection

In the following, we will discuss the dynamics of the same type of electron bunch (such as considered in the previous case), which is injected off-axis in the laser wakefield at the maximum accelerating field as presented in figure 3.4. In this scenario, when the bunch is injected off-axis into the focusing region of the wakefield, the individual electrons in the bunch will oscillate about the axis with different betatron frequencies depending on their initial positions and momenta. As the bunch is initially located off-axis, the betatron oscillations in this case provide a stronger influence compared to the on-axis injection. This is because the focusing force of the wakefield is stronger compared to that on axis. We have simulated this situation and the results are presented in figure 3.6. It can be seen that, after the same acceleration distance (as in the on-axis case) the calculated longitudinal cross-section of

the bunch shows a "snake-like" distribution while the normalized transverse emittance grows by more than a factor of 10. This means that, in comparison with the bunch in Fig. 3.5(b), the bunch quality reduces considerably.

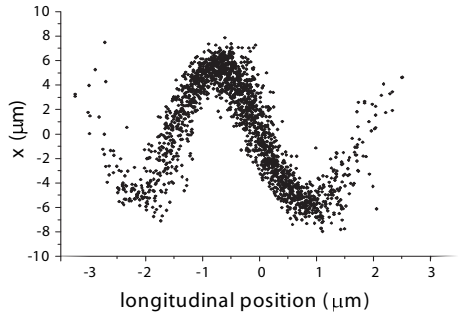

Figure 3.6: The calculated longitudinal cross-section of the bunch after acceleration in a 5 cm plasma channel for off-axis injection. The bunch shows a "snake-shape" distribution.

The shown results indicate that injection into a second stage laser wakefield accelerator requires a control of high precision with regard to correctly positioning the injected bunch, otherwise, the bunch quality would degrade despite increasing bunch energy.

3.4 Conclusions

We have studied the dynamics of electron bunches produced by laser wakefield acceleration when propagating through vacuum and during acceleration in a second stage laser wakefield accelerator. We have shown that strong bunch dynamics already occurs upon a millimeter scale propagation distance in both cases. When the bunch is propagating in vacuum, the bunch duration remains on the order of femtoseconds, while the bunch radius and normalized transverse emittance grow considerably. This indicates a degradation of the bunch focusability, which means that the bunch cannot be focused back to the same radius as it was at the exit of plasma. However, for higher energy bunches, at the GeV-level, the bunch quality can be preserved during propagation in vacuum and also over a considerable distance.

Furthermore, we have investigated a novel experimental design to boost the energy that can be obtained in laser wakefield acceleration, by so-called staging. Here, the bunch from a first laser wakefield accelerator is injected into a second laser wakefield accelerator (another stage may follow). We found that, due to the finite size of the bunch injected into the second stage, different parts of the bunch will perform different betatron oscillations during the second acceleration. This leads to a degradation of the bunch quality despite of increasing energy. For off-

axis injection, we found that the bunch quality reduces even faster. This indicates that very strict alignment procedures are needed for staging laser wakefield accelerators.

4

Front to end modeling and design of the experiment

In order to design an experiment for the first demonstration of laser wakefield acceleration with external electron bunch injection, we studied, as the first step, the transverse and the longitudinal dynamics of an electron bunch provided by a photocathode linear accelerator. Our model predicts that the bunch, with a kinetic energy of 2.88 MeV, a charge of 5 pC and an energy chirp imposed by the linac, can be considerably compressed by a factor of 8 to a duration of 250 fs with appropriately designed magnetic fields. In the second step of modeling, we follow the dynamics of the bunch as it is focused by a next set of magnetic fields to be designed that the bunch enters a plasma channel such that it approximately matches the spot size of the drive laser pulse (30 μm). The final step of calculations describes the trapping, compression and acceleration of the injected bunch in the wakefield of a TW laser pulse. After optimization of the parameters in all of the three named steps, this yields an experimental design which should be capable of generating highly relativistic bunches with $\approx$ 750 MeV energy, $\approx$ 1 % relative energy spread, and an extremely short duration (6 fs), after acceleration in a 5.4 cm long plasma channel. Note that, this output bunch energy is comparable with that produced from conventional accelerators housed in larger facilities. In the experimental design presented here, this seems to be possible just on a centimeter-scale.[This chapter is based on the article A. Irman, M.J.H. Luttikhof, A.G. Khachatryan, F.A. van Goor, J.W.J. Verschuur, H.M.J. Bastiaens, K.-J. Boller, J. Appl. Phys., 102, 024513(2007)]

4.1 Introduction

Controlled acceleration of electron bunches in a laser wakefield is still a great challenge and an important issue for many future applications, e.g., table-top VUV and X-ray free electron lasers [28], radiotherapy with high-energy electrons [83]. It is widely accepted that this goal is best to be achieved by separating the controlled production and injection of electron bunches from the acceleration process itself. In this approach, the bunches are generated initially by a photo-cathode linear accelerator where the bunch properties, e.g., energy, charge, emittance and beam sizes, can be reliably controlled. Afterwards these bunches are to be transported and injected into a plasma channel where they would be trapped and accelerated to higher energies by a laser wakefield.

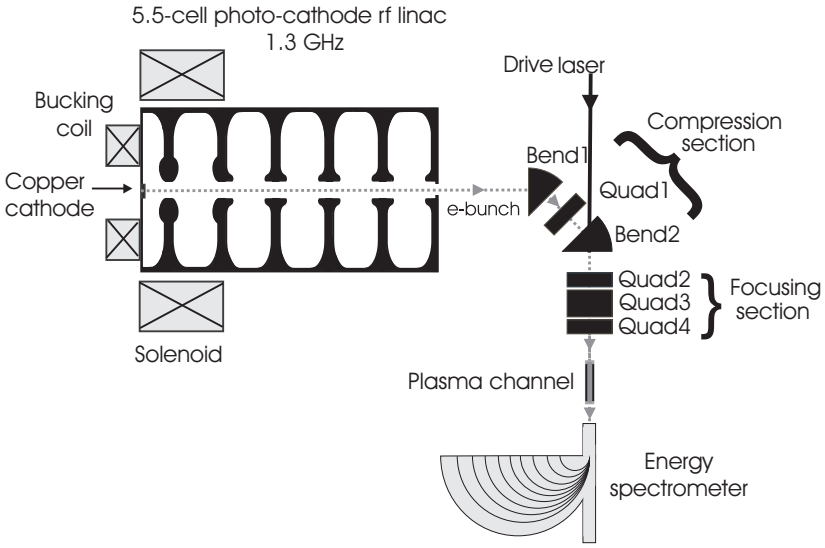

Figure 4.1: Schematic drawing of a photo-cathode rf linear accelerator, an electron beam transportation system, which includes compression- and focusing sections, and a plasma channel. In this channel, laser wakefield acceleration to be demonstrated as driven by a TW laser.

For a successful experimental demonstration of the described approach, it is crucially important that the complete system is carefully designed. This creates an extremely challenging problem in that, due to the very large number of parameters involved, the design process becomes very complicated. The degree of complexity is so big, and experimental changes of parameters are so slow and costly, so that insufficient understanding of the details dramatically increases the risk of failure. In order to reduce this risk to the merely experimental level of technological limits, we have performed a comprehensive modeling of the electron bunch dynamics starting from the photo-cathode, through the rf linac, along the electron beam trans-

portation system, which includes bunch compression and focusing sections, and during the laser wakefield acceleration along a plasma channel. With this modeling we have arrived at an experimental design which is schematically shown in Fig. 4.1. And with a careful analysis and optimization, we have chosen for the most promising setting of the operational parameters as will be described in chapter 5.

As discussed in chapter 2 (section 2.3.1) that, to demonstrate the generation of high-quality electron bunches from laser wakefield acceleration, the bunch trapping process should be completed on a distance (the trapping distance $L_{tr} \approx 2\gamma_0^2 l_0$) which is considerably shorter than the acceleration length (L_{acc}). For a conventional capillary discharge plasma channel [49, 50], the acceleration length is typically about 5 cm. Accordingly, to enable the use of existing plasma channel technology, we prepare the trapping distance to be considerably less than the acceleration length by choosing a low-energy and a short-duration of injected bunch as will be explained in the following.

The minimum total energy[1] of an electron which will be trapped in the plasma wake wave created with the laser parameters available to us (see chapter 5 for experimental details) is ≈1 MeV for on-axis electrons and increases to ≈2.5 MeV for electrons at the periphery of the drive laser pulse [23]. In order to trap the on-axis as well as the off-axis electrons, maximizing the fraction of electrons that are trapped after injection, we chose a total energy of ≈3.4 MeV for the injected bunches, this is well above the lowest stable operational mode of our linac [84]. This linac was originally designed to deliver electron bunches with a maximum total energy of 6 MeV, but a total energy of ≈3.4 MeV may be obtained by decreasing the rf field amplitude inside the linac while keeping the electron launching phase close to its optimum value. The latter is important because, in this case, the electron energy at the linac exit is less sensitive to a jitter between the phase of the rf field and the UV pulse on the cathode [84].

The details to be presented on our particle tracking simulations (section 4.2) on generation and acceleration of an electron bunch inside the linac predict a bunch duration of ~1.7 ps (defined as twice the root-mean-square (rms) value) at the linac exit for a total energy of 3.4 MeV and a charge of 5 pC. These bunch parameters would give a trapping distance $L_{tr} \approx 4.5$ cm inside the plasma channel, which is still too long to arrive at a small energy spread after laser wakefield acceleration, since $L_{tr} \sim L_{acc}$. Therefore, as described in the following, we adopt a magnetic bunch compression scheme for shortening the length of the injected bunch, so that the trapping distance becomes considerably less than the length of the plasma channel.

As will be described in detail below, we found in our simulations that the electron bunch shows a time-energy correlation (also named chirp) along the bunch length acquired during acceleration in the linac. In order to compress the bunch, we consider, design and realize a magnetic compression section which is installed downstream from the linac. The compression section is designed to provide a non-isochronous property to the bunch trajectory, this means that it introduces an energy-

[1] Total energy of an electron is defined as $E_o = m_e c^2 \gamma$, where m_e is the mass of electron, c is the speed of light and γ is the relativistic factor. Total energy relates to the kinetic energy via $E_k = E_o - m_e c^2$.

dependent path length on the electrons so that higher-energy electrons follow a longer path than lower-energy electrons. Thus a proper tuning of parameters of the compression section should give the required chirp compensation resulting in a compression of the bunch. In our actual design, the compression section consists of two subsequent 45^0 bending magnets with a quadrupole placed in the middle between the bending magnets as shown in Fig. 4.1. The function of the quadrupole is to compensate for the increase in the bunch size in the transverse direction, in the bending plane behind the first bending magnet.

The compression section is then followed by a quadrupole triplet which we designed to transversely focus the electron bunches to match the spot size of the drive laser in the channel, thereby increasing the number of electrons which would interact with the wakefield. The transverse focusing can induce an additional bunch lengthening at the focus due to the different path lengths of the electron trajectories, because off-axis electrons travel a longer distance compared to on-axis electrons. However, in our modeling we found that this effect can be minimized by a careful choice of the strength of the solenoid field in the linac such that both the transverse beam size and the normalized transverse emittance are at their minimum.

As a comparison, the design of our electron beam transportation system differs strongly from that proposed earlier, e.g., at the TU-Eindhoven [69] and for the ALPHA-X project at the University of Strathclyde [85], where a folding-mirror with a hole is used to couple the electron bunch into the drive laser beam line. In our design, besides the advantage of bunch compression, the bending magnets allow the electron bunch and the drive laser to propagate co-linearly avoiding the use of the coupling hole. The coupling hole may disturb the field pattern of the high intensity drive laser.

The remaining part of this chapter is organized as follows: In section 4.2, we analyze the transverse and the longitudinal dynamics of an electron bunch while it is undergoing acceleration inside the rf linac. The transverse dynamics includes the transverse beam size and the transverse normalized emittance. The longitudinal dynamics is determined by the average energy, the energy spread, the electron bunch duration and the time-energy correlation. Section 4.3 presents the working and details on the magnetic compression section for shortening the bunch. Magnetic focusing is presented in section 4.4. Finally, in section 4.5, the acceleration dynamics of the bunch inside the laser wakefield is described. Here we present the kinetic energy and bunch quality expected to be when injecting bunches from the linac as described.

4.2 Bunch dynamics in photo-cathode linear accelerator

Electron beams for our laser wakefield acceleration experiment are produced by a radio-frequency photo-cathode linear accelerator (rf linac), see Fig. 4.1. A fast-response photocathode made from copper is placed at the back-wall of this accel-

erator. When it is illuminated by an ultra violet or an infrared laser pulse, a bunch of free electrons is released via single or multi-photon ionization, respectively. These electrons are accelerated in the 5.5-cell linac that operates at an rf frequency of 1.3 GHz. The mode excited in the individual cavities (cells) is the TM_{010} mode which has its electric field vector pointing in the z direction (propagation axis) and its magnetic field vector parallel to the surface of the cavity. A static focusing field in the z-direction created by a solenoid around the cavity is applied to compensate for the transverse growth of the bunch diameter caused by the Coulomb force during acceleration. A bucking coil field is used to zero the focusing in the plane of the cathode surface where electrons are released. This prevents undesirable growth of the bunch emittance near the cathode, where energy of the electrons is quite low. Hence, the initial emittance of the electron bunch depends only on the difference between the photon energy and the cathode work function. This situation is known as the photo-cathode delivering electrons with a thermal emittance [86].

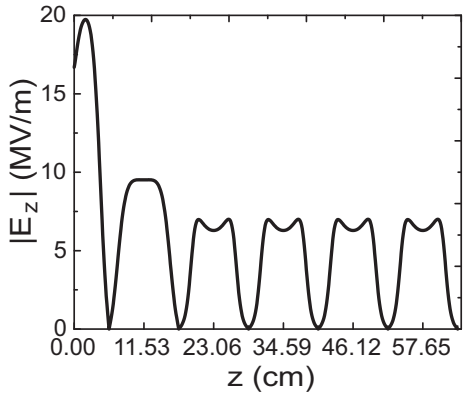

Figure 4.2: The calculated on-axis electric field in the linac. The rf wavelength is λ_{RF} = 23.08 cm. The maximum on-axis accelerating field in the first half cell is 19.94 MV/m, in the second cell is 9.52 MV/m and is 7 MV/m in the remaining 4 cells.

We performed numerical studies to investigate and optimize the electron bunch dynamics during acceleration in the linac. The electromagnetic field inside the linac was calculated by the SUPERFISH code [87]. An example of the calculated on-axis accelerating electric field is presented in Fig. 4.2 [84]. The field is an axially-symmetric, standing wave with the highest amplitude occurring in the first half cell. The spatial distribution of the focusing solenoid field and the bucking field were also calculated with the SUPERFISH code. The electron bunch dynamics was simulated by using the general particle tracer (GPT) code [72] in which the previously named and calculated fields, the rf field, the bucking coil and solenoid fields, have been imported. The 3D space-charge model was implemented into the GPT to calculate the Coulomb force effect on the bunch during its acceleration [78, 79]. Intro-

ducing the space-charge effect is important for the following reasons. The Coulomb force causes the bunch to expand in all directions depending on the charge density, i.e., the charge per unit volume. A higher charge density, such as that which occurs in a bunch of small size, results in a stronger Coulomb force which is encountered by an individual electron in the bunch. However, for moving particles, the Coulomb force decreases in a manner inversely proportional to the square of the relativistic factor [88]. Therefore, Coulomb repulsion is weak at relativistic velocities, but this force becomes very important when considering low energy bunches which is the case in design until the bunch enters wakefield.

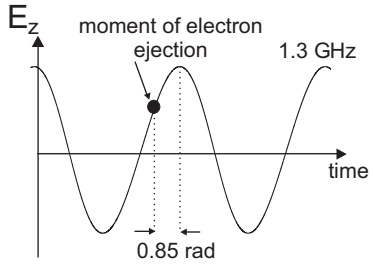

Figure 4.3: The rf phase at the cathode evolving in time. Electrons are ejected at the phase -0.85 rad with respect to the phase of the maximum rf field.

In the model, we consider that the photo-cathode is illuminated by a 40 fs (FWHM) long UV pulse focused to a radius of 0.6 mm and that the electrons are ejected from the cathode surface isotropically [89]. The initial transverse and longitudinal distributions of the emitted electrons are assumed to possess a Gaussian profile imposed by the laser pulse profile. For the demonstration experiment, the charge within a bunch is considered to be 5 pC, which is well below the beam loading limit for a laser wakefield calculated from the parameters based on the experimental specifications of our setup (section 4.5). Furthermore, the effect of image charges on the cathode surface is neglected since it has a minor effect on the bunch [90, 91]. The initial kinetic energy of the electrons after photoemission has been calculated via the following [92]

$$E_k(\varphi_0) = h\upsilon - \Phi_{copper} + b\sqrt{\beta E_z(\varphi_0)}, \tag{4.1}$$

where υ is the optical frequency of UV light of a wavelength of 267 nm (photon energy 4.65 eV), Φ_{copper} = 4.6 eV is the work function of copper and $b = \sqrt{e/4\pi\epsilon_0}$, in which e is the electron charge and ϵ_0 is the vacuum permittivity. The parameter β is an empirical field enhancement factor that depends on the cathode surface properties. For example, a perfectly flat, clean surface has a value β equal to 1, while a rough surface has a higher value for β [93]. $E_z(\varphi_0)$ is the accelerating field on the cathode at the launching phase φ_0 (phase of the rf field at the cathode when electrons are ejected, see Fig. 4.3) relative to acceleration on crest.

The maximum bunch energy is obtained at a launching phase $\varphi_0 = -0.85$ rad as

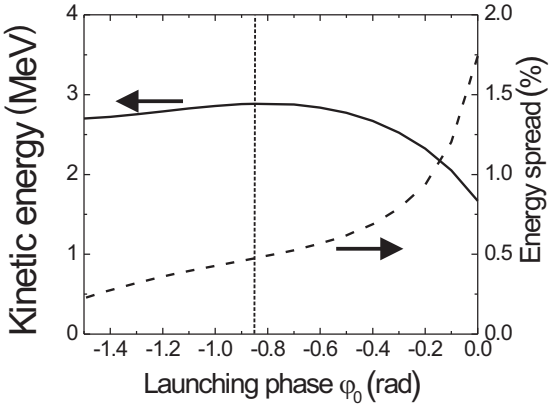

Figure 4.4: Calculated average kinetic energy of an electron bunch as a function of the launching phase at the exit of the linac (the solid line) plotted for the rf field amplitude presented in Fig. 4.2. The maximum kinetic energy is found at the optimum launching phase of 0.85 rad before the crest of the rf field as indicated with the vertical dotted line. The calculated relative energy spread of the bunch is shown as the dashed curve.

presented in Fig. 4.4. However, it is important for our experiments that the bunch energy here is also less sensitive to a jitter between the phase of the rf field and the timing of the UV pulse on the cathode. This will be explained in more detail in chapter 5.7. The negative sign for the launching phase indicates that the injection occurs before the crest of the rf field. Outside the range of -1.5 rad to 0 rad, electrons are out of phase with respect to the rf field. Thus, no accelerated electrons can then be expected at the linac's exit. The relative energy spread of the bunch, defined as $\delta E_{rms}/\langle E\rangle$, where δE_{rms} is the root-mean-square (rms) value and $\langle E\rangle$ is the average energy, as a function of launching phases was calculated and is plotted as the dashed line in Fig. 4.4. At the optimum launching phase ($\varphi_0 = -0.85$), the relative energy spread is found to be at the reasonably low value of 0.47 %.

4.2.1 Transverse bunch dynamics

The calculated transverse dynamics of the bunch during acceleration is shown in figure 4.5. These results were obtained by considering the bunch as injected from the photo-cathode at the optimum launching phase of $\varphi_0 = -0.85$. We further assumed a reduced rf field amplitude inside the linac to yield lower average kinetic energy of 2.88 MeV. Simultaneously we varied the strength of the focusing solenoid field B_{sol}.

From the calculations, we found that, if there is no focusing field, when the solenoid field is set to zero ($B_{sol} = 0$), the Coulomb forces result in a considerable growth of the bunch radius during acceleration. This is the dashed line in Fig.

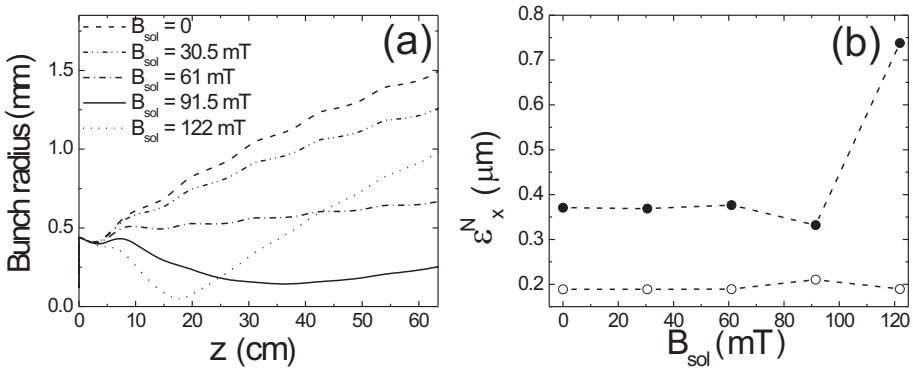

Figure 4.5: Calculated bunch dynamics during acceleration in the linac for the optimum launching phase $\varphi_0 = -0.85$ rad. As the focusing field increases, the position of the focus shifts toward the linac's cathode as shown in Fig. 4.5(a). Fig. 4.5(b) shows the effect of the focusing field on the transverse normalized emittance of the bunch at the exit of the linac. The filled and empty dots were calculated with and without the Coulomb force effect, respectively, for 5 pC charge.

4.5(a). In this case, the bunch radius at the linac exit is rather large, 1.5 mm. It can also be seen that, as the strength of B_{sol} is increased, the radius at the exit reduces and reaches a minimum of 0.25 mm for $B_{sol} = 91.5$ mT. By increasing the focusing field further, the bunch will be focused more tightly inside the linac. However, behind the focus, the radius grows very rapidly, as shown with the dotted line, and reaches large value at the exit of the linac.

To obtain a measure for the spatial quality of the accelerated bunches, we used the normalized transverse emittance, which is defined, for instance, in the transverse x-direction, as [94]:

$$\epsilon_x^N = \sqrt{\langle (x-\langle x\rangle)^2\rangle \langle (p_x-\langle p_x\rangle)^2\rangle - \langle (x-\langle x\rangle)(p_x-\langle p_x\rangle)\rangle^2}. \tag{4.2}$$

Here p_x is the x-component of the electron momentum, normalized to $m_e c$, where m_e is the rest mass of electron and c is the speed of light, x is the position of the electron and $\langle x\rangle$, $\langle p_x\rangle$ denotes taking the average position and momentum of all electrons in a bunch. The electron distribution in the (x, p_x) phase-space is actually a projection of the hyper-volume occupied by the electrons in the six-dimensional phase-space, i.e., (x, p_x, y, p_y, z, p_z), in which Liouville's theorem is applied, see Appendix B for details. The normalized emittance for the other coordinates y and z, ϵ_y^N and ϵ_z^N, repectively, can be found from equation (4.2) by replacing x and p_x by $y(z)$ and $p_y(p_z)$.

Next, we have calculated the influence of the focusing field from the solenoid on the transverse normalized emittance of the bunch at the exit of the linac. The results are diplayed in Fig. 4.5(b). Without the focusing field, the normalized emit-

tance at the exit is 0.37 μm. At the minimum bunch size at the exit, 0.25 mm, the normalized emittance is found to be also at a minimum, $\epsilon_x^N = 0.33$ μm. In this case, the focusing field balances the Coulomb expansion to obtain the smallest transverse bunch size as well as the normalized transverse emittance. This is important in order to minimize an additional bunch lengthening during focusing into the plasma channel, as will be explained in section 4.4. In the case of tight focusing inside the linac, i.e., for $B_{sol} = 122$ mT, the transverse emittance is found to be larger than with weaker focusing fields. In this situation, the Coulomb force contributes to an extra transverse momentum of the electrons, particularly, at the time when electrons are very close to each other (in the focus). In comparison, the normalized transverse emittances of the bunch calculated without the Coulomb force effect are plotted as the empty dots in Fig. 4.5(b). As expected, the normalized transverse emittances of the bunch are nearly constant, i.e., independent of the solenoid strength, and in general smaller than with the Coulomb force.

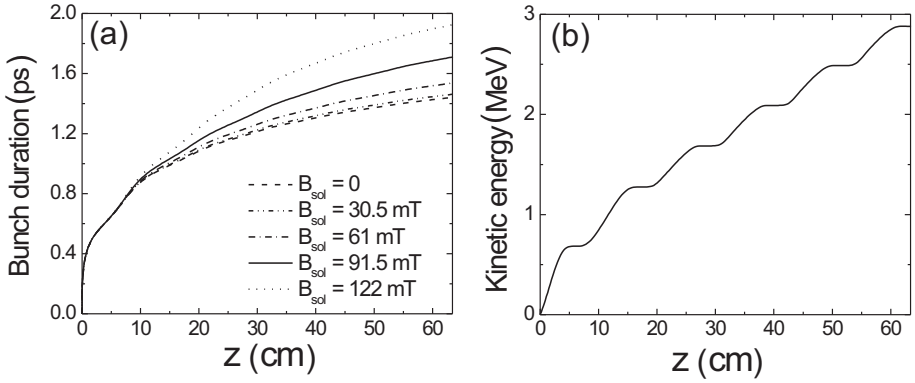

Figure 4.6: (a) Calculated duration of an electron bunch during acceleration inside the linac for different solenoid field strengths. The bunch is launched at the optimum phase $\varphi_0 = -0.85$ rad. The bunch becomes longer as the solenoid field increases. (b) The calculated kinetic energy of the bunch is found independent of the solenoid strength as all curves for different solenoid strengths coincide.

4.2.2 Longitudinal bunch dynamics

The longitudinal effects on the bunch duration has been investigated in calculations and the results are displayed in Fig 4.6 (a). It can be seen that the focusing field leads to an extra bunch lengthening, i.e., the bunch becomes longer for a larger setting of B_{sol}. For $B_{sol} = 91.5$ mT, the bunch duration at the exit of the linac is expected to become 1.7 ps or 508 μm, i.e., showing 0.3 ps extra lengthening compared to the case when there is no focusing field ($B_{sol} = 0$). The bunch lengthening is caused by the fact that the off-axis electrons travel a longer distance compared to

the on-axis electrons during focusing. In contrast, the energy of the bunch is found to be independent of the focusing field as shown in Fig. 4.6(b). But here, the bunch energy shows a strong dependence on the launching phase as was described earlier in Fig.4.4.

In order to investigate the possibility of a bunch compression in the bending section, the energy chirp in the bunch was studied. The origin of such chirp is as follows. In the early stage, the electrons emitted from the cathode are accelerated instantaneously by the rf field starting from almost zero energy and a very small volume in space. This results in a strong Coulomb expansion in the longitudinal as well as in the transverse directions. In particular, the bunch becomes relatively long, so that electrons, depending on their position, feel a different accelerating field. In the case we consider, the front electrons experience a higher accelerating field compared to the trailing electrons, thus yielding a chirp.

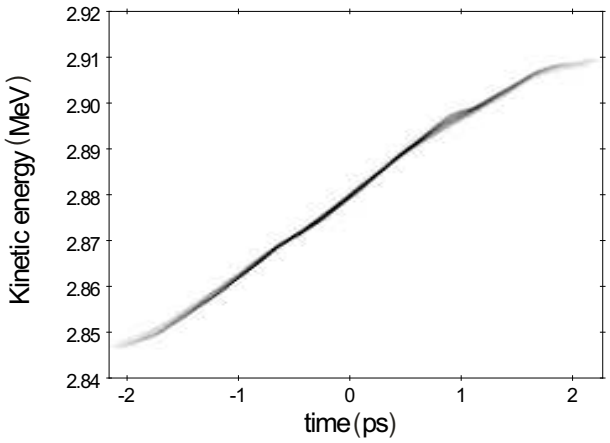

Figure 4.7: Calculated longitudinal phase-space density of the bunch at the exit of the linac for the launching phase $\varphi_0 = -0.85$ rad. The average kinetic energy and relative energy spread are 2.88 MeV and 0.47 %, respectively. The setting used for the solenoid field is $B_{sol} = 91.5$ mT. The time $t = 0$ corresponds to the centre of the bunch.

In order to give an impression of the shape and size of the chirp in the linac, we performed calculations for a typically chosen setting. Figure 4.7 shows the calculated longitudinal phase-space density of the bunch at the exit of the linac for the optimum launching phase $\varphi_0 = -0.85$ rad. It can be seen that, for this bunch, the chirp is positive, which means that the front-part electrons have a higher energy than the end-part. But polynomials fitted to the shown data show that the chirp is not simply a linear function but also contains a slight quadratic component, $\delta(z) = \kappa z + \mu z^2 + O(z^3) + \overline{E_k}$ [95]. Here $\delta(z)$ is the kinetic energy as a function of electron position z, $\overline{E_k}$ is the average kinetic energy, κ and μ are coefficients for the first and the second order chirp, and $O(z^3)$ stands for smaller terms of higher

order.

From the fit, we obtained $\kappa = 58.63$ MeV m^{-1} and $\mu = -552.70$ MeV m^{-2} and an average kinetic energy $\overline{E_k}$ of 2.88 MeV. After this characterization of bunch acceleration in the linac, the next step is to analyze the propagation of these bunches through the following bending sections in order to find appropriate parameter settings for the temporal compression of the bunches by compensating the chirp.

4.3 Magnetic bunch compression section

As explained in the previous section, without a temporal compression, the length of the bunches produced by the linac would be too long to be trapped in the wakefield within a length much shorter than the 5 cm length of the plasma channel. To shorten the bunches, we designed the following magnetic compression section. The compression provides a 90^0 turn in total [96, 97]. This consists of two subsequent 45^0 bending magnets with a compensating quadrupole placed in the middle as shown in figure 4.1. The choice of this approach is motivated by it's simplicity and that it also provides a negative first-order momentum compaction factor R_{56} [95], which is suitable for compensating the typical chirp produced by our linac as was presented in Fig. 4.7. The nonlinearity of the chirp results in an extra bunch lengthening by a factor $T_{566}\delta(z)^2$, where T_{566} is the second-order momentum compaction factor. It is well known that a proper ratio R_{56}/T_{566} is needed to optimize the bunch compression [95, 98].

The spatial distribution of the magnetostatic field of the bending magnets in our compressor system was calculated using the 3D COMSOL multiphysics modeling [99], discussed in detail in chapter 5. Such modeling is important because it should provide a realistic field which also involves the fringe fields, i.e., extension of the magnetic fields outside the magnet's gap. This field is, then, imported to the GPT code to calculate the bunch dynamics along the compression section.

In our simulations, the strategy to optimize the bunch compressor is as follows. First, we represented the compression section as a first-order 6×6 transfer matrix as described in appendix B. Then, we considered a single electron which initially has a longitudinal position z_i and a transverse position x_i. The electron's longitudinal position behind the compressor, z_f, depends on its initial transverse position, x_i, its initial transverse divergence, x_i' ($x_i = (dx/dz)_i$), and its energy chirp, $\delta(z)$, via $z_f = R_{51}x_i + R_{52}x_i' + z_i + R_{56}\delta(z)$ where R_{51}, R_{52} and R_{56} are the compression parameters which relate to the radius and angle of the bending section, the field strengths of the bending magnets and the quadrupole, and the distance between the bending magnets. In order to obtain the shortest bunch, we minimized the transverse effects by setting $R_{51} = R_{52} = 0$ (achromatic system [100]). Furthermore, R_{56} needs to match with $-z_i/\delta(z)$, which, in the case of linear chirp, gives $R_{56} = -1/\kappa$ (where κ is given in the definition of the chirp function $\delta(z)$ in section 4.2). The parameters found from this linear approach for a single electron were, then, used as starting values for the numerical optimization of an electron bunch with the GPT code. This optimization aimed to correct the compressor parameters such that also a compensation of the higher-order chirp terms is achieved. Another

important criterium for this optimization is that the transverse bunch dimensions behind the compressor need to be as small as possible to avoid additional bunch lengthening due to the path length difference in the following focusing section.

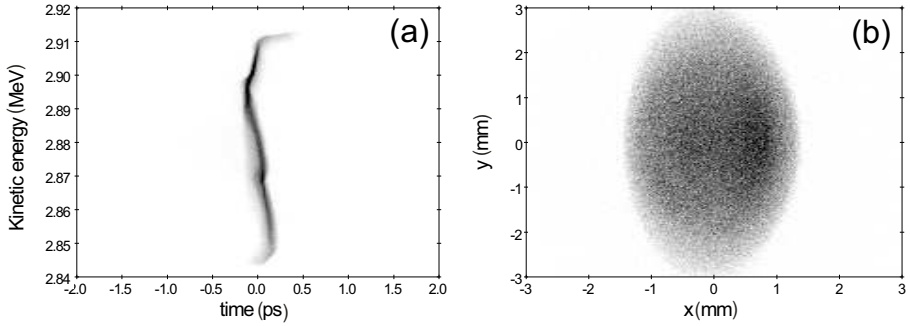

Figure 4.8: calculated properties of the electron bunch behind the compression section for a setting of $\varphi_0 = -0.85$ rad and $B_{sol} = 91.5$ mT. The longitudinal phase-space density is shown in part (a) and the beam cross section in part(b).

Fig. 4.8(a) shows the calculated longitudinal phase-space distribution of the bunch after the optimized compression section. In comparison with the longitudinal phase-space distribution before compression (Fig. 4.7), one sees that the distribution is rotated counter-clock wise and aligns approximately parallel with the energy axis. In the time domain, the bunch is compressed from ≈ 2 ps before the compression section down to ≈ 250 fs, yielding a considerable compression by a factor of 8. The transverse bunch cross-section can be seen in Fig. 4.8(b). The rms bunch sizes in the x- and y-directions behind the compressor are 0.7 mm and 1.3 mm, respectively. The remaining ellipticity is due to the fringe field, which leads to the bunch expansion in the non-bending plane direction, i.e., in the y-direction.

4.4 Magnetic bunch focusing section

The transverse size of the bunch behind the compressor section is still much larger than the laser spot size (≈ 30 μm), which means that only a small part of the bunch would interact and possibly be trapped in the laser wakefield without any further means. In order to avoid this, we designed a set of magnetic lenses to focus the compressed bunch and match it to the spot size of the drive laser. The magnetic lenses were chosen as a quadrupole triplet (a set of three quadrupole magnets, Quad2-4 in Fig. 4.1). The reason a quadrupole triplet was chosen is that this can also reduce the ellipticity of the bunch and thereby provide an approximately round spot size in the focus. The triplet can be considered as the equivalent of an achromatic lens for light-optic.

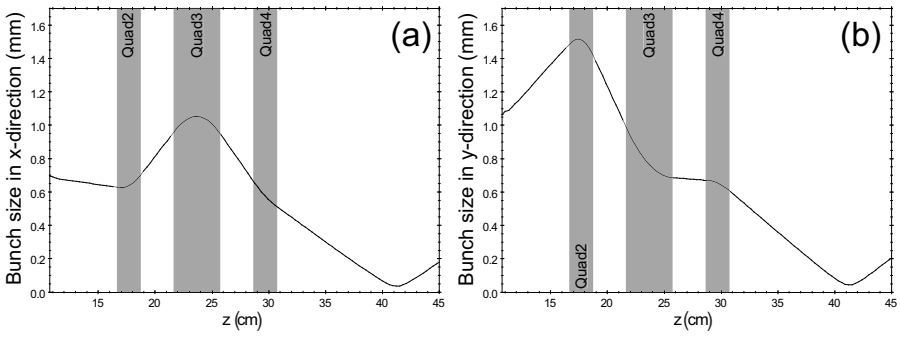

Figure 4.9: Calculated evolution of bunch size in the x-direction (a) and in the y-direction (b) during focusing in the magnetic focusing section. The position of the focus, i.e., where the channel entrance is located, is at $z = 41.2$ cm.

A single quadrupole provides a magnetic field which can focus a bunch in one direction, e.g., the x-direction, but it simultaneously defocuses the bunch in the other direction, e.g., the y-direction, described in chapter 5. In order to have an approximately round and sufficiently small focus for our compressed bunch, we optimized the magnetic field strengths, the physical sizes and distances of each individual quadrupole magnet within the triplet by using the GPT code. Figure 4.9 shows the typical evolution of the bunch sizes along the focusing section in the x- and y- directions. When the compressed bunch is propagating through the quadrupole 2 (Quad2), the bunch size in the y-direction decreases (Fig. 4.9(b)) and at the same time the bunch size grows in the other direction (Fig. 4.9(a)). As the bunch travels inside the quadrupole 3 (Quad3), the focusing and defocusing directions are exchanged, namely, the bunch is now focused in the x-direction while in the y-direction it is defocusing. As a result, the bunch size in the x-direction reduces while in the y-direction the bunch size is constant. This is due to the defocusing force from Quad3 compensating for the focusing induced previously by Quad2 in the y-direction. In the last quadrupole (Quad4), the bunch is focused back in the y-direction, i.e., the same direction as with Quad2. This focusing leads to a small bunch size in both the x- and y-directions at the focus of the quadrupole triplet. The position of the focus is placed at a distance of 10 cm with regard to the last quadrupole, approximately where the entrance to the plasma channel is located. The bunch cross-section, calculated in the focus, is shown in Fig. 4.10(a). It can be seen that the bunch size in the x and y directions are 35 μm (rms) and 40 μm (rms), respectively. In spite of this rather tight focusing, we found that the bunch duration is not increased noticeably, i.e., it remains approximately as short as $\approx$ 250 fs as shown in Fig. 4.10(b). This means that the bunch lengthening due to the path length differences between on-axis and off-axis electrons during the focusing

is negligible.

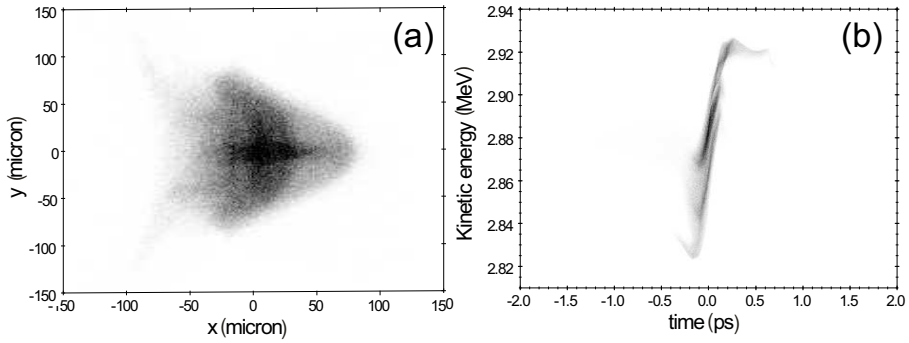

Figure 4.10: (a) Calculated cross-section of the bunch in the focus. (b) Calculated longitudinal phase-space distribution of the bunch in the focus. These results are obtained with the same linac parameters as in figure 4.8.

Looking back to figure 4.9, it can be seen that the bunch will diverge behind the focus. We found in our calculations that the bunch size increases by a factor of 1.7 both in the x- and y- directions after a propagation of 1 cm from the focus. This bunch divergence should be taken into consideration when maximizing the number of electrons that could be trapped in the wakefield. This will be discussed in the next section. The described compression and focusing are promising values but they are still achieved at the cost of the beam quality. Particularly, the relative energy spread slightly grows from 0.47 % at the exit of the linac to 0.56 % at the entrance of the plasma channel while the normalized emittance increases considerably, from 0.3 μm to 0.9 μm in the x-direction and from 0.3 μm to 1.6 μm in the y-direction. Fortunately, these bunch parameters can be well accepted in our scheme with injection in front of the laser pulse as will be described in section 4.5.

4.5 Laser wakefield acceleration

To investigate also the final step of laser wakefield acceleration, the bunch parameters obtained from the GPT code described above were imported into our three dimensional numerical code to calculate the trapping, compression and acceleration in the laser wakefield. We used the parameters for the drive laser and the plasma channel as outlined in the experimental specifications of our setup as discussed in chapter 5. These are a laser pulse duration of 35 fs (FWHM), a peak intensity of 2×10^{18} W/cm^2 ($a_0\approx0.97$), a wavelength of 0.8 μm and a spot radius of 30 μm at the entrance of the plasma channel. The channel is designed to an on-axis density of 8.6×10^{17} cm^{-3}, which corresponds to a plasma wavelength of 36 μm.

Fig. 4.11 shows the energy and relative energy spread calculated for the injected linac-electrons along the acceleration length in the plasma channel. It can be seen

that the energy of the electron bunch grows very rapidly (solid line) and reaches its maximum of 744 MeV after a propagation distance of 5.4 cm inside the channel. The relative energy spread in the bunch, indicated as the dashed line, increases at the beginning of the process but then decreases rapidly to a low value of 1.1 % at the end of the channel. The increase of the relative energy spread during the trapping process is due to the contribution of electrons which are already trapped and gain energy while there are still electrons at the trailling edge of the bunch which just enter the trapping region and still are at a low energy.

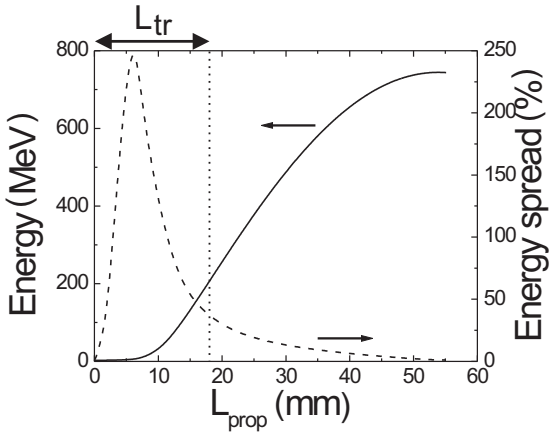

Figure 4.11: The average energy and the relative energy spread of the trapped electrons during trapping and acceleration inside the laser wakefield. A maximum energy of 744 MeV and a lowest energy spread of 1.1 % are reached at propagation distance L_{prop} of 5.4 cm in the channel.

The longitudinal and transverse compression of the bunch during trapping and acceleration is shown in Fig.4.12. It can be seen that, after the trapping process is completed at a propagation distance of about 1.8 cm (L_{tr}), the bunch attains extremely small sizes of 1.7 μm (rms) in the x-direction and 1.3 μm (rms) in the y-direction. Moreover, the accelerated bunch is very short, in particular, the FWHM duration of the bunch is only 6 fs, corresponding to a longitudinal size as short as 1.8 μm. Snapshots of these trapping, compression and acceleration processes are presented in Fig. 2.9 and Fig. 2.10 in section 2.3.1, chapter 2.

We found in our simulations that, to maximize the number of trapped electrons, the bunch should be focused inside the plasma channel, i.e., at a distance of about 4 mm from the entrance, instead of focusing at the entrance of the channel. This way, the injected bunch reaches its minimum size within the trapping distance. The trapped and accelerated bunch calculated for this focusing possesses a total charge of 2.4 pC (compared to 5 pC injected), which means that a significant fraction of ≈ 48 % of the injected electrons are trapped. The calculated normalized transverse emittances at the exit of plasma are ϵ_x^N=3.8 μm and ϵ_y^N=2.5 μm, respectively. As an

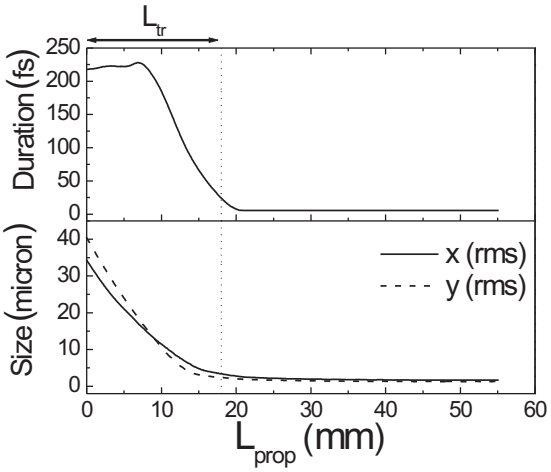

Figure 4.12: The compression of the bunch in the wakefield. After about the trapping distance $L_{tr} \approx 1.8$ cm, the bunch size shrinks considerably in 3D space. At the exit of the channel (5.4 cm length), the bunch sizes are 1.7 μm and 1.3 μm in the x and y directions, respectively and the bunch duration is 6 fs.

overview, the input and output parameters for our LWFA experiment are summarized in Tab. 4.1. As one can see from the table, the bunch accelerated by the laser wakefield is ≈330-times shorter, and has a transverse size being ≈250 and ≈190-times smaller than the bunch before the compressor. This means that the volume occupied by the bunch shrinks enormously, by a factor of $\approx 1.6 \times 10^7$. Hence, the electron concentration in the bunch increases with the same factor of $\approx 7.7 \times 10^6$, because only ≈48 % of the injected electrons are trapped. The named small sizes, the high concentration (charge density), in combination with high energy, make laser wakefield accelerated bunches unique because such bunches cannot be generated by conventional accelerator technology.

The injected bunch propagates some distance inside the plasma before the trapping process is completed. In our case, this distance is about 1.8 cm. During this propagation, the bunch interacts with the plasma which may lead to complicated bunch dynamics. The bunch can excite its own wakefield which is called a plasma wakefield [43]. The plasma wakefield can influence the bunch properties and also alter the laser wakefield. To estimate the strength of such effects we consider an electron bunch longer than plasma wavelengths, provided according to our calculations by the linac ($k_p \sigma_b = 2\pi\sigma_b/\lambda_p >> 1$ where σ_b is the injected bunch length and λ_p is the plasma wavelength). The maximum plasma wakefield amplitude generated by the bunch itself $E_{z,b0}$ can then be approximated by the expression [24]

$$E_{z,b0}[MV/cm] \approx 9.2 \times 10^{14} \frac{N_e}{n_p[cm^{-3}](\sigma_b[\mu m] r_b[\mu m])^2}. \tag{4.3}$$

Bunch parameters	Before the compressor	The injected bunch	At the exit of plasma channel
Energy	2.88 MeV	2.88 MeV	744 MeV
Energy spread	0.47%	0.56%	1.1%
Norm. emittance			
ϵ_x^N	0.3 μm	0.9 μm	3.8 μm
ϵ_y^N	0.3 μm	1.6 μm	2.5 μm
Bunch length	2 ps	250 fs	6 fs
Transverse size:			
x (rms)	0.33 mm	35 μm	1.7 μm
y (rms)	0.33 mm	40 μm	1.3 μm

Table 4.1: Bunch parameters for the proof-of principle LWFA experiment with external injection in front of the laser pulse. The injected bunch charge is 5 pC. The on-axis plasma density is 8.6×10^{17} cm^{-3}, the channel length is 5.4 cm, the laser spot size is 30 μm, the peak intensity is 2×10^{18} W/cm^2.

In this equation, N_e is the total number of electrons in the bunch and r_b is the bunch radius. From the named approximation, we find that the plasma wakefield generated by the injected bunch is in the order of a few tens of kV/cm. Compared to the energy of the injected bunch of 2.88 MeV and the amplitude of the laser wakefield of a few hundreds of GV/m, the energy gained or lost by the electrons in the plasma wakefield during the trapping process can thus be safely neglected. For the envisioned parameters of our experimental setup, note that for a higher bunch concentration and a longer propagation distance the bunch dynamics may be strong, and the theoretical description of the acceleration would have to be extended with the named addition effects.

Furthermore, the trapped bunch can also generate its own wakefield during the laser wakefield acceleration inside the plasma channel. If the amplitude of this plasma wakefield is comparable to the laser wakefield amplitude, the plasma wakefield modifies the laser wakefield, particularly, in the trailing part of the bunch (because no plasma wakefield is generated in front of the bunch). This situation is known as beam loading [101–103]. As a result, the laser wakefield acceleration would be disturbed. To investigate whether beam loading would play a role in our design of the experiment, we determined the maximum allowable total number of electrons in the trapped bunch as described in reference [23]

$$N_{tot,load} \approx 1.4 \times 10^7 \frac{(R)^2}{T} E_{z,max} \lambda_p[\mu m]. \tag{4.4}$$

Here, $R = k_p r_b$, $E_{z,max}$ is the maximum laser wakefield amplitude normalized to the non-relativistic wave-breaking field, $T = 1 - RK_1(R)$ in which $K_1(R)$ is the modified Bessel function. In this case, the length of the trapped bunch is assumed to be small ($k_p \sigma_b << 1$). For the parameters of the trapped bunch which are described above in Tab. 4.1, the total charge for the beam loading limit is found to be about 24 pC. The total charge which is being used for our demonstration experiment is 5 pC. This is well below the beam loading limit and thus justifies neglecting beam

loading in our experimental design.

4.6 Conclusions

In conclusion, we have arrived at a realistic set of parameters that should allow the first experiment demonstrating laser wakefield acceleration with external injection. In this experiment, an electron bunch generated by an rf photocathode linac is injected into a plasma channel in front of the drive laser pulse.

To maximize the chance for success in this unique approach, we have performed comprehensive numerical simulations and optimization to come to an integral design. For this, the generation, pre-acceleration in an rf linac, propagation through a bunch compression section, a focusing section, injection in the plasma channel have been numerically modeled. These calculations show that the electron bunch acquires an energy chirp during propagation through the linac and exits the linac with an average energy of 2.88 MeV, a duration of 1.7 ps, and a transverse size of 250 μm. The transverse size of the bunch and its duration increases to 330 μm and 2 ps respectively during propagation between the exit of the linac and the entrance of the compression section. The bunch is then compressed by the compression section (a non-isochronous section) which compensates for the energy chirp in the bunch. This yields a bunch duration of 250 fs after the compression section. Then, the temporally compressed bunch is spatially focused with a quadrupole triplet to a rms transverse size of 35 μm and 40 μm in the two transverse directions. Thereby, the spatial volume occupied by the bunch reduces by more than a factor of 600. This makes it possible to use the bunch for injection into a laser wakefield to achieve acceleration towards hundreds of MeV energy. The simulations predict that bunches with an energy of about 0.75 GeV and with about 1% relative energy spread can possibly be obtained from our planned experiment. Our detailed simulations clearly indicate the experimental possibility for controlled injection and acceleration of an electron bunch generated by a conventional rf linac in a laser wakefield.

5

Experimental setup and characterization experiments

In this chapter, we describe the experimental setup that we designed and constructed to carry out the first demonstration of laser wakefield acceleration with external bunch injection. This includes a terawatt laser system, a photo-cathode rf linear accelerator, an electron bunch transportation line and a capillary discharge plasma channel. The terawatt laser was designed to be based on the chirped pulse amplification (CPA) technique using Ti:sapphire (Ti:Sa) crystals as the active medium. In this technique, a low-energy laser pulse is generated in a Kerr-lens mode-locked oscillator and is temporally stretched by a grating stretcher before its energy is boosted in a chain of energy amplifiers. The laser output, temporally compressed and spatially focused, is directed into the plasma channel to excite a laser wakefield. The linac, which provides the electron bunches to be injected into the wakefield, is described here as well, followed by a description of the bunch transportation system which contains magnetic bunch compression and focusing sections. The optimum design parameters for these sections were found from our modeling explained earlier in chapter 4. The plasma channel, which is designed to obtain waveguiding of the drive laser pulse through the plasma, is based on a pulsed discharge in a hydrogen-filled capillary made of alumina. The output end of the plasma channel, where the accelerated bunches would exit, is directed towards an electron spectrometer with which the energy spectra of the accelerated bunch can be measured. We also describe here how all of these elements have been tested individually and in a mutually synchronized fashion. These tests show that we successfully realized a unique setup which should be suitable for the demonstration of controlled laser wakefield acceleration within the year 2009.

5.1 Introduction

The strong electric fields that occur in plasma waves driven by high-intensity laser pulses are of great interest for electron acceleration. A central property of the laser wakefield accelerator is that the wavelength of the accelerating field is typically of the order of tens of microns, which is about four orders of magnitude shorter than the wavelengths used in conventional rf accelerators. This enormous reduction in scale length has several important consequences. Firstly, there is a dramatic reduction in the size and costs of these plasma accelerators compared to those of microwave driven linear accelerators. Secondly, experiments and simulations have shown that the high-energy bunches generated using this approach possess strongly reduced dimensions in space and time, such as femtosecond bunch durations, and could therefore be used as a new tool in physical research. However, it is the third consequence that provides the most demanding challenge, namely that to produce high-quality accelerated bunches (bunches with low energy spread) the duration of the electron bunch to be injected must be brought to a microscopic scale as tiny as a small fraction of the plasma wavelength. This challenge can also be translated into a femtosecond scale precision with which the bunches are to be injected. In other words, it appears that the strongly reduced dimension in a laser wakefield accelerator requires femtosecond bunches and femtosecond time-precision of injection. Such short bunches cannot be generated by existing linear accelerators. This issue is the so-called injection problem and has remained the central problem in laser wakefield acceleration.

In this thesis, we present our experimental approach to provide a solution to the injection problem. In the previous chapters, we have described the basic theory followed by a comprehensive modeling with numerous sets of parameters to arrive at a realistic design of an experimental setup that should allow for the first time demonstration of laser wakefield acceleration with external bunch injection. In this chapter, we describe all the experimental components needed to form a setup ready for operation. This also includes the issues related to a proper timing and synchronization of these components.

A schematic drawing of the experimental setup for a laser wakefield accelerator is presented in figure 5.1. A TW-laser generates light pulses with an energy of $\sim$ 480 mJ, a duration of $\sim$40 fs (full width at half maximum) and 800 nm central wavelength by the chirped pulse amplification (CPA) technique. A small fraction of the laser pulse (of about 50-100 μJ) is split-off from the main beam and focused onto a fast-response cathode made of copper, which is placed at the front of the first acceleration cavity of the linac. When the cathode is illuminated by this infra-red laser pulse, a bunch of free electrons is emitted. Although the photon energy is below the cathode work function, this occurs at sufficiently high intensities. Then an electron consecutively absorbs more than one photon to overcome the surface potential barrier, which is three-photon absorption in our case. This method was chosen rather than using an ultra-violet laser pulse (based on single-photon absorption) because the setup is more simple. In particular there is no need to use a third-harmonic generator to convert the infra-red pulses to

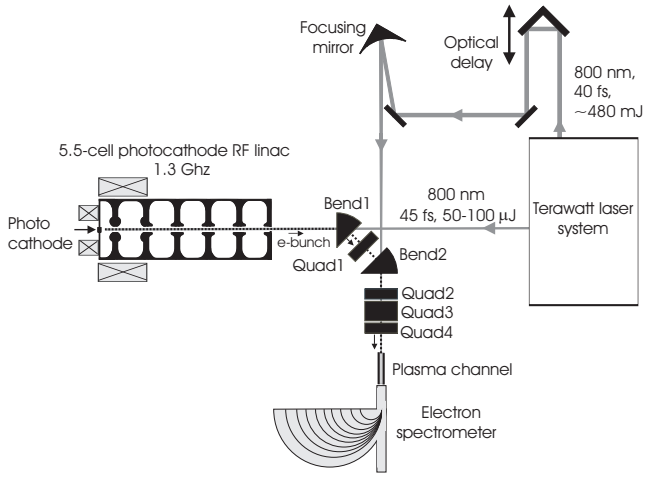

Figure 5.1: Schematic drawing of the experimental setup for our laser wakefield accelerator

the ultra-violet. Although three-photon absorption is generally considered weaker than single-photon absorption, here it is sufficiently strong to provide the required bunches of low charge (~5-10 pC) without laser ablation of the cathode surface [104]. After pre-acceleration inside the linac, the bunch is transported to the channel via a compression section, consisting of two subsequent 45° bending magnets (Bend1, Bend2), a quadrupole magnet (Quad1), and a focusing section consisting of further quadrupole magnets (Quad2, Quad3, Quad4). A major part of the laser pulse is directed to an off-axis parabolic mirror which then focuses the radiation to the entrance of the plasma channel. The gaps in the bending and focusing elements are of sufficient size to allow the transmission of the drive laser pulses without clipping. The time delay between the bunch and the pulse is controlled by an optical delay stage with a high accuracy, once the oscillator of the TW-laser is locked to the rf oscillator of the linac.

5.2 The terawatt laser system

In order to excite a large amplitude laser wakefield, a high-intensity laser pulse, with a duration of the order of the period of the plasma wave, is required. To achieve such pulses, we have designed a laser system based on the chirped pulse amplification (CPA) technique using Ti:sapphire (Ti:Sa) crystals as the active medium [105, 106]. A schematic overview of our laser system is presented in figure 5.2. It consists of six stages in total, namely, an oscillator, a pulse stretcher, a regenerative amplifier, two stages of four-pass amplifiers and a vacuum compressor. In the oscillator, a Ti:Sa crystal is pumped at a wavelength of 532 nm with an average power of 3.5 W by a cw frequency-doubled Nd:YVO_4 laser (Spectra Physics-

Millennia V). A train of femtosecond pulses is generated by means of the Kerr-lens mode-lock mechanism [107]. A prism pair is used to compensate for the material dispersion in the cavity, thus, maintaining an ultra-short pulse duration. The oscillator produces pulses of about 28 fs pulse duration (FWHM) with a central wavelength of 800 nm, at a repetition rate of 81.25 MHz. To allow synchronization of the laser pulses to the electron bunches from our linac, this repetition rate was chosen such that the 16^{th} harmonic of it is equal to the (fixed) 1.3 GHz frequency of the linac. Details about this synchronization will be discussed later in section 5.7. An average power of about 300 mW is measured at the output of the laser oscillator, which corresponds to an energy per pulse of about 3.7 nJ.

In order to avoid any damage of optical components or gain media during amplification in the subsequent amplifier stages, the pulse intensity needs to be kept below the damage threshold of all optical elements in the subsequent path of the light. This can be done in two ways, namely decreasing the peak power[1] and increasing the spot size of the pulse. The peak power can be reduced by stretching the pulse in time, i.e., increasing the pulse duration, while the spectral bandwidth remains unchanged. Such stretching of pulses can be done by propagating them through a dispersive element such that different frequency components in the pulse follow paths with different optical lengths. However, it is important that the phase relation between the frequencies in the stretched pulse remains well-controlled and known with regard to the initial pulse. This is because, in order to restore the original pulse duration at the end of the energy amplification, one has to be able to compensate for the total dispersion caused by the optical elements placed in the beam. For the desired stretching of the oscillator pulse, grating stretchers are commonly used, where the required dispersion is provided by letting the various spectral components of the pulse propagate across paths of different geometrical lengths between pairs of gratings with sufficiently large width. Since, it is very difficult to fabricate high-quality gratings with a large enough size, the stretching factor is usually limited by the availability of the gratings. To obtain a large stretching factor, e.g., 2×10^4, typically requires grating with a width of 25 cm. To further limit the intensity during amplification, an increasing of the laser spot size requires the use of optical components (lens, mirrors, gain crystals) of sufficient size. The most critical components are sufficiently large Ti:Sa crystals of sufficiently high quality, e.g., high-homogeneity across the whole crystal. Typically, in the last amplifier stage, the beam size is magnified to a few centimeters in diameter.

In our laser system, we decided to use a pulse stretcher based on an aberration-free Öffner design [108]. Here, different frequency components of the pulse, which are dispersed by a grating, are redistributed in time so that the lower frequencies are in the leading part and the higher frequencies are placed in the trailing part of the pulse. To safely amplify the pulse energy up to the level of a Joule, we designed our stretcher to stretch the pulse from the initial 28 fs duration to about 500 ps, i.e., a stretching factor of about 18000 times. The spectral bandwidth was measured to be about 32 nm.

[1] Peak power of a Gaussian profile laser pulse can be estimated via $P_{peak} = 0.939 E_{pulse}/\tau_o$, where E_{pulse} and τ_o are the pulse energy and the FWHM pulse duration, respectively.

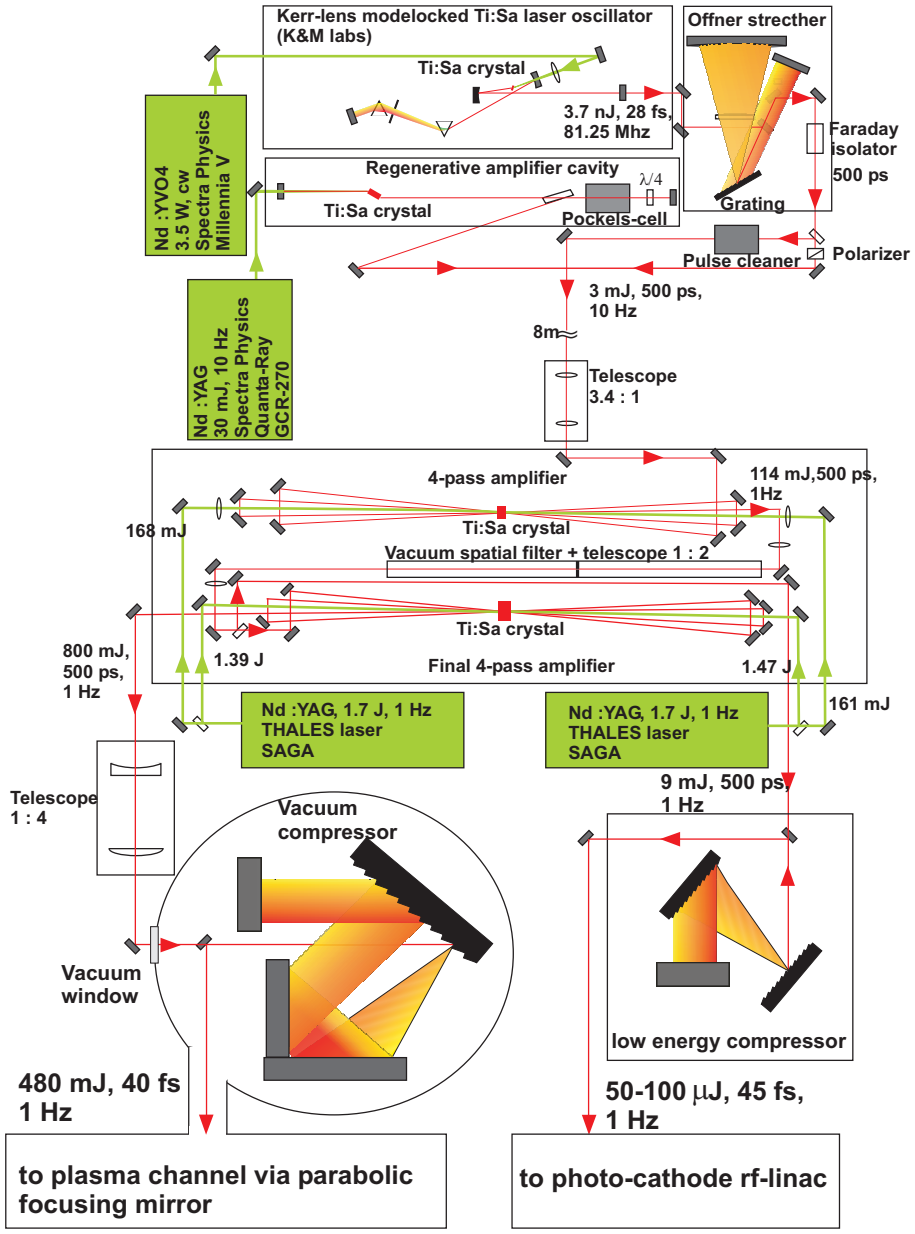

Figure 5.2: Overview of the 12 terawatt laser system at the laser physics and non-linear optics group (LPNO) at the University of Twente

From the train of the stretched pulses, one pulse is selected by a pulse picker made of a combination of a Pockels cell, a quarter-lambda plate and a polarizing beam splitter. The energy of the picked pulse is amplified in three stages. For the first amplifier stage, we use a regenerative amplifier. This amplifier is a resonator-type amplifier where the pulse performs many round-trips through the same gain crystal to build up its energy. We chose this configuration because the following advantages. The total amplification gain can reach values, as large as 10^6, boosting the pulse energy to the mJ level. Regenerative amplification also prevents the build-up of amplified spontaneous emission (ASE) which can deplete the gain before the stored energy in the crystal can be extracted by the pulse. Finally, a high beam quality can be obtained because the regenerative amplifier enhances the energy on the fundamental stable-cavity mode, which has a Gaussian profile. The gain medium of our regenerative amplifier (Ti:Sa crystal) is pumped at a wavelength of 532 nm with 30 mJ pulse energy by a frequency-doubled Nd:YAG laser (Spectra Physics Quanta-Ray GCR-270) at a repetition rate of 10 Hz. After about 20 round-trips, the pulse energy reaches its saturation and is coupled out from the cavity. Saturation means that a large fraction of the energy stored in the active medium has been transformed into the energy of the amplified pulse. Operating the regenerative amplifier close to saturation (in its final round-trips) is important to obtain a pulse-to-pulse stability of laser output. Otherwise, fluctuations of the injected pulse as well as the moment of injection would cause energy fluctuations of the amplified pulse. The regenerative amplifier produces an output pulse energy of about 3 mJ.

We observed that the pulse picker could not fully isolate one pulse out of the train of pulses from the laser oscillator due to the limited polarization contrast of the polarizing beam splitter used in the pulse picker. As a result, the main pulse is preceded by several pre-pulses. Although their energies are much lower compared to that of the main pulse (typically a factor of 10^2 lower), they can potentially absorb the energy stored in the gain medium of the subsequent amplifiers before the main pulse arrives, thereby reducing the energy gain for the main pulse. To suppress these unwanted pre-pulses, we constructed a so-called pulse cleaner which consists of a second Pockels cell, a half-lambda plate and a polarizing beam splitter. By properly timing the Pockels cell, pre-pulses can be eliminated down to a factor of $\sim 10^4$, thus ensuring that only the main pulse depletes the gain of the next amplifier stages.

For the second and final amplifier stages, we use multi-pass amplifiers. Directed by arrays of mirrors, the laser pulse passes through the gain medium four times. In designing the 4-pass amplifier, we started by modeling the amplification based on the one-dimensional Franz-Nodvik theory [109]. Although this model is rather simple, it describes the amplification process very well because it considers losses in the amplifying system and gain saturation in the gain medium quite realistically. Further, we again chose a design where the gain was saturated at the 4^{th} pass. Because the pump energy is much larger than in the regenerative amplifier, the gain per pass is much higher and the pump power is used more efficiently. A second difference from the regenerative amplifier is that the quality of the output beam profile from the multi-pass amplifier is for a large part determined by the

beam profile of both the input and the pump beam. This might become problematic if the input beam as well as the pump beam profile is not good.

In the second amplifier stage, a Ti:Sa crystal with a diameter of 12 mm and a length of 18 mm is pumped at a wavelength of 532 nm with a total pulse energy of ~320 mJ (a total pump fluence of 2.2 J/cm^2) by two frequency-doubled Nd:YAG lasers (Thales SAGA 230/10) at both surfaces at a repetition rate of 1 Hz. To better follow the detailed growth of pulse energy, we measured the pulse energy after each pass through the crystal. The results are plotted in Fig. 5.3(a). It can be seen that a pulse energy of about 114 mJ is obtained at the exit of the second amplifier. The 1D model, plotted as the filled boxes, predicts a value only slightly higher (about 10% higher after the 4th pass) than the measured data. This is probably due to the gain profile of the crystal, which was not included in the model, is not homogeneous.

In addition to the pulse energy measurements, we characterized the transverse beam profile at the exit of the amplifier in order to investigate whether or not the amplification is homogeneous across the beam. For measuring the transverse beam profile, a charge coupled device (CCD) camera was used in combination with a set of beam splitters for attenuation. A typical result is shown in Fig. 5.4(a). It can be seen that the beam profile is not a smooth Gaussian profile. It turns out that this profile closely resembles the profile of the pump beam.

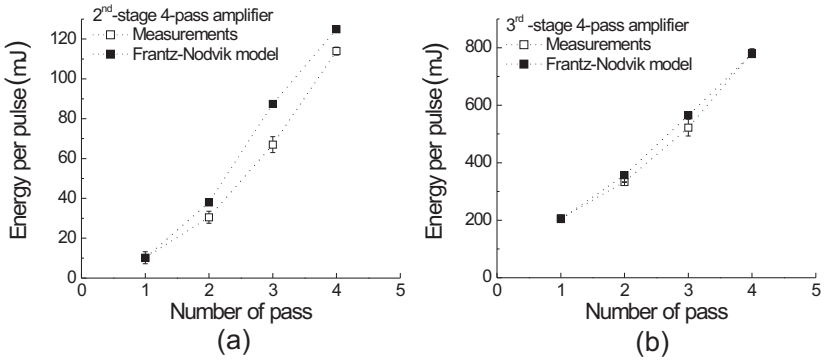

Figure 5.3: Pulse energy per pass measured in the second and third 4-pass amplifier is plotted as the empty symbols in part (a) and (b), respectively. The bold symbols show the pulse energy calculated using the Frantz-Nodvik theory.

To avoid possible damage of the gain medium or other optical components, such beam shape cannot be tolerated in the final amplifier. It is thus important to improve the beam quality. In an effort to improve beam quality, we decided to filter the pulse spatially before it is sent into the final amplifier. This is done by placing a small pinhole in the focal plane of a telescope consisting of two positive lenses. The first positive lens creates the two-dimensional Fourier transform of the input pulse in its focal plane. The pinhole only transmits the central part of the focused beam which is close to a Gaussian profile. The second positive lens is used to perform

the inverse Fourier transform of the pulse transmitted by the pinhole. To prevent a damage of the pinhole by the very high laser intensity in the focus, the pinhole was designed to have a geometry similar to that of a tapered capillary made of glass and it is placed inside a vacuum vessel. In this approach, the unwanted radiation is diffracted from the central part of the focused beam, and should not contribute to the final beam profile behind the second positive lens. To verify the proper working of the spatial filter, we measured the beam profile with a CCD camera after filtering. A typical result is shown in Fig. 5.4(b). One can see that the pulse now shows a Gaussian profile and is thus suitable to be injected into the final amplifier stage.

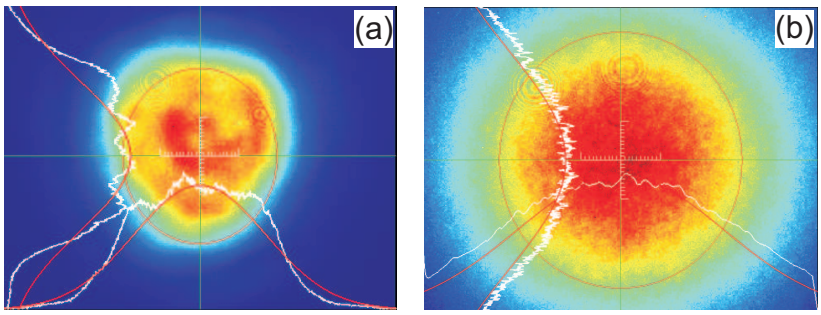

Figure 5.4: Beam profiles measured in front of and behind the spatial filter are presented in part (a) and (b), respectively.

The third (final) amplifier is performed analogous to the second amplifier. A Ti:Sa cystal with 20 mm diameter and 15 mm length is pumped at both surfaces with a total pulse energy of 2.8 J (a total pump fluence of 2 J/cm^2) by two frequency-doubled Nd:YAG lasers (Thales SAGA 230/10) at a repetition rate of 1 Hz. To characterize the performance of the final amplifier, the measured pulse energy for each pass is plotted in figure 5.3(b). It can be seen that the pulse energy grows with each pass and reaches an energy of 790 mJ at the exit of the amplifier. Again, it can be seen that the Frantz-Nodvik model agrees quite well with the experimental data which indicates that the amplification across the beam is close to homogeneous as can be expected from a flat-top pump beam profile.

The output pulse from the final amplifier is sent through an optical delay line before it enters a vacuum compressor. This delay line is chosen in order to optimize later the timing between the drive laser pulse and the injected electron bunch in the plasma channel. A highly precise timing down to the femtosecond scale is possible since the drive laser pulse and the bunch originate from the same pulse.

As the final step to reach the TW-peak power, the duration of the amplified pulse is temporally compressed by a grating compressor (placed in vacuum to avoid air breakdown) which aims to approach the initial pulse duration of the oscillator pulse. Such a compressor works in the opposite way as the pulse stretcher and can also compensate for the extra dispersion that the pulse accumulates in the numerous optical components that are used in the amplifier chain. To properly design the

compressor, we used a software ZEMAX [110] which calculated the total dispersion caused by the stretcher and all the optical components in the beam path, and then optimized the grating angle and effective distance in order to obtain the shortest pulse. Fine tuning of the compressor was done experimentally. In order to analyze the temporal shape and duration of the output from the compressor, a Grenouille-FROG setup was assembled [111]. This setup is capable of tracing the phase of each frequency component within the pulse, so that the chirp introduced in the stretcher and the optical components in the beam path can be optimally compensated to obtain the shortest pulse duration. We found that for the optimum configuration of the compressor, the pulse duration was measured to be about 40 fs (FWHM) at the exit of the compressor with a spectral bandwidth of about 24 nm (FWHM). This pulse duration is longer than the initial duration of the oscillator pulse (~28 fs). This difference is mainly explained by gain narrowing during the amplification process, because the spectral bandwidth reduces from initially about 32 nm to 24 nm. Additionally, higher-order dispersion introduced in the system could possibly not be compensated for by the compressor. As a further characterization, we measured the pulse energy behind the compressor which is about 474 mJ (at an input energy to the compressor of 790 mJ). This means that the efficiency of the compressor is about 60 %, as expected from the specification of the grating (four reflections with a grating efficiency of about 90% per reflection).

The output from the compressor (a beam with approximate 5 cm diameter) is directed to an off-axis parabolic mirror with a focal length of 2.5 m. The mirror focuses the beam into the entrance of the plasma channel where we measured the vertical and horizontal spot sizes of 40 μm and 35 μm, respectively. The ellipticity observed in the focus was also recognized in the beam already behind the final amplifier. We found that this is due to the profile of the pump beams in the crystal of the final amplifier stage. In the focus, we estimate an intensity of 5×10^{17} W/cm^2.

When comparing these current laser parameters, particularly the pulse energy, to those we used in the modeling described in chapter 4, one can see that the pulse energy produced by our laser system is about a factor of 2.1 lower. This choice is made for speeding up the basic demonstration experiments before attempting to obtain refined and improved results via further increasing the peak power. In fact, we have a possibility to increase the output energy of our laser system by installing an additional pump laser (Quantel Nd:YAG, pulse energy up to 4 J at 532 nm in single-shot mode) which we already have. However, this pump laser still requires maintenance before it can be implemented into our laser system.

To investigate the influence of our experimentally available laser parameters (the pulse energy, duration and peak intensity) on the generation of a wakefield and the acceleration process, we recalculated the model, taking these current parameters into account. We found that the minimum kinetic energy needed for the injected electrons to be trapped (trapping threshold) on the axis of the generated wakefield is ≈1.9 MeV. This is about a factor of 4 higher than to the trapping threshold found from the initial calculations as described in chapter 4. As a consequence, it would lead to a reduction of the number of trapped electrons in the wakefield. In these new calculations, where we injected a 5 pC bunch, we obtained a num-

ber of trapped electrons of ≈7 % (0.35 pC) instead of ≈48 % (2.4 pC) calculated initially. Furthermore, we found that the final bunch energy after the acceleration process decreases because with the current conditions the amplitude of the generated wakefield is about a factor of 3.6 lower when compared to the initial calculations. After acceleration over 5 cm in the channel, the final bunch energy was calculated to be about 200 MeV with a relative energy spread of about 2 %.

In order to know whether these final bunch parameters, particularly the total charge, can be tolerated in the demonstration experiment, we continue the analysis by evaluating our detection system. To detect the accelerated bunch, a phosphor screen (Kodak Lanex) was installed of about 1.4 m behind the plasma channel. As the screen is hit by the bunch, it emits light which will be captured by a gated CCD camera. Our model, described in chapter 3, predicts that the radius of the 0.35 pC bunch from the laser wakefield acceleration would grow to about 3.5 mm, resulting in a number of electrons per unit area of 6×10^4 mm^{-2}, at the phosphor screen. With the same method, Masuda, et.al. [124] reported also much lower numbers 10^4 electrons/mm^2.

The calculations mentioned and estimations show that our first demonstration experiment for laser wakefield acceleration with external bunch injection should indeed be feasible using the current laser parameters. Later, after the demonstration experiment, we expect to improve the final bunch parameters (bunch energy, trapping efficiency and energy spread) by increasing the output energy of our laser system and thereby the amplitude of the generated wakefield. For the latter modification we have an additional pump laser available.

5.3 The linac

The linac including its control system had originally been designed and built by the Los Alamos National Laboratories, however, for a different purpose (driving a THz free-electron laser) and for higher kinetic energies (up to 6 MeV) [112, 113]. Also, the linac was originally designed for much higher electron currents using a different photo-cathode (Cs-Te) of higher conversion efficiency and a long response time [84]. The original design and build aimed on rather long (tens of picoseconds) bunches which would not have been useful for our purpose. For our laser wakefield experiment, in which bunches of shorter duration and lower kinetic energy are required, a first step was to replace the slow cathode with a fast-response cathode (Cu) so that the linac would produce bunches of sub-picosecond duration as the cathode is illuminated by femtosecond laser pulses.

To generate the electron bunches, the copper cathode is placed on the back wall of the linac and illuminated by a small fraction of the energy of the infra-red laser pulses from the drive laser system. This radiation is split-off from the main beam by a beam sampler which is placed just behind the spatial filter as depicted in Fig. 5.2. Since the duration of the pulse is still rather long in this stage, ~500 ps, the pulse is sent through a grating compressor, which was designed for a low energy laser pulse. Behind this compressor, the pulse is about 45 fs and the pulse energy is chosen to be about 100 μJ. The laser pulse is transported and focused on the copper

cathode with a radius of about 0.6 mm. Based on the experimental results from Brogle *et.al.* in reference [104], we estimated that an electron bunch with a charge of about 5 pC would be generated with such a pulse. To avoid any disturbance of the bunch due to any asymmetry of the accelerating field that would occur with off-axis propagation in the linac, it is required that the laser pulse hits the center of the cathode. We checked this alignment via a viewport with a telescope, while alignment was done via a remote controlled mirror, which directs the laser beam, steered from the control room.

The microwave power that drives the linac originates from an oscillator-amplifier system. The continuous-wave crystal oscillator generates a highly stable of 40.625 MHz at a mW power-level which is frequency multiplied into the microwave range of 1.3 GHz. This signal is split into two parts. The first part is sent into a synchronization device, where it is compared with the 16^{th} harmonic of the laser oscillator repetition rate in order to synchronize the rf phase and the arrival time of the laser pulse on the cathode in the linac. The second part is sent into a series of microwave amplifiers to generate adjustable power levels of several megawatts, before feeding the microwave into the linac enhancement cavity using a microwave waveguide.

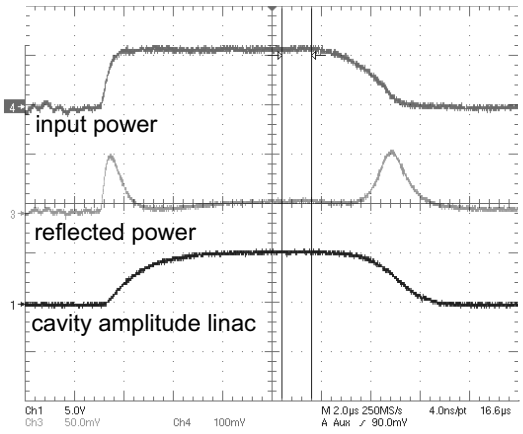

Figure 5.5: The measured input- and reflected power as well as the cavity amplitude of the microwave in the linac cavity at resonance.

To achieve pre-acceleration as desired and to avoid a large shot-to-shot energy jitter of the bunches, a proper timing of the injection of the electrons from the cathode is required. Injection should occur near the peak of the microwave pulse where the power is almost constant. In order to find the corresponding time window, we measured the injected and reflected power and also the power stored inside the linac cavity as a function of time at resonance[2] with the cavity. Typical results are

[2] At resonance, the length of the cavity of the linac matches with the rf wavelength.

presented in figure 5.5. It can be seen that, at resonance, the reflected power becomes minimum and the rf power stored in the cavity reaches its maximum. From Fig. 5.5, one can see that there is a time window of about ~1.2 μs (indicated as the two vertical lines) within which the cavity amplitude is almost as constant as desired (less than 1 % relative variation). Thus, releasing electrons within this time window would lead to acceleration with minimized shot-to-shot fluctuation of the kinetic energy.

5.4 The electron beam transportation line

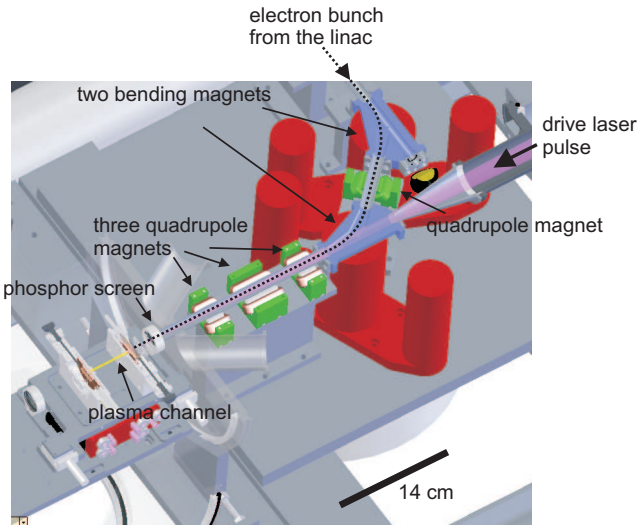

Figure 5.6: Setup of the electron bunch transportation line. It consists of bending and focusing sections. The bending section is formed by two 45° bending magnets and a focusing (quadrupole) magnet. The focusing sections consists of three quadrupole magnets.

After pre-acceleration in the linac, bunches are to be transported to the plasma channel via a beam transportation line. To explain the working of this transportation line, we present the cross-section of this beam line in figure 5.6. When a bunch from the linac is propagating through the first bending magnet, where the magnetic fields are pointing downwards, the Lorentz force changes the propagation direction of the bunch resulting in a curved path. At the exit of the first magnet, the direction of the bunch is changed about 45° with regard to the axis of the linac. Behind the first bending magnet, a focusing (quadrupole) magnet is placed. Its function is to compensate for the increase of the bunch size in the transverse direction of the bending plane. When the bunch propagates through the second bending magnet, where the magnetic field is also pointing downwards, its direction changes again

resulting in a total deflection angle of 90° with regard to the axis of the linac. Behind the second bending magnet, the bunch propagates co-linearly with the drive laser pulse toward the plasma channel. Finally, three quadrupole magnets are installed to focus the bunch so that the transverse size of the bunch approximately matches the laser spot size at the entrance of the plasma channel.

Besides its function to achieve overlap of the bunch with the drive laser beam, the bending section has another important function, namely to compress the bunch in time yielding a shorter bunch duration compared to that at the linac exit. This is possible with our described design which provides a non-isochronous trajectory. This means that it introduces an energy-dependent path length to the electrons such that higher-energy electrons follow a longer path than lower-energy electrons. By propagating typical bunches from the linac, where faster electrons are leaving before slower ones (an energy chirped bunch), through the bending section, the electrons would arrive at the same time behind the bending section, which leads to a short bunch duration. Our simulations presented in chapter 4 predict that the bunch duration at the exit of the second bending magnet would be about 8 times shorter than at the linac exit.

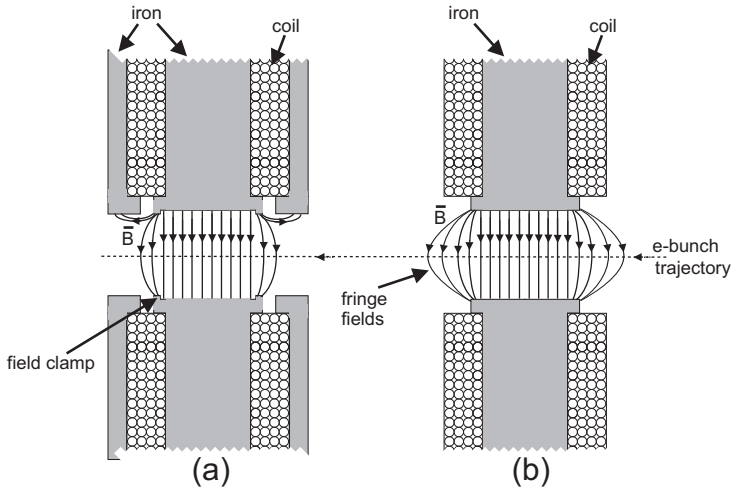

Figure 5.7: Design schematic of our bending magnet (a). The fringe fields are reduced with field clamps in combination with an iron shielding around the coil. For comparison, the magnetic field lines in a standard dipole magnet are presented in part (b). Here, the fringe fields extend over large distances outside the magnet's gap.

As parts of the described bending section are non-standard, we applied extra attention in the design. To design the bending magnet, we used the 3D COMSOL multiphysics modeling tool [99]. This modeling is important because it provides a full (three-dimensional) calculation of the magnetic field distributions involved.

There are two main requirements that must be fulfilled by the design, namely that the gap between the pole faces is to be large enough to permit the transmission of the drive laser without clipping it and, that the fringe fields[3] are as short as possible. The latter is important in order to minimize the expansion of the transverse size of the bunch in the non-bending plane direction, which may lead to additional bunch lengthening during focusing into the plasma channel. The difficulty in this optimization is that these two parameters are coupled, i.e., for an increasing gap the fringe fields become larger as well. In order to minimize the fringe fields for a large gap between the pole faces, we introduced, so called, field clamps at the edges of the pole faces in combination with an iron shielding around the coil. To see the difference between this design compared to a standard dipole magnet, we schematically show the cross-section of the magnets in figure 5.7. One can see that in our bending magnet (Fig. 5.7(a)) the field lines of the fringe fields make shortcut paths to the iron shielding around the coil which results in a sharp drop-off of the field along the electron bunch trajectory. In the case of a standard dipole magnet (Fig. 5.7(b)), the field lines of the fringe fields extend over much wider distances outside the magnet's gap.

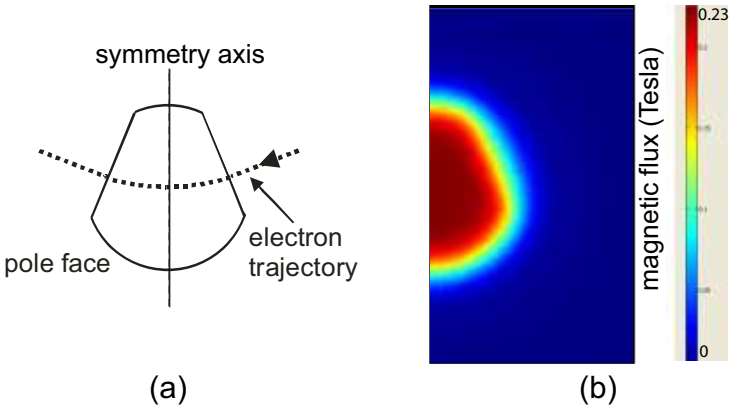

Figure 5.8: In part (a), the pole face of the bending magnet is shown. The dotted curve presents a trajectory of an electron through the magnet. In part (b), the calculated magnetic flux on the bending plane located in the middle of two pole faces is shown for a half of the bending magnet.

In order to analyze the results from the modeling done with the COMSOL software, we present the designed pole face and the calculated magnetic flux in figure 5.8. The pole face is shown together with the trajectory of a test electron in Fig. 5.8(a). Taking the considerations described earlier into account, the gap between the pole face was chosen to be 15 mm. The calculated magnetic flux on the bending plane located in the middle of two pole faces, i.e., at a distance of 7.5 mm from

[3] Fringe fields are extension of the magnetic fields outside the magnet's gap as shown in Fig. 5.7.

each face, is presented in Fig. 5.8(b). Since the geometry of the bending magnet is symmetric with regard to the symmetry axis of the pole face, only a half of the magnetic flux is shown. One can see that the magnetic flux is homogeneous in the center of the magnet. This homogeneity is important so that individual electrons in the bunch traveling along different trajectories experience essentially the same magnetic field during propagation inside the magnet.

To investigate whether the drop-off of the fringe fields can be tolerated for our experiment and also to allow a quantitative comparison with measurements of the magnetic field, we calculated the fringe fields along the propagation direction for an on-axis trajectory (at the middle of the gap) and for a trajectory 3 mm above the axis. The results are presented in Fig. 5.9 as the stepped curve, where the steps are due to the numerical step size used in the model. To simulate the bunch dynamics during propagation along the bending section as discussed in chapter 4, we fitted the stepped curve in Fig. 5.9 with the following expression for the fringe field reported in references [72, 114],

$$B_y(z) = \frac{B_0}{1+\exp(b_1(z-dl)+b_2(z-dl)^2)}, \tag{5.1}$$

where $B_y(z)$ is the magnetic field along the propagation axis (z) and B_0 is the maximum value of the field. The parameter dl changes the effective length of the magnet (the length of the path on which the electrons experience a constant field along the propagation direction). The parameter b_1 affects the steepness of the drop-off of the magnetic field to outside the gap while b_2 is a second order correction. The fitted curve is plotted in Fig. 5.9 as the solid line. When using the parameters obtained from the fit, the model as was described in chapter 4 predicted that the bunch from the linac can be compressed by a factor of 8 yielding to a short bunch duration of about 250 fs. Based on these calculations, we decided that the described design can be used for our experiment.

After fabrication, we tested and calibrated the magnets by measuring the magnetic flux along the propagation axis using a Gauss meter (F.W. Bell, series 9900 gaussmeter, HTM 95-0608). In this experiment, we set the current through the coil of the bending magnet to 2 A. This current results in a magnetic field strength of 234 mT measured in the middle of the gap. This field strength is chosen based on our modeling described in chapter 4. The results are presented as the filled dots in figure 5.9. It can be seen that there is very good agreement with the modeling for both the on-axis field (Fig. 5.9(a)) as well as at 3 mm off-axis (Fig. 5.9(b)). This indicates that we have successfully fabricated the magnets which possess properties as required. A second important issue of performance can be a thermal limit of operation. To investigate this, we measured the temperature of the coil as a function of time and, also, the corresponding magnetic flux. We observed that the temperature of the coil increases by about 15° C after 2.5 hours operation. However, this increase did not form a problem because, at the same time, we observed that magnetic flux is almost constant (±0.01 mT) during this period.

The design of the quadrupole magnets optimized along the the lines described above is shown in figure 5.10 [113]. The strength of the magnetic field on the prop-

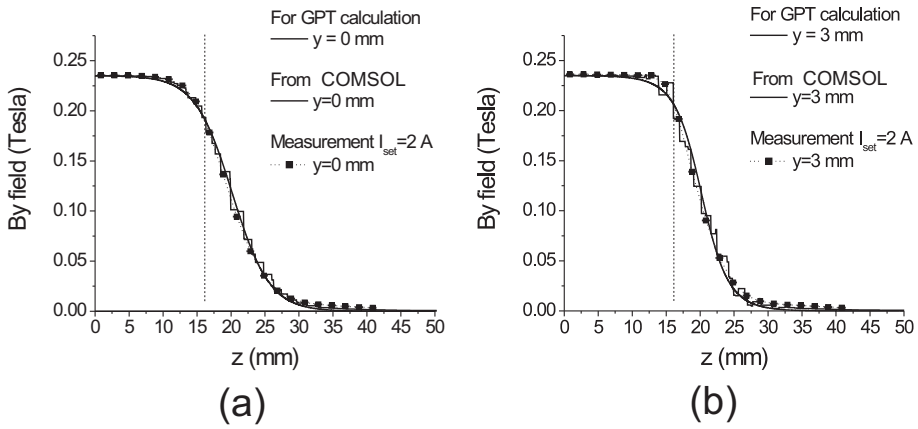

Figure 5.9: In part (a), the calculated magnetic field (in the middle of the gap) along propagation direction (z) is shown as the stepped curve. The solid line is a result from fitting the stepped curve with equation (5.1) which is used to calculate the bunch dynamics described in chapter 4. The filled dots show the measurement results. In part (b), we show the magnetic field at 3 mm above the propagation axis, which is a result from COMSOL modeling (stepped curve), the solid curve is derived from the fitting of the stepped curve and the filled dots are obtained from measurements. The vertical dashed line is the physical edge of the pole face.

agation axis is zero and, ideally, increases linearly toward the pole faces of the magnets. In the configuration shown, the magnetic field lines focus the bunch only in the horizontal plane and whereas there is a defocusing in the vertical plane. To enable adjustable focusing in both directions a quadrupole triplet is required, where three quadrupole magnets are placed behind each other with different focusing directions.

5.4.1 Testing of the beam transportation line

After all the magnets were constructed and assembled in the beam transportation line as shown in figure 5.6, we performed a test experiment to characterize the transportation line, that is bunch propagation experiments along this transportation line. In this experiment, we switched off all the quadrupole magnets in order to only test the bending magnets. The motivation for this test was to see whether the bunch could indeed be directed to the plasma channel without focusing. For the observation of the bunch, we used a phosphor screen (Kodak Lanex) which is placed in front of the plasma channel. When electrons hit this screen, it emits light which is imaged on a gated CCD camera (4 Picos Stanford Computer Optics Inc.).

As starting parameters, the rf amplitude in the linac was set to 40% of its maximum value and the electron bunch was launched from the cathode at the optimum

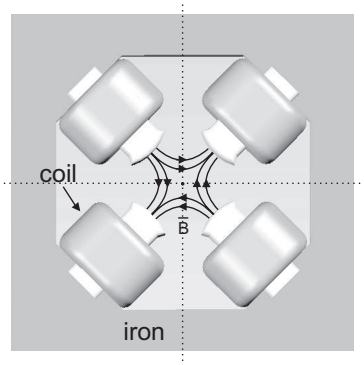

Figure 5.10: Schematic of a focusing (quadrupole) magnet. The magnetic field is zero at the center (propagation axis) and increases linearly to a maximum at the pole faces.

phase. To analyze the working of the beam transportation line, we recorded images of consecutive shots of electron bunches. The results from nine consecutive shots are presented in figure 5.11. Here, both bending magnets were operated at a current of 1.3 A, creating a magnetic flux of 183 mT in the middle of the magnets. One can see that the bunch has an elliptical shape. This is what is expected, due to the energy spread in the bunch. Namely, in this configuration, the bending section can also be considered as an electron spectrometer, where electrons with slightly different energies follow slightly different paths with different lengths and output bending angles, resulting in an elliptical density distribution in space as observed at the screen. Based on the same arguments, the shot-to-shot fluctuation of the bunch position on the screen can be used to determine the shot-to-shot fluctuation of the kinetic energy of the bunches. As can be seen in Fig. 5.11, the position of the spot is observed to shift to the left side of the cross line for a few shots, e.g., shot no. 1, 3, 6, 8 and 9.

In order to quantify these findings for a comparison with the input parameters of the model in chapter 4, we determined both the kinetic energy and the shot-to-shot energy fluctuation of the bunch as indicated in Fig. 5.12. From the measured magnetic field strength of 183 mT, we calculate a kinetic energy of the bunch of about $\approx$2.2 MeV, which is roughly in the range of what we have assumed for the model input. The shot-to-shot fluctuation can be estimated by evaluating two trajectories followed by electrons with the relativistic factor γ and $\gamma + \Delta\gamma$. The energy

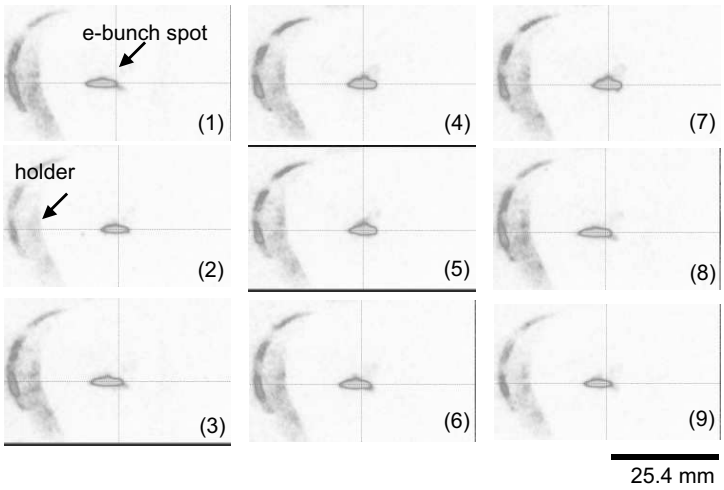

Figure 5.11: Images of nine consecutive shots of electron bunches on a phosphor screen located in front of the plasma channel. The scale bar is 25.4 mm.

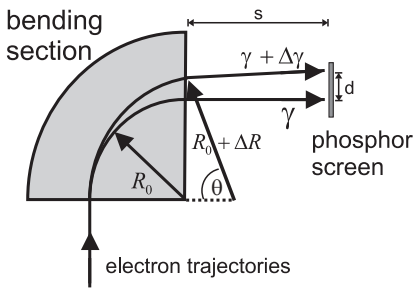

Figure 5.12: Illustration of two electrons with slightly different energies propagating in a bending section. The higher-energy electron follows a longer trajectory than the lower-energy electron. After propagation over a distance s behind the magnet, the two electrons will be separated by a distance d.

fluctuation can be calculated as

$$\frac{\Delta\gamma}{\gamma} = \frac{\sqrt{\left(\frac{e}{m_e c}\right)^2 B_y^2 (R_o + \Delta R)^2 + 1}}{\sqrt{\left(\frac{e}{m_e c}\right)^2 B_y^2 R_o^2 + 1}} - 1, \tag{5.2}$$

where e and m_e are the charge and mass of the electron, c is the speed of light, B_y is

the magnetic field and R_o is the Larmor radius of electrons with a relativistic factor γ. In our design R_o amounts to 48.5 mm. The parameter $R_o + \Delta R$ is the radius of a trajectory followed by the electrons with a relativistic factor $\gamma + \Delta\gamma$. The parameter ΔR can be calculated by considering the distance between the two electrons on the phosphor screen (d) and the distance from the magnet to the screen (s). In our setup, s is 28 cm. With $\Delta R = \{(R_o + d - s \cdot \tan(90 - \theta)) / \sin(\theta)\} - R_o$, where θ is the deflection angle for electrons with $\gamma + \Delta\gamma$, ΔR was calculated. From the central spot of the image, we obtained d=1.27 mm, as the standard deviation, so that the energy fluctuation is found to be 1.7%. This fluctuation is slightly larger than we expected and assumed in the model. This fluctuation probably arises from our operating the linac at a somewhat lower kinetic energy. Indeed, the minimum kinetic energy required for stable operation as reported in reference [115] is slightly higher, at about 2.5 MeV. Nevertheless, the described test experiment yielded the important proof that the bunch transport line works as planned. In the actual laser wakefield experiments, one would simply increase the rf amplitude and also the current in the bending magnets to obtain electron bunches with kinetic energy of about 2.9 MeV.

5.5 The plasma channel

In a laser wakefield accelerator, optical guiding of high-intensity laser pulses is essentially required to extend the acceleration length up to the dephasing length[4]. This is important in order to obtain maximum bunch energy from the acceleration process. In the absence of guiding, the acceleration length is fundamentally limited by diffraction to a characteristic distance determined by the Rayleigh length as illustrated in Fig. 5.13(a).

An attractive technique to guide a high-intensity laser pulse is to couple the beam into a preformed plasma channel as shown in Fig. 5.13(b), where the density of the plasma is minimum on axis and increases with increasing distance from the axis. Waveguiding in such a channel works as follows. The phase velocity of light in a plasma increases as the plasma density increases, and this leads to a curving of the wavefront of the beam, i.e., a steady re-focusing during propagation. When this focusing balances the defocusing effect of diffraction, the laser beam diameter becomes constant, this is also called waveguiding.

A promising technique used to transiently create the described type of plasma channel is to use a slow discharge in a hydrogen-filled capillary made from alumina [49, 50]. In this technique, the discharge ionizes the gas. Subsequent heating of plasma by the electron current yields a rise of the on-axis temperature. Because the plasma temperature at the capillary wall is lower than on-axis and the pressure inside the capillary is essentially homogeneous, a density profile is formed with its lowest electron density on axis as desired for guiding.

Due to its proved working, we have decided to implement the described type of plasma channel in our experiment. The setup for our plasma channel, which was

[4] The dephasing length is the maximum travel distance within which electrons can gain energy before they outrun the wakefield and enter its decelerating phase.

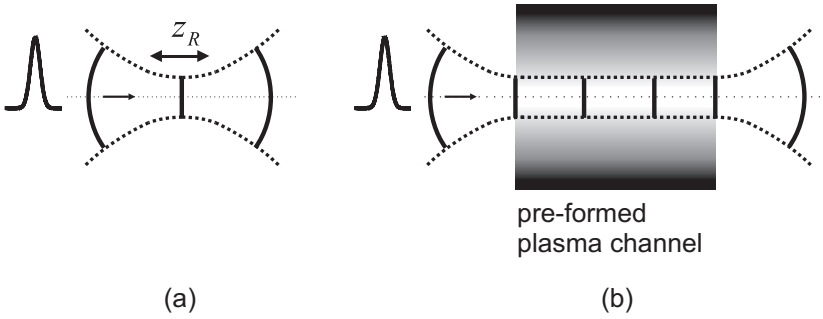

Figure 5.13: In part (a), a focused laser pulse diffracts with a characteristic distance determined by the Rayleigh length (z_R). In part (b), a preformed plasma channel provides a gradient of the refractive index such that the wavefront of a laser pulse curves in a focusing direction. Balance between the focusing and diffraction can guide a laser pulse over distances beyond the Rayleigh length.

developed at the FOM-Institute for Plasma Physics Rijnhuizen [116], is presented in figure 5.14. An alumina capillary with an inner diameter of 306 μm and a length of 3 cm is mounted between two electrodes, namely a high voltage- and grounded electrode. The hydrogen gas is injected continuously via small holes drilled in the capillary wall near both ends of the capillary. The hydrogen gas inlet is regulated with a valve controlled by a pressure controller in order to keep the pressure inside the capillary constant for each shot. Both ends of the capillary are closed with a shutter. The purpose of this construction is to keep the pressure along the capillary homogeneous and, at the same time, restrict the average flow-rate of gas into the interaction chamber. This is important because the chamber is connected with the linac which has to operate at a relatively high vacuum (10^{-6}-10^{-8} mbar). In order to avoid a microwave field induced breakthrough in the accelerator cavities, the shutters are only opened for about 30 ms during the acceleration experiment. The entire plasma channel setup is mounted on a 5-axis translation stage (Motorized Wide Five-Axis Tilt Aligner Model 8082, New Focus), which allows alignment with high precision of the capillary with regard to the electron bunch.

For our laser wakefield acceleration experiment, there are two considerations for choosing the parameters of the plasma channel (the plasma density and the channel radius). Firstly, the plasma density is chosen such that a resonant laser wakefield can be excited by the drive laser pulse. This can occur when the duration of the drive laser pulse is of the order of the plasma wavelength. The optimum on-axis plasma density (n_p) can be found via the expression $n_p[cm^{-3}] = 1.766 \times 10^{21} / \left(\tau_0[fs]\right)^2$ as described in reference [117], where τ_0 is the FWHM pulse duration in fs. Based on our laser parameters in the focus (at the entrance of the plasma channel) as described earlier in section 5.2, the required plasma density is calculated to be about 1.1×10^{18} cm^{-3}. Numerical studies done by Broks *et.al.* [117]

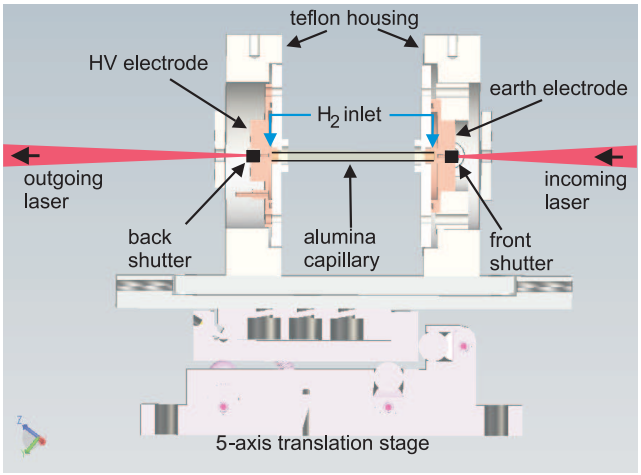

Figure 5.14: Setup of the capillary discharge plasma channel

yielded a relation between the hydrogen filling pressure and the on-axis density in the capillary which is expressed by,

$$p_{H_2}[mbar] = \frac{n_p[cm^{-3}] - 0.27 \cdot 10^{18}}{1.787 \cdot 10^{16}}, \tag{5.3}$$

where p_{H_2} is the filling pressure of the hydrogen gas in mbar. In our case, to obtain the required plasma density of 1.1×10^{18} cm^{-3}, the expression yields an optimum filling pressure of about 46 mbar.

As the second consideration, the channel radius is chosen to match the laser spot size such that the laser beam can be guided through the plasma channel. Broks [117] showed that for a fixed filling pressure, the channel radius depends strongly on a chosen radius of the capillary, via $r_c[\mu m] = 7.801 \cdot p_{H_2}[mbar]^{-0.25} \cdot R_{cap}[\mu m]^{0.5625}$, where r_c and R_{cap} are the matched spot size and the capillary radius, respectively, in μm. According to this expression, for the optimum filling pressure and the intended focusing of our laser beam, a capillary diameter of about 300 μm is required to get waveguiding of the laser beam through the plasma channel.

The capillary (3 cm long and 306 μm inner diameter) is placed inside the interaction chamber with a background pressure of about 10^{-6} mbar. A pulsed discharge in the capillary is driven by rapidly discharging of a capacitor of 2.7 nF (previously charged to a voltage between 20 kV to 24 kV). The current was measured directly on the earth connection inside the chamber using a 1/10 Ohm resistive current probe. To characterize the working of the plasma channel, we measured the current through the capillary as a function of time during the discharge. Typical results are presented in Fig. 5.15 for the case in which the capillary was filled with 46 mbar H_2, and the charging voltage was 24 kV. One can see that a maximum current of about 300 A is obtained approximately 100 ns after the initiation of the

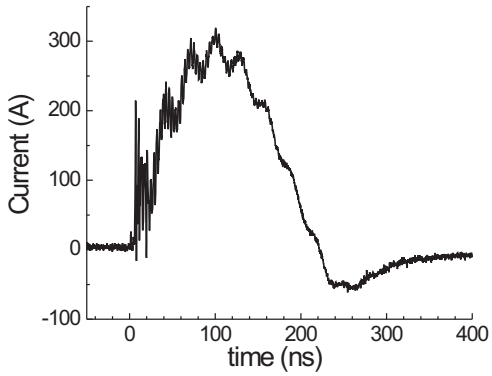

Figure 5.15: Discharge current through the capillary measured as a function of time. The charging voltage of the pulser capacitance was 24 kV and the capillary (306 μm diameter and 3 cm long) was filled with 46 mbar H_2.

discharge. Similar results had been reported by Spence *et.al.* [50]. Accordingly the measurements confirm that our setup works as expected. In order to characterize the guiding properties of the plasma channel, the next step is to perform guiding experiments of our TW laser through this plasma channel.

5.5.1 Guiding of high-intensity laser pulses with the plasma channel

In this section, we report guiding of high-intensity pulses from our laser system through a 3-cm-long capillary discharge waveguide. By analyzing the spatial, temporal and spectral properties of the transmitted laser pulse, we identify a suitable time window where ionization induced spectral shifts are minimum and the overall transmission is maximum. Based on these results, we verified the presence of a certain time window suitable the injection of the drive laser pulse and the electron bunch into the plasma channel to perform the laser wakefield acceleration experiment.

The experimental setup for guiding high-intensity laser pulses in the plasma channel is shown in figure 5.16. The laser pulse is focused into the entrance of an alumina capillary where we measured the vertical and horizontal spot sizes of 40 μm and 35 μm, respectively. In the focus, we estimate the peak intensity of 10^{17} W/cm^2. The capillary (3 cm long and 306 μm inner diameter) is filled with hydrogen gas at a filling pressure of 46 mbar. Any laser light transmitted by the capillary is brought outside the vacuum vessel and attenuated via a reflection from an uncoated mirror placed about 1 m behind the capillary exit. This mirror is mounted

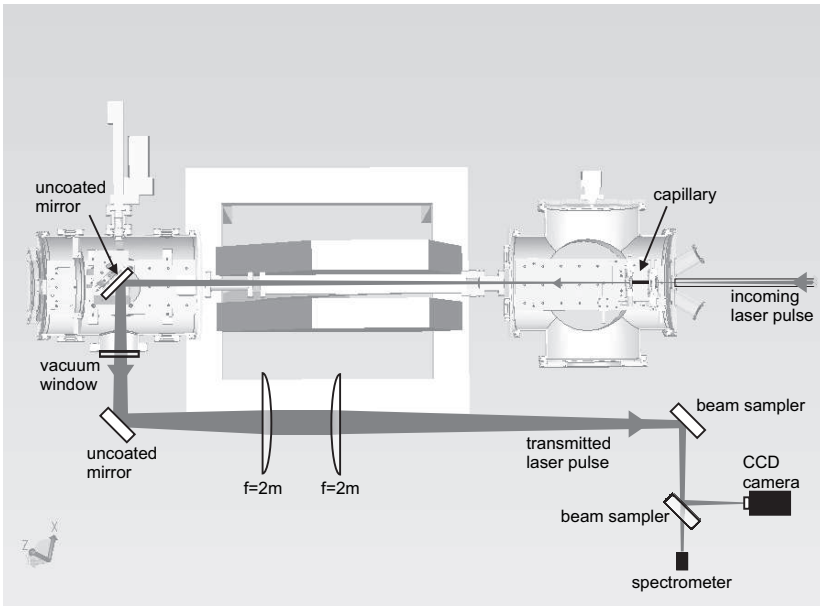

Figure 5.16: Experimental setup for guiding high-intensity laser pulses in a plasma channel.

on a motorized translation stage so that it can be slid out of the beam path to prepare the investigation of electron bunches along the same path. After a second attenuating reflection from an uncoated mirror placed outside the vacuum, the laser spot from the exit of the plasma channel is imaged on a CCD camera (PixeLINK camera) using a telescope optics based on two positive lenses (f= 2 m). The camera is triggered with a signal derived from the laser pulse to record an image of the transmitted laser pulse for each shot. Further, a small fraction of the transmitted laser pulse is directed to a spectrometer (USB2000 OceanOptics) to measure any spectral changes that the laser light might undergo in the plasma channel.

In order to analyze the guiding of the laser pulse propagating through the plasma channel, the spatial and spectral profile of the transmitted laser pulse for different injection time are plotted in Fig. 5.17 and Fig. 5.18, respectively. For example, when the laser pulse was injected before the discharge pulse, the H_2 gas is still in neutral condition. In this case, we observe only a weak transmission of the laser pulse with an irregular beam profile as shown in the first image in Fig. 5.17. Measurement of the spectrum of this laser pulse (as plotted with the curve 1 in Fig. 5.18) shows spectral broadening which is marked with two distinct peaks, namely a peak originating from the initial laser pulse at 805 nm and an additional strong peak at 780 nm. This strong peak, which is blueshifted from the initial spectrum, may be caused by ionization of the neutral gas by the intense laser pulse [118–120]. The ionization induced by the rising slope of the laser pulse causes a rapid increase of

the electron density and, hence, a decrease of the refractive index. Such a change of the refractive index in time leads to self-phase-modulation which can be seen as a spectral broadening and blueshift of the propagating laser pulse.

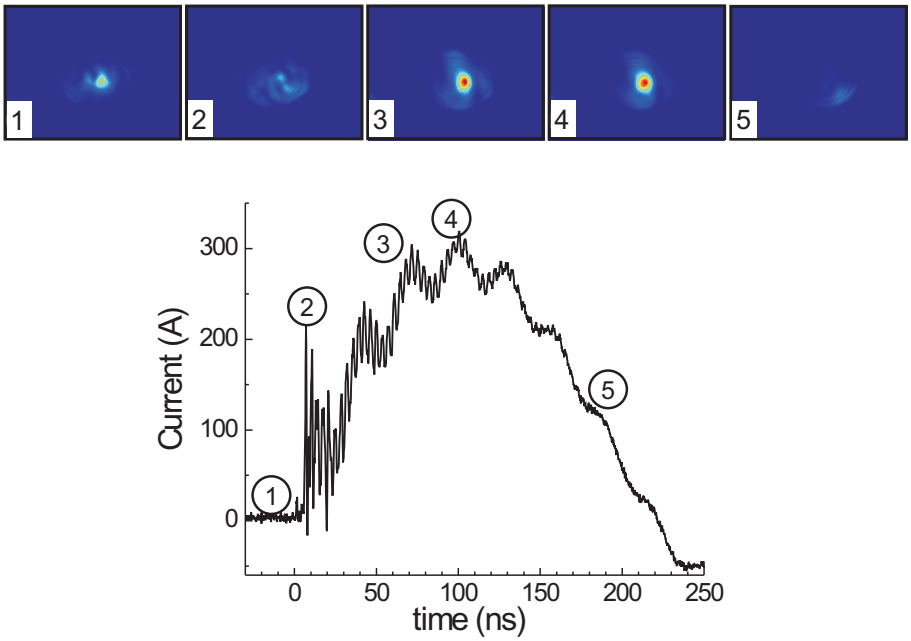

Figure 5.17: At the top part, beam profiles of the transmitted laser pulses through the plasma channel are presented. The images are recorded for different injection times of the laser pulse with respect to the time of discharge ignition. Image 1 is obtained for injection before the discharge pulse. Image 2 until 5 are recorded for injection at 6 ns, 60 ns, 100 ns and 190 ns after the discharge pulse. At the bottom part, the measured current through the capillary is shown together with the injection times for which the profiles were measured.

It can further be seen that when the laser pulse is injected shortly after the start-up of the discharge current pulse (t= 6 ns), the transmitted beam profile becomes significantly distorted as shown in the image 2 in Fig. 5.17. To explain this situation, more detailed information about the state of the plasma in this period is required. Measurements of the plasma density profile of the same waveguiding capillary using an interferometry technique [57, 121] showed that, shortly after the breakdown phase of the discharge, the plasma density becomes spatially very irregular, thereby deteriorating waveguiding. Further, the spectral measurement shows that the 780 nm peak in the spectrum is less dominant compared to the 805 nm peak as shown in the curve 2 in Fig. 5.18. This may be due to a reduction of the laser-induced-ionization since at this moment some part of the gas has been ionized (or partly

ionized) during the rising part of the discharge current.

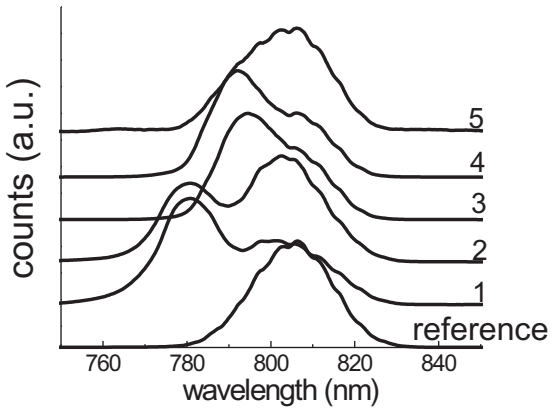

Figure 5.18: The measured spectra of the transmitted laser pulses as were presented in Fig. 5.17. As a reference, the spectrum of the laser pulse was measured before the capillary.

With injection times at 60 ns and 100 ns after the onset of the discharge current pulse, we record a significant improvement of the transmitted beam profile as shown in the images 3 and 4 in Fig. 5.17. The beam profile possesses a near Gaussian profile distribution as expected from single-mode propagation through the plasma waveguide. Here, also the measured current through the capillary is approaching its maximum. This indicates that the plasma is fully ionized and that the desired channel structure of the plasma has been formed. These observations are in good agreement with numerical simulations [122, 123] and interferometric measurements [57, 121]. In the spectral measurement shown in Fig. 5.18, despite the likely assumption that the plasma is fully ionized, we still observe that the peak of the spectrum shifts by about 10 nm to shorter wavelengths. This may be due to laser induced ionization of neutral (or partially ionized) H_2 gas outside the capillary, in the vacuum-plasma transition regions in front of the capillary and behind it. However, the spectral signature of this effect seems to be small and one may thus conclude that also the temporal perturbation of the transmitted laser pulse is small.

Further delay (t=190 ns) resulted in a degradation of the transmitted beam profile as can be seen in the image 5 in Fig. 5.17. The measured current through the capillary is decreasing in this period. This indicates that the channel structure of the plasma is weakened and about to disappear. Plasma density measurements using interferometry [121] indicate that partial recombination of electrons and ions occurs in this period and the channel profile becomes more shallow, thus loosing its waveguiding property. Furthermore, we observed that the time window for a

good guiding is about 100 ns which is in good agreement with experimental results reported in references [121, 124, 125].

5.6 The electron spectrometer

The last part of the experimental setup is a diagnostic device which will be used to measure the energy spectra of the accelerated bunches by the laser wakefield. In figure 5.19 we present an overview of the electron bunch diagnostic as installed so far. The electron spectrometer is placed at about 50 cm behind the plasma channel, and a phosphor screen (Kodak Lanex) placed about 70 cm behind the spectrometer. The electron spectrometer is based on a dipole magnet where electrons with different energies are deflected to different angles. In order to distinguish the light generated by the bunch from the transmitted drive laser light, a 13 μm thick aluminium foil is used to block the transmitted drive laser. The foil is placed about 20 cm in front of the screen. Fluorescence images generated by bunches arriving on the screen can then be captured with a gated CCD camera (4 Picos Stanford Computer Optics Inc.).

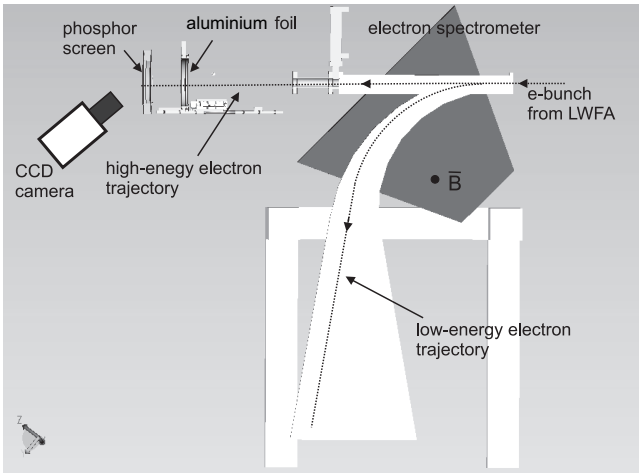

Figure 5.19: Overview of our diagnostic setup to measure the energy spectra of electron bunches from laser wakefield acceleration

The measured magnetic flux of the spectrometer is adjustable but limited to a maximum of 284 mT. This field strength would bend electrons with a kinetic energy of 25 MeV by an angle of 90° with respect to the direction of the input beam. The high-energy bunches, as we expect to generate with laser wakefield acceleration, would make a much smaller angle and go almost straight to hit the phosphor screen. We estimate that for the case of a 750 MeV bunch, the spot would be located at about 18 mm below the propagation axis at a deflection angle of only 1.5 degrees.

5.7 The timing and synchronization

Our front-to-end modeling of laser wakefield acceleration with external bunch injection as described in chapter 4, yielded a set of optimum parameters for an experimental demonstration. Most of these parameters were then experimentally realized as described in previous sections. One central parameter in the model is the proper timing of the external bunch injection with regard to the wakefield. Our special injection scheme is extremely tolerant in the sense that even long (subpicosecond) bunches are trapped and compressed into a bunch of femtosecond duration. However, not only a low relative energy spread is achieved but also a low shot-to-shot fluctuations of the kinetic energy, the scheme requires a timing with a precision on the scale of a picosecond.

In this section, we describe the realization of a suitable timing scheme. This scheme serves two goals. The first is to set the injection time of the drive laser pulse and the electron bunch to the time window in which the plasma channel is ready for waveguiding. The second goal is to synchronize the phase of the rf field and the laser pulse on the cathode inside the linac for the named mutual timing of the injected bunches with regard to the wakefield. This is done by a phase-locking of the 16^{th} harmonic of the laser oscillator repetition rate to the 1.3 GHz microwave master oscillator of the rf-linac. For this, the cavity length of the laser oscillator is adjusted such that the repetition rate of the laser oscillator follows the frequency of the microwave master oscillator.

To explain the working of the synchronization to more detail, the timing scheme for our laser wakefield acceleration experiment is shown in figure 5.20. A 1 Hz signal from a pulse generator is used to trigger the timing module of the linac. After being triggered, this module sends out a 1 Hz signal to trigger the various sub-systems of the linac, including the klystron, a high voltage pulse line, and also to trigger the timing module (Thales masterclock) of the laser system. Further, the masterlock is set to use an external clock derived from the repetition rate frequency of the Ti:Sa laser oscillator (81.25 MHz). This is done to reduce the jitter between the optical pulses and the electrical pulses generated by the masterclock. The masterclock also sends out a 1 Hz signal to trigger the Pockels cells of the pulse picker and the pulse cleaner in the laser amplifier chain, as well as a thyratron that applies the discharge voltage across the capillary. This 1 Hz signal is also used to trigger the Q-switches of the pump lasers. However, the flash lamps of the pump lasers require a trigger signal at 10 Hz repetition rate in order to maintain temperature of the Nd:YAG rods in the pump laser in order to maintain the specified beam parameters for the pump laser output. The 10 Hz trigger pulses are generated by a pulse generator. However, we observed a large jitter of about 100 ns between the 10 Hz signal and the 1 Hz signal delivered from the linac's timing module. This jitter is too large, particularly, for our regenerative amplifier where pumping of the gain crystal and the extraction of an amplified pulse requires a time precision of less than one nanosecond. This jitter is due to the fact that the timing module of the linac has its own free running internal clock with a frequency of 10 MHz. To synchronize these signals, we built a synchronization device (sync.1 in Fig. 5.20) which has function to exchange one

out of every ten pulses in the 10 Hz pulse train with the pulse triggered by the 1 Hz timing module of the linac. This means that one of every ten pulses in the 10 Hz train always matches the 1 Hz signal. Then, this 10 Hz signal is used as the second reference for the masterclock which triggers the flash lamps of the pump lasers.

Since, the Pockels cell of the pulse picker is triggered with the same signal as the thyratron of the plasma channel, we observed no jitter between the arrival time of the laser pulse at the plasma channel and the trigger signal of the thyratron. However, after the thyratron was switched on, the discharge current through the channel was observed to have a jitter of about 12.5 ns. In order to verify whether this 12.5 ns jitter can be tolerated, we compared this time jitter with the time window where a proper guiding in the plasma channel was observed. Since long guiding window of the plasma channel was measured to be about 100 ns [121, 124, 125], this jitter does not seem to be a problem.

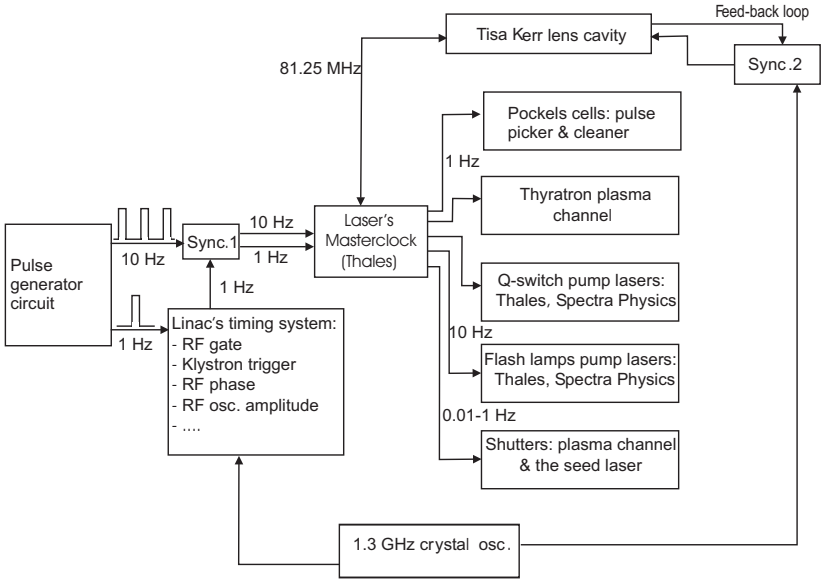

Figure 5.20: Timing and synchronization scheme for our laser wakefield acceleration experiment

For optimum bunch acceleration inside the linac, the electrons have to be injected at a specific phase of the rf field (the optimum launching phase). This means that the arrival time of the laser pulse on the cathode has to be synchronized to the rf phase with high precision. For this purpose, we have built a synchronization circuit (sync. 2 in Fig. 5.20) which is based on phase-locking of the 16^{th} harmonic of the laser oscillator repetition rate to the microwave master oscillator of the linac. For this circuit, we used the same approach as used in the synchronization at DESY in Hamburg [126], because their tests had shown a sufficiently low jitter of better than 1 ps. To explain the working of our circuit, a block diagram of the

synchronization setup is presented in figure 5.21. The 81.25 MHz frequency of the laser pulse is detected by a very fast photodiode, which converts the light pulses to electrical pulses. These pulses contain many harmonics of the laser repetition frequency which make it possible to extract the 16^{th} harmonic component with a bandpass filter resulting at a frequency near 1.3 GHz. Further, the phase of the extracted 1.3 GHz oscillation is compared with a mixer to the reference phase originating from the 1.3 GHz master oscillator of the linac. If the phases are not equal, the mixer outputs an error signal. This signal enters a lowpass filter to eliminate higher frequencies, e.g., the remaining 1.3 GHz, before it enters a PI (Proportional-Integrator) regulator circuit. This regulator has the function of evaluating the error signal and generating a signal that can be used for the necessary adjustment of the laser repetition rate. The repetition rate of the laser is changed via the cavity length by moving the outcoupling mirror with a piezo transducer. With this synchronization, we measured a time jitter of about 3 ps. In the next section, we will describe the expected effects of this 3 ps jitter on the accelerated bunch from laser wakefield acceleration.

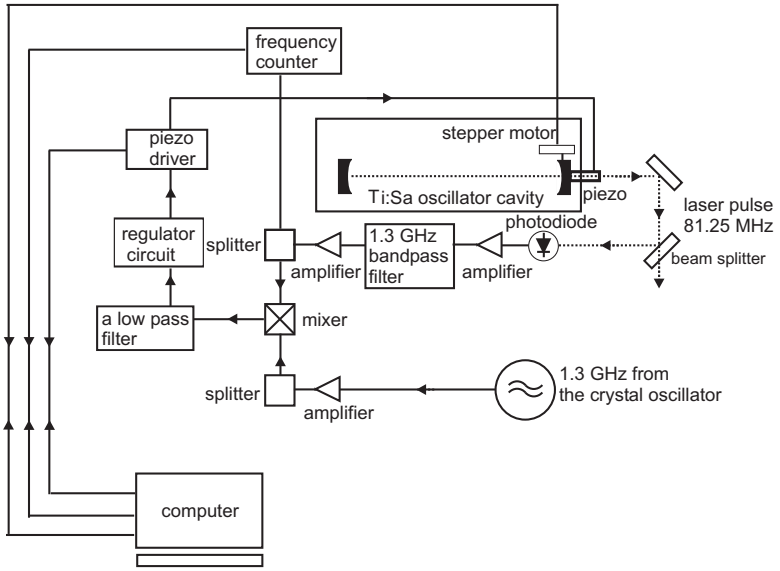

Figure 5.21: Block diagram of the synchronization circuit used to phase-lock the microwave master oscillator [126]

5.7.1 Expected shot-to-shot energy fluctuations

As we have discussed in chapter 4 (section 4.2) electrons from the photo-cathode need to be injected in the optimum phase of the rf field to achieve a proper acceleration in the linac. For this injection, the arrival time of the laser pulse on the

cathode is to be synchronized to the optimum phase of the rf field with a high precision. Typically such synchronization requires a time precision of a fraction of the rf period, e.g., a ps-precision for the given 1.3 GHz rf frequency. However, in the experiment there is always some residual jitter as illustrated in figure 5.22 and here we inverstigate its influence on the subsequent wakefield acceleration. When the injection phase is set at φ_0, the laser pulses will arrive at the cathode at different phases of the rf field around the set point due to the time jitter ($\Delta\varphi_0$) of the laser pulse with regard to the rf phase. As a consequence, the emitted electron bunches experience a different initial rf phase in each individual shot which leads to a shot-to-shot energy fluctuation after acceleration in the linac. As these electron bunches are to be transported to the plasma channel, they would arrive at different times with regard to the arrival time (Δt_0) of the drive laser pulses. As a consequence, these injected bunches would be trapped at different longitudinal positions inside the plasma channel for each shot and leaving different lengths for the remaining acceleration. This results in a shot-to-shot energy fluctuation of the average kinetic energy of the accelerated bunch.

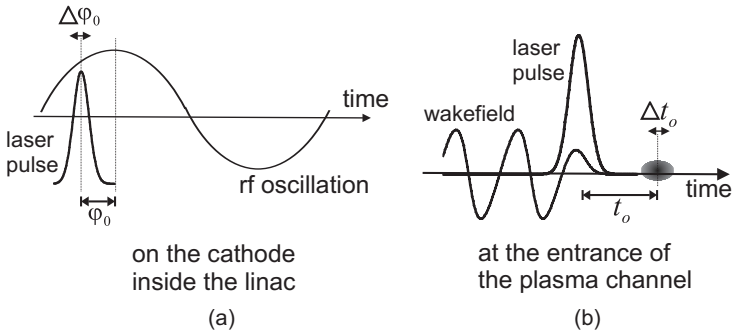

Figure 5.22: Part (a), illustration of the time jitter between the arrival time ($\Delta\varphi_0$) of the laser pulses and the optimum phase of the rf field on the cathode inside the linac. Part (b), illustration of the arrival time jitter (Δt_0) of the injected bunches with regard to the drive laser pulses inside the plasma channel.

After this qualitative discussion, we continue to give also a quantitative estimation of its importance for the 3 ps timing jitter that we have measured. Based on our calculations in chapter 4, the optimum launching phase of our linac was found to be $\varphi_0 = -0.85$ rad. By varying the launching phase around this optimum phase, we calculated the arrival time of the bunch at the entrance of the plasma channel. These calculations were done by using the optimized parameters of the beam transportation line as presented in chapter 4. The results of the calculations are displayed in Fig. 5.23(a) where the calculated arrival time is plotted versus the launching phase. The optimal launching phase is indicated as the vertical line and the corresponding arrival time is set to zero in the graph as a reference time. One can

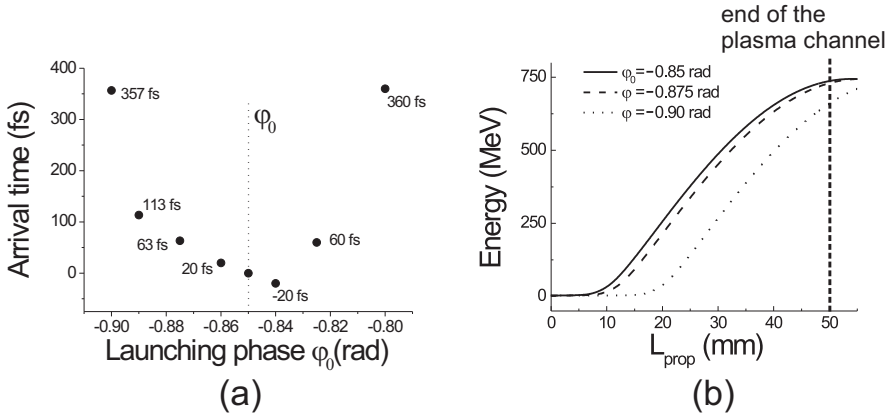

Figure 5.23: In part (a), the calculated arrival time of the laser pulse at the entrance of the plasma channel for different launching phases. In part(b), the calculated bunch energy during acceleration in the laser wakefield acceleration for three launching phases as calculated in part (a).

see that with ±0.025 rad deviation from the optimum launching phase ($\varphi_0 = -0.85$ rad), which corresponds to about ±3 ps time interval, the bunch would arrive at the plasma channel about 60 fs later than when the bunch was launched at $\varphi_0 = -0.85$ rad. This arrival time delay increases considerably for larger deviations. To calculate the influence of such variations in arrival time on the wakefield acceleration, we used the same wakefield as presented in chapter 4 (section 4.5). As examples, in figure 5.23(b) we plot the calculated bunch energy during acceleration in the laser wakefield for bunches launched at $\varphi = -0.85$, -0.875 and -0.9 rad. One can see that after acceleration over 5 cm, for $\varphi = -0.875$ rad (delay of 3 ps with regard to the optimum phase), the bunch energy would only be reduced by a small fraction of 1 % compared to the optimum launching phase. For comparison, a much more noticeable reduction of the bunch energy is calculated for launching at the $\varphi = -0.9$ rad (6 ps delay). Namely, in this case, the energy of the accelerated bunch is found to be 10% lower, which is a ten-fold decrease with regard to a 3 ps delay although the delay has only doubled. We conclude from this that our synchronization, which gives an experimentally proven precision of better than 3 ps, would lead to a shot-to-shot energy fluctuation of about 1%, which is comparable to the intrinsic energy spread of about 1% (from the acceleration process as described in chapter 4), and can thus be tolerated in a first experiment.

5.8 Summary

In summary, we have successfully designed, constructed and tested an experimental setup that would allow the first demonstration of laser wakefield acceleration

with external bunch injection. Our laser delivers 12 TW peak power and is focused to the entrance of a plasma channel to generate a laser wakefield suitable to demonstrate trapping, bunch compression and acceleration. Electron bunches, which have to be injected into the wakefield, are produced by a linac and transported into the channel via a bunch transportation line. The parameters found in electron bunch propagation experiments are in good agreement with our design values. Furthermore, a plasma channel that guides the drive laser pulse, was designed based on a pulsed discharge in a hydrogen filled-capillary. Test experiments showed that the plasma channel works as expected and that the measured parameters are in good agreement with those reported by other groups.

A successful guiding experiment of the high intensity drive laser pulses was achieved in a 3-cm-long capillary discharge waveguide. The capillary was filled with hydrogen gas at a filling pressure of 46 mbar and pulsed with a charging voltage of 24 kV. With proper timing of the discharge, we confirmed that the laser profile at the exit of the capillary possesses a Gaussian profile distribution as expected from single-mode propagation through the plasma waveguide. A small spectral blueshifting was measured in the laser spectra which we interpret as caused by laser ionization induced self-phase-modulation in residual neutral hydrogen in front and behind the otherwise fully ionized plasma in the channel. The measured time window available for waveguiding is found to be about 100 ns long, which is much larger than any possible jitter in the experiment. In contrast, outside this time window, we observed bad guiding visible as an irregular beam profile and a weak pulse intensity at the exit of the channel. Moreover, in this case, the spectra showed a strong spectral blueshifting.

Further, we setup a diagnostic device to resolve the energy spectra of electron bunches accelerated by a laser wakefield accelerator. Finally, we synchronized the arrival time of the laser pulse to the phase of the rf field on the cathode with a precision better than 3 ps. We calculated that this precision is well tolerable for a first demonstration experiment because the resulting 1% shot-to-shot energy fluctuation of electron bunches after acceleration are as small as the intrinsic energy spread from the wakefield acceleration.

6

Summary, conclusions and following steps

This thesis has described the modeling, design and setup of an experiment which aims on the first demonstration of laser wakefield acceleration with external electron bunch injection. Our comprehensive modeling of the entire laser wakefield accelerator predicted that such an accelerator could generate relativistic electron bunches of high quality and extremely short durations over a very short acceleration distance in a controlled manner. Such bunches can open the way for subsequent research steps in the forefront of relativistic interaction of light with matter.

The key problem we have addressed in this thesis is the, so-called, injection problem. To obtain a high-quality electron bunch from laser wakefield acceleration, the bunch must be injected into the plasma wave with high temporal and spatial precision of the order of a fraction of the plasma wavelength, which is typically only a few tens of microns. These requirements demand extremely small sizes in both transverse and longitudinal directions of the bunch, and temporal and spatial control on a femtosecond time- and micrometer scale, respectively. Such small dimensions are considered beyond the state-of-the-art of technology and thus alternative injection methods need to be found.

To provide a solution to the injection problem, a novel method to inject an electron bunch with large dimensions into a laser wakefield had been proposed by one of us [21–23]. This method was implemented into the design criteria of the experimental setup presented in this thesis. In that approach, an electron bunch provided by a conventional linear accelerator is injected into a plasma channel shortly before the arrival of a high-intensity laser pulse. In the channel, the bunch is then overtaken by the laser pulse. Subsequently, the excited wakefield follow-

ing the laser pulse traps, compresses and accelerates the bunch to ultra-relativistic energies. Based on our theoretical calculations, it is expected that this results in bunches of unprecedented small dimensions; micrometer-sized femtosecond electron bunches with low energy spread.

This thesis describes the essential experimental steps taken toward the first demonstration of laser wakefield acceleration with external bunch injection:

Step 1: Front-to-end modeling and design of the experiment
The very large number of parameters involved makes careful design of the complete system crucially important. In order to reduce the risk of failure in the experiment, we comprehensively modeled of the entire laser wakefield accelerator. The model covers all necessary steps including: the generation of an electron bunch from a photo-cathode, bunch propagation and pre-acceleration in an rf-linac, temporal bunch compression, and focusing of the bunch with magnetic fields. Finally the model describes injection, trapping and acceleration of this bunch in a wakefield generated by a multi-TW laser pulse guided in a plasma channel. After a careful analysis and optimization, we have chosen the most promising combination of the operational parameters that we can access.

The optimization was done based on the requirement that the drive laser pulse and its wakefield should overtake the bunch within a fraction of the acceleration length. This is necessary in order to obtain a low relative energy spread after the acceleration process. To enable the use of existing plasma channel technology, which yields plasma channels with length of typically 5 cm, the duration and kinetic energy of the injected bunch were chosen such that the bunch is compressed toward the region where a maximum accelerating wakefield exists within a propagation distance of approximately 1.8 cm. Our model of laser wakefield acceleration predicts a maximum energy of around 750 MeV, with a relative energy spread of about 1%, obtained after acceleration in a 5 cm long plasma channel. Note that this output energy is comparable to that from a conventional accelerator, which would have a large size. With the experimental design presented here, equal ouput seems to be possible but with acceleration on a centimeter-scale.

Step 2: Construction of the experimental setup
To demonstrate the approach, we have constructed an experimental setup based on the optimized parameters obtained from the modeling. The main elements of the setup include: a multi-TW laser system, a capillary discharge plasma channel, a photo-cathode rf-linac, and an electron beam transportation line. Furthermore, we developed a timing and synchronization scheme and devices, which allows the elements mentioned operate in a mutually synchronized fashion.

As the first element, we have constructed a laser system using the technique of chirped pulse amplification. The laser system uses Ti:Sa crystals as the gain medium and currently produces a pulse energy of about 475 mJ with a duration of 40 fs which corresponds to a peak power of about 12 TW. The laser pulse is focused into the entrance of the plasma channel where we measured a spot size of 40 μm and 35 μm in the transverse x- and y-directions, respectively. In the focus, we estimate

a peak intensity of 5×10^{17} W/cm^2. When comparing these laser parameters, particularly the pulse energy, to those we used in the modeling described in chapter 4, the pulse energy is about a factor of 2.1 lower. This choice is made for speeding up the basic demonstration experiments before attempting to obtain refined and improved results via further increasing the peak power. Our model was used in order to investigate the influence of our experimentally available laser parameters (the pulse energy, duration and peak intensity) on the generation of the wakefield and the acceleration process. We found that the minimum kinetic energy for the injected electrons to be trapped (trapping threshold) on the axis of the generated wakefield is ≈1.9MeV. This is about a factor of 4 higher than to the trapping threshold found in the initial calculations as described in chapter 4. This is well within the kinetic energy that can be delivered by the rf-linac but, as a first consequence, one would expect a reduction of the number of trapped electrons in the wakefield. In the calculations, where we injected a 5 pC bunch, we obtained a trapping efficiency of ≈7 % (0.35 pC) instead of ≈48 % (2.4 pC) with full laser power. A second consequence is that the final bunch energy (after the wakefield acceleration) would decrease due to the lower amplitude of the generated wakefield. We calculate that the latter amounts to about a factor of 3.6. After acceleration over 5 cm in the channel, the final bunch energy would then about 200 MeV with a relative energy spread of about 2 %.

In order to determine whether the final bunch parameters, particularly the lower charge of the bunches, can be tolerated for the demonstration experiment, we continue the analysis by considering our detection system. To detect the accelerated bunch, a phosphor screen (Kodak Lanex) is installed at a position of about 1.4 m behind the plasma channel, at the location of the electron spectrometer. As the screen is hit by electrons the emitted light will be captured by a gated CCD camera. Our model described in chapter 3 predicts that the radius of the expected (0.35 pC) bunches from the laser wakefield acceleration would grow to about 3.5 mm, resulting in a number of electrons per unit area of 6×10^4 electrons/mm^2, at the phosphor screen. Masuda, et.al. [127] reported that a phosphor screen (Kodak Lanex) can detect electron concentrations as low as 10^4 electrons/mm^2. Accordingly we can expect that this 0.35 pC bunch can be detected with our detection system.

Based on these recent calculations, the planned demonstration experiment for laser wakefield acceleration with external bunch injection can indeed be carried out using the current laser parameters. Later, after the demonstration experiment, we expect to improve the final bunch parameters (bunch energy, trapping efficiency and energy spread) by increasing the output energy of our laser system and thereby the amplitude of the generated wakefield. For the latter modification we have an additional pump laser available.

As the next essential element, we have carefully designed and constructed the electron beam transportation line which functions as a temporal and transverse bunch compressor. Measurements of the magnetic fields of the individual magnetic elements revealed parameters which are in good agreement with the design values. This indicates that the temporal compression and spatial focusing properties of the constructed beam transportation line are comparable with those we used

in the numerical model. Due to heat dissipation inside the coils of the magnetic elements and the maximum current that can be delivered by the power supplies, we concluded that the beam line could transport electron bunches as desired with a maximum kinetic energy of about 4 MeV.

The smallest element, the plasma channel, is formed inside an alumina capillary filled with a hydrogen gas that is fully ionized with a pulsed discharge. The filling pressure, which determines the on-axis plasma density, is chosen such that a resonant wakefield is excited by the laser pulse. Based on the current pulse duration, we calculated that a filling pressure of about 46 mbar is required. Further, the choice of the radius of the capillary ($\approx$153 μm) was based on the requirement of optimum guiding of the laser pulse through the channel for a given filling pressure, i.e., the channel radius is such that it matches the laser spot size at the entrance of the capillary.

Finally, we have synchronized the drive laser pulse, the injected electron bunch and the plasma channel with various synchronization devices that span in largely different time intervals, from the range of seconds to the range of picoseconds. A time jitter of about 12.5 ns was measured between the discharge current in the plasma channel and the arrival time of the drive laser pulse at the channel. Note that this jitter is much smaller than the time window (of about 100 ns) in which good guiding was observed. Further, we measured a time jitter better than 3 ps between the phase of the rf field of the linac and the arrival time of the laser pulse on the cathode inside the linac. Based on our calculations, this time jitter would lead to a shot-to-shot fluctuation of the final bunch energy of less than 1 % after the laser wakefield acceleration process. After the demonstration experiment, the next experimental step would be the improvement of the synchronization device to achieve a time jitter better than 1 ps.

Step 3: Essential tests of the experimental setup
After the individual elements, such as the TW laser, the rf-linac, the electron beam transportation line and the plasma channel, had been tested separately, we performed two essential experiments involving the complete setup. The first experiment performed was bunch generation and pre-acceleration inside the linac followed by bunch propagation through the beam transportation line to the entrance of the capillary. Based on the results of this experiment, we determined the energy of the bunch and its shot-to-shot energy fluctuation discovering that both were fully in the planned range. Secondly, we performed an experiment of guiding high-intensity laser pulses through the plasma channel. Based on the analysis of the spatial, temporal and spectral properties of the transmitted laser pulse, we observed successful waveguiding within a certain, optimum temporal window after the ignition of the discharge as expected. These experiments show that our experimental setup works and is ready for the laser wakefield acceleration experiment planned within the year 2009.

6.1 Following steps

In this part, we discuss some final issues that will become important during the subsequent demonstration experiments. These issues serve to guarantee with some experimental procedures that the electron bunch from the linac will have a sufficiently good overlap, temporally as well spatially with the wakefield in the plasma channel. More specifically, the spatial overlap needs to be controllable on the scale of a few tens of micrometers and the temporal overlap on the scale of a few picosecond. If the goal was to overlap *two light pulses* with the previously named precision, this would certainly be an easy task. Both micrometer and picosecond precision can easily be checked, e.g. by relying on a nonlinear effect in a suitable medium, such as in an intensity cross-correlation experiment using a nonlinear optical crystal. Here, however, the goal is to overlap a pulse of *light (photons)* with a bunch of *particles (electrons)*. Then a cross-correlation is not trivial at all. The reason for this is that it is difficult to find physical effects that depend on the parameters of both *photons* and *electrons*, and which is also a strong effect suitable for experimental observation. A known possibility for measuring temporal overlap is what is called electro-optical gating [128, 129], which works as follows. The bunch is sent along the side of a nonlinear optical crystal, such that the Coulomb field of the bunch induces a transient change of the refractive index in the crystal. This change can then be probed with the light pulse, provided that the bunch and the pulse are propagating in parallel with sufficiently a small delay. The installment of such electro-optical gating is, however, quite complex and it is not of much use for measuring spatial overlap as well.

Our strategy for performing such an experiment is as follows. We will make use of optical radiation (called transition radiation) [2]. Such radiation is instantaneously generated when relativistic electrons cross the interface between two media, such as the surface of an aluminium foil (interface between vacuum and metal). The emission time of the generated radiation can then be compared with the arrival time of the drive laser pulse with a sufficiently fast optical detector. For detecting the radiation (picosecond precision as was discussed in the end of chapter 5) we will make use of a streak camera. The technique, to measure the passage of the bunch via transition radiation has the additional advantage that the properties of the emitted radiation closely resembles the spatial properties of the bunch.

The next issue is that of a proper spatial alignment of the electron bunch with the laser pulse along the axis of the plasma channel and the wakefield structure. Keeping the capillary at a fixed position and then steering the electron bunch through the capillary would be an intricate approach. The reason is that it is experimentally difficult to steer the location of an electron beam independent from its direction of propagation. Particularly as the steering would need to be carried out with high precision, given the rather high aspect ratio of the wakefield structure and the capillary (about 60 μm width of the wakefield structure and about 306 μm inner diameter of the capillary, compared with 5 cm length of the capillary).

To overcome this problem, we will use the propagation axis of the injected bunch as the reference for the alignment of the plasma channel, as well as for the laser

beam. For this purpose the capillary is mounted on a high accuracy motorized 5-axis alignment stage, while the parabolic focusing mirror for the laser beam and a preceding mirror is equipped with a motorized precision alignment as well. On the capillary alignment stage, we also installed two phosphor screens, one placed at the front side of the capillary and the other one at the backside. The front phosphor screen carries a pinhole of the same diameter as the inner diameter of the capillary and which is on axis with the capillary. As the first step, we align the capillary with regard to the electron bunch by observing a light signal from the back phosphor screen, captured by our gated CCD camera. A good alignment is indicated by the brightest light signal from the back phosphor screen and when, at the same time, there is no signal observed from the front phosphor screen. This indicates a maximum number of electrons propagating through the pinhole as well as through the capillary. After this alignment process is completed, these phosphor screens can be slid out of the beam path but can also be put back in a reproducible manner to the original position. As the final step, the beam of the drive laser is aligned to get optimum waveguiding through the plasma channel as was presented in chapter 5 (section 5.5.1).

After the named alignment procedure, the main experiments are to be performed. As the first step we fine-tune the time delay between the laser pulse and the injected bunch. Upon such tuning, the goal is to observe at the phosphor screen placed behind the electron spectrometer a tiny spot of fluorescence, indicating that electron bunches are arriving with only a few millimeters in size. In this first experiment the magnetic field of the spectrometer can be switched off as only the effect of proper timing between bunch injection and wakefield is being investigated. In this case bunches from the capillary would propagate in a straight line toward the screen. The relatively small size of the expected fluorescent spot (about 1.4 m behind the exit of the plasma channel) would be indicative for a successful acceleration of the electrons due to the small divergence angles (order of mrad) that have been observed with bunches from other laser wakefield experiments (e.g. in the bubble regime). In contrast, when there is no laser wakefield acceleration, the divergence of the bunch (and thus the size of the fluorescent spot) would be expected to be much larger, namely as large as given by the bunch and focusing parameters of the linac and the beam transportation line. After having obtained the optimum time delay, for the second step we plan to investigate the energy distribution of the accelerated bunches by turning on the magnetic field of the spectrometer. Based on the deflection distance of the spot at the phosphor screen with regard to the initial position of the spot, this should reveal information about the kinetic energy spectra of the electron bunches. Similar measurements would aim to maximize the trapping efficiency, for which the timing as well as the spatial alignment will be optimized. The experimental data can then be compared with the theoretical prediction as in chapter 4 and this could provide a first confirmation of the proper working and control of laser wake field acceleration with external bunch injection.

A

A.1 Electron beam theory

A.1.1 Liouville's theorem

The state of a bunch, consisting of N particles which are clustering in a small volume, is normally described by a density function in the six-dimensional phase-space, i.e., $f(\boldsymbol{r},\boldsymbol{p})$ where $\boldsymbol{r}$ and $\boldsymbol{p}$ each contain three position and momentum coordinates, respectively. The number of particles in an infinitesimal volume dr^3dp^3 in the phase-space at a time t is $dN = f(\boldsymbol{r},\boldsymbol{p},t)dr^3dp^3$. Assuming that there are no collisions between particles, that emission or absorption of electromagnetic radiation by the particles can be neglected and that the collective macroscopic field arising from the bulk beam charge and the current density is very small [94], the evolution of the phase-space density function, $f(\boldsymbol{r},\boldsymbol{p})$, under the influence of a Hamiltonian force can be described as follows:

$$\frac{df}{dt} = \frac{\partial f}{\partial t} + \sum_i^N \left(\frac{d\boldsymbol{r}_i}{dt} \cdot \nabla_{\boldsymbol{r}_i} f + \frac{d\boldsymbol{p}_i}{dt} \cdot \nabla_{\boldsymbol{p}_i} f \right).$$

Since $dr/dt = \partial H/\partial p$ and $dp/dt = -\partial H/\partial r$, we have

$$\begin{aligned} \frac{df}{dt} &= \frac{\partial f}{\partial t} + \sum_i^N \left(\frac{\partial H}{\partial p_i}\frac{\partial H}{\partial r_i}\frac{df}{dH} - \frac{\partial H}{\partial r_i}\frac{\partial H}{\partial p_i}\frac{df}{dH} \right), \\ \frac{df}{dt} &= \frac{\partial f}{\partial t}. \end{aligned}$$

If neither creation nor destruction of the particles are allowed, Liouville's theorem states that the phase space density of the particles in a Hamiltonian system is conserved ($\partial f/\partial t = 0$), which yields

$$\frac{df}{dt} = 0. \tag{A.1}$$

A.1.2 Electron motion in a magnetic field

An electron experiences the Lorentz force, i.e., $\boldsymbol{F} = -e[\boldsymbol{E} + (\boldsymbol{v}/c \times \boldsymbol{B})]$ as it travels through an electromagnetic field. As an illustration, shown in Fig. A.1, when an electron moves in the horizontal plane (the x-z plane) through the homogenous transverse magnetic field (B_y) there is a balance between the Lorentz force and the centrifugal force. This yields a circular orbit, where the radius R depends on the electron momentum p_0 and the strength of the magnetic field B_y. This relation between the named parameters is also known as the cyclotron relation:

$$\frac{1}{R} = \frac{e}{cp_0} B_y. \tag{A.2}$$

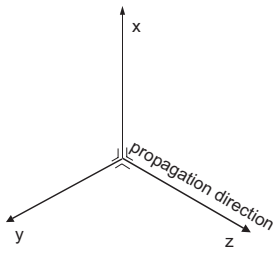

Figure A.1: Cartesian coordinate to describe the propagation of an electron in a magnetic field.

The magnetic field around an electron can be regarded as a sum of multi-poles (see eq. (A.3), each of which has a different effect on the beam path.

$$\begin{aligned} \frac{e}{cp_0} B_y(x) &= \frac{e}{cp_0} B_y(0) + \frac{e}{cp_0} \left[\frac{dB_y}{dx} \right]_{x=0} x + \frac{1}{2!} \frac{e}{cp_0} \left[\frac{d^2 B_y}{dx^2} \right]_{x=0} x^2 + \\ &\quad \frac{1}{3!} \frac{e}{cp_0} \left[\frac{d^3 B_y}{dx^3} \right]_{x=0} x^3 + \ldots \\ &= \frac{1}{R} + kx + \frac{1}{2!} mx^2 + \frac{1}{3!} ox^3 + \ldots, \end{aligned} \tag{A.3}$$

where $1/R$ is named the dipole field component, which is used to steer the beam. The term kx is the quadrupole field, which yields a beam focusing effect. The third term which describes the sextupole field $mx^2/2!$ can be used to compensate for chromaticity. The octupole field $ox^3/3!$ can used to compensate higher-order errors. In fact, each field component can be applied independently by using a corresponding magnetic element. These elements form the basics to design a transport beam line in accelerators.

In order to study a trajectory followed by an electron as it moves in a magnetic systems, a transformation from the cartesian coordinates to curvilinear coordinates is needed [2]. In case of linear beam optics where only the two lowest

multipoles are considered, i.e., dipole and quadrupole, the general equation of motion of the electrons can be written as follows:

$$\begin{aligned} x''(z) + \left[\frac{1}{R^2(z)} - k(z)\right] x(z) &= \frac{1}{R(z)} \frac{\Delta p}{p_o}, \\ y''(z) + k(z)\, y(z) &= 0, \end{aligned} \tag{A.4}$$

where $x(z)$ and $y(z)$ are the position of electron in x- and y-axis as a function of z. x'' and y'' are the second derivatives of $x(z)$ and $y(z)$ in respect to z. The momentum deviation Δp is $\Delta p = p - p_0$ and the quadrupole strength $k(s) = (e/cp_0)dB_y/dx$. The quadrupole is focusing if $k(s) < 0$ and defocusing if $k(s) > 0$. The solution of equation (A.4) is the basis for the transfer matrix formalism of the beam optics.

A.1.3 Transfer matrix

The transfer matrix theory describes particle motion relative to a known main equilibrium orbit. It employs two assumptions, i.e., firstly, particle motions are paraxial and secondly, the transverse focusing force varies linearly with displacement from the main axis and is independent of the transverse velocity. By using the transfer matrix method, one can easily trace an electron trajectory through a system of magnetic elements. In this method, a magnetic element is represented as a matrix **M** whose determinant is equal to 1. At any arbitrary position in the beam line, an electron can be represented as a vector (single column matrix) whose components are the position, angle, and the momentum. If the initial condition for an electron is $(x_0, x_0', y_0, y_0', z_0, \delta_0)$, where x and y are lying on the transverse plane, z and $\delta = \Delta p/p_0$ are on the propagation axis with p_0 the momentum, the electron after a magnetic element **M** can be described as

$$\begin{pmatrix} x_1 \\ x_1' \\ z_1 \\ z_1' \\ l_1 \\ \delta_1' \end{pmatrix} = \mathbf{M} \cdot \begin{pmatrix} x_0 \\ x_0' \\ z_0 \\ z_0' \\ l_0 \\ \delta_0' \\ , \end{pmatrix}$$

where **M** is

$$\begin{pmatrix} R_{11} & R_{12} & 0 & 0 & 0 & R_{16} \\ R_{21} & R_{22} & 0 & 0 & 0 & R_{26} \\ 0 & 0 & R_{33} & R_{34} & 0 & 0 \\ 0 & 0 & R_{43} & R_{44} & 0 & 0 \\ R_{51} & R_{52} & 0 & 0 & 1 & R_{56} \\ 0 & 0 & 0 & 0 & 0 & 1 \\ . & & & & & \end{pmatrix}$$

The matrice element for the matrix **M** are actually the solution of the equations (A.4). In a system of magnets, the total transfer matrix can be obtained by multiply-

ing the transfer matrix for each element.

$$\mathbf{M_T} = \mathbf{M_N} \cdots \mathbf{M_2} \cdot \mathbf{M_1}. \tag{A.5}$$

For example, a bending magnet, in which the magnetic field is directed along the y-axis and assuming $\Delta p/p_0 = 0$, the matrix $\mathbf{M}$ of the bending magnet has the components $R_{11} = \cos(s/R)$, $R_{12} = R\sin(s/R)$, $R_{21} = -1/R\sin(s/R)$, $R_{22} = \cos(s/R)$, $R_{33} = 1$, $R_{34} = s$, $R_{43} = 0$, $R_{44} = 1$ and the remaining components are zero. The parameter R is the Lamour radius and s is the propagation axis.

A.1.4 Magnetic compression

A longitudinal compression of an electron bunch canachieved by propagating the beam through a dispersive beam line with an energy dependent path length. In this beam line, electrons with a higher energy will travel a longer distance than a lower energy electrons, and the bunch becomes shorter. In order to design the bunch compressor, one needs to know the time-energy correlation (chirp) of the initial bunch. Usually, this relation shows a non-linear dependency due to a higher order harmonic of the rf field in the accelerator or an energy modulator. Then, one needs to find an appropriate compressor scheme to compensate the chirp, e.g., so-called chicane, s-chicane, F0D0 arc, dog-leg [95]. In our case, we found that electrons at the head of the bunch have higher energy than those at the tail of the bunch for which we adapt a compression section which provides 90 degree turn in total. The compressor has two-subsequent 45 degree bending magnets with a focusing quadrupole in the middle. The first-order transfer matrix for our compressor is follows:

$$\mathbf{M_{Com}} = \mathbf{M_{bend2}} \cdot \mathbf{M_{drift2}} \cdot \mathbf{M_{quad}} \cdot \mathbf{M_{drift1}} \cdot \mathbf{M_{bend1}}. \tag{A.6}$$

where $\mathbf{M_{bend1}}$ and $\mathbf{M_{bend2}}$ are the transfer matrix for the first and the second 45-degree bending magnet. $\mathbf{M_{quad}}$ and $\mathbf{M_{drift}}$ are the transfer matrix for the quadrupole and the drift motion in free space between the bending magnet and the quadrupole.

Bibliography

[1] T. Tajima and J. M. Dawson. *Laser electron accelerator*. Phys. Rev. Lett., 43:267, 1979.

[2] K. Wille. The physics of particle accelerators. Oxford University Press, Great Clarendon Street, Oxford OX2 6DP, 2000.

[3] D. Strickland and G. Mourou. *Compression of amplified chirped optical pulses.* Optics Comm., 56:219, 1985.

[4] P. Maine, D. Strickland, P. Bado, M. Pessot, and G. Mourou. *Generation of ultrahigh peak power pulses by chirped pulse amplification.* IEEE J. Quantum Electron., 24:398, 1988.

[5] D. Umstadter, S.-Y. Chen, A. Maksimchuk, G. Mourou, and R. Wagner. *Nonlinear Optics in Relativistic Plasmas and Laser Wake Field Acceleration of Electrons.* Science, 273:472, 1996.

[6] A. Modena, Z. Najmudin, A. E. Dangor, C. E. Clayton, K. A. Marsh, C. Joshi, V. Malka, C. B. Darrow, C. Danson, D. Neely, and F. N. Walsh. *Electron acceleration from the breaking of relativistic plasma waves.* Nature, 377:606, 1995.

[7] K. Nakajima, D. Fisher, T. Kawakubo, H. Nakanishi, A. Ogata, Y. Kato, Y. Kitagawa, R. Kodama, K. Mima, H. Shiraga, K. Suzuki, K. Yamakawa, T. Zhang, Y. Sakawa, T. Shoji, Y. Nishida, N. Yugami, M. Downer, and T. Tajima. *Observation of ultrahigh gradient electron acceleration by a self-modulated intense short laser pulse.* Phys. Rev. Lett., 74:4428, 1995.

[8] C. Coverdale, C. B. Darrow, C. D. Decker, W. B. Mori, K. A. Tzeng, K. C. Marsh, C. E. Clayton, and C. Joshi. *Propagation of intense subpicosecond laser pulses through underdense plasma.* Phys. Rev. Lett., 74:4659, 1995.

[9] C. E. Clayton, K. A. Marsh, A. Dyson, M. Everer, A. Lal, W. P. Leemans, R. Williams, and C. Joshi. *Ultrahigh-gradient acceleration of injected electrons by laser-excited relativistic electron plasma waves.* Phys. Rev. Lett., 70:37, 1993.

[10] K. Nakajima. *Recent progress on laser acceleration.* Nucl. Instrum. Methods Phys. Res. A., 455:140, 2000.

[11] N. H. Matlis, S. Reed, S. S. Bulanov, V. Chvykov, G. Kalintchenko, T. Matsuoka, P. Rousseau, V. Yanovsky, A. Maksimchuk, S. Kalmykov, G. Shvets, and M. C. Downer. *Snapshots of laser wakefields.* Nat. Phys., 2:749, 2006.

[12] S. P. D. Mangles, C. D. Murphy, Z. Najmudin, A. G. R. Thomas, J. L. Collier, A. E. Dangor, E. J. Divall, P. S. Foster, J. G. Gallacher, C. J. Hooker, D. A. Jaroszynski, A. J. Langley, W. B. Mori, P. A. Norreys, F. S. Tsung, R. Viskup, B. R. Walton, and K. Krushelnick. *Monoenergetic beams of relativistic electron from intense laser-plasma interactions.* Nature, 431:535, 2004.

[13] C. G. R. Geddes, Cs. Tóth, J. van Tilborg, E. Esarey, C. B. Schroeder, D. Bruhwiler, C. Nieter, J. Cary, and W. P. Leemans. *High quality electron beams from a laser wakefield accelerator using plasma-channel guiding.* Nature, 431:538, 2004.

[14] J. Faure, Y. Glinec, A. Pukhov, S. Kiselev, S. Gordienko, E. Lefebvre, J. P. Rousseau, F. Burgy, and V. Malka. *A laser-plasma acccelerator producing monoenergetic electron beams.* Nature, 431:541, 2004.

[15] A. Pukhov and J. Meyer-Ter-Vehn. *Laser wakefield accelerator: the highly nonlinear broken-wave regime.* Appl. Phys. B, 74:355, 2002.

[16] W. P. Leemans, B. Nagler, A. J. Gonsalves, Cs. Tóth, K. Nakamura, G. R. Geddes, E. Esarey, C. B. Schroeder, and S. M. Hooker. *GeV electron beams from a centimeter-scale accelerator.* Nature Phys., 2:696, 2006.

[17] N. A. M. Hafz, T. M. Jeong, I. W. Choi, S. K. Lee, K. H. Pae, V. V. Kulagin, J. H. Sung, T. J. Yu, K.-H. Hong, T. Hosokai, J. R. Cary, Ko D.-K., and J. Lee. *Stable generation of GeV-class electron beams from self-guided laser-plasma channels.* Nature Photonics, 2:571, 2008.

[18] J. Osterhoff, A. Popp, Zs. Major, B. Marx, T. P. Rowlands-Rees, M. Fuchs, M. Geissler, R. Hörlein, B. Hidding, S. Becker, E. A. Peralta, U. Schramm, F. Grüner, D. Habs, F. Krausz, S. M. Hooker, and S. Karsch. *Generation of stable, low-divergence electron beams by laser wakefield acceleration in a steady-state-flow gas cell.* Phys. Rev. Lett., 101:085002, 2008.

[19] J. Faure, C. Rechatin, A. Norlin, A. Lifschitz, Y. Glinec, and V. Malka. *Controlled injection and acceleration of electrons in plasma wakefields by colliding laser pulses.* Nature, 444:737, 2006.

[20] C. G. R. Geddes, K. Nakamura, G. R. Plateau, Cs. Tóth, E. Cormier-Michel, E. Esarey, C. B. Schroeder, J. R. Cary, and W. P. Leemans. *Plasma density gradient injection of low absolute momentum spread electron bunches.* Phys. Rev. Lett., 100:215004, 2008.

[21] A. G. Khachatryan. *Trapping, compression and acceleration of an electron beam by the laser wake wave.* JETP Lett., 74:371, 2001.

[22] A. G. Khachatryan. *Trapping, compression, and acceleration of an electron bunch in the nonlinear laser wakefield.* Phys. Rev. E., 65:046504, 2002.

[23] A. G. Khachatryan, F. A. van Goor, K. J. Boller, A. J. W. Reitsma, and D. A. Jaroszynski. *Extremely short relativistic-electron-bunch generation in the laser wakefield via novel bunch injection scheme.* Phys. Rev. ST. Accel. Beams, 7:121301, 2004.

[24] A. G. Khachatryan, M. J. H. Luttikhof, A. Irman, F. A. van Goor, J. W. J. Verschuur, H. M. J. Bastiaens, and K. J. Boller. *Conceptual design of a laser wakefield acceleration experiment with external bunch injection.* Nucl. Instrum. Methods Phys. Res. A., 566:244, 2006.

[25] A. Irman, M. J. H. Luttikhof, A. G. Khachatryan, F. A. van Goor, J. W. J. Verschuur, H. M. J. Bastiaens, and K. J. Boller. *Design and simulation of laser wakefield acceleration experiment with external electron bunch injection in front of the laser pulse.* J. Appl. Phys., 102:024513, 2007.

[26] Z. Huang and K.-J. Kim. *Review of x-ray free-electron laser theory.* Phys. Rev. ST. Accel. Beams, 10:034801, 2007.

[27] H.-P. Schlenvoigt, K. Haupt, A. Debus, F. Budde, O. Jäckel, S. Pfotenhauer, H. Schwoerer, E. Rohwer, J. G. Gallacher, E. Brunetti, Shanks. R. P., S. M. Wiggins, and D. A. Jaroszynski. *A compact synchrotron radiation source driven by a laser-plasma wakefield accelerator.* Nature Phys., 4:130, 2008.

[28] F. Grüner, S. Becker, U. Schramm, T. Eichner, M. Fuchs, R. Weingartner, D. Habs, J. Meyer-Ter-Vehn, M. Geissler, M. Ferrario, L. Serafini, S. B. Van Der Geer, H. Backe, W. Lauth, and S. Reiche. *Design consideration for table-top laser-based VUV and X-ray free electron lasers.* App. Phys. B, 86:431, 2007.

[29] H. Schwoerer, B. Liesfeld, H.-P. Schlenvoigt, K.-U. Amthor, and R. Sauerbrey. *Thompson-backscattered x rays from laser-accelerated electrons.* Phys. Rev. Lett., 96:014802, 2006.

[30] A. Rousse, K. Ta. Phuoc, R. Shah, A. Pukhov, E. Lefebvre, V. Malka, S. Kisselev, F. Burgy, J. P. Rousseau, D. Umstadter, and D. Hulin. *Production of a keV X-ray beam from synchrotron radiation in relativistic laser-plasma interaction.* Phys. Rev. Lett., 93:135005, 2004.

[31] K. Ta. Phuoc, S. Corde, R. Shah, F. Albert, R. Fitour, J.-P. Rousseau, F. Burgy, B. Mercier, and A. Rousse. *Imaging electron trajectories in a laser wakefield cavity using betatron x-ray radiation.* Phys. Rev. Lett., 97:225002, 2006.

[32] S. Kneip, S. R. Nagel, C. Bellei, N. Bourgeois, A. E. Dangor, A. Gopal, R. Heathcote, S. P. D. Mangles, J. R. Marqués, A. Maksimchuk, P. M. Nilson, K. Ta. Phuoc, S. Reed, M. Tzoufras, F. S. Tsung, L. Willingale, W. B. Mori, A. Rousse, K. Krushelnick, and Z. Najmudin. *Observation of synchrotron radiation from electrons accelerated in a petawatt-laser-generated plasma cavity.* Phys. Rev. Lett., 100:105006, 2008.

[33] A. G. Khachatryan, F. A. van Goor, and K. J. Boller. *Coherent and incoherent radiation from a channel-guided laser wakefield accelerator.* New Journal of Physics, 10:083043, 2008.

[34] V. Malka, J. Faure, Y. A. Gauduel, E. Lefebvre, A. Rousse, and K. Ta. Phuoc. *Principle and applications of compact laser-plasma accelerators.* Nature, 4:447, 2008.

[35] Y. Kitagawa, T. Matsumoto, T. Minamihata, K. Sawai, K. Matsuo, K. Mima, K. Nishihara, H. Azechi, K. A. Tanaka, H. Takabe, and S. Nakai. *Beat-wave excitation of plasma wave and observation of accelerated electrons.* Phys. Rev. Lett., 68:48, 1992.

[36] Y. Glinec, J. Faure, L. Le. Dain, S. Darbon, T. Hosokai, J. J. Santos, E. Lefebvre, J. P. Rousseau, F. Burgy, B. Mercier, and V. Malka. *High resolution γ-ray radiography produced by a laser-plasma driven electron source.* Phys. Rev. Lett., 94:025003, 2005.

[37] L. M. Gorbunov, S. Yu. Kalmykov, and P. Mora. *Laser wakefield acceleration by petawatt ultrashort laser pulses.* Phys. Plasmas, 12:033101, 2005.

[38] D. F. Gordon, R. F. Hubbard, J. H. Cooley, B. Hafizi, A. Ting, and P. Sprangle. *Quasimonoenergetic electrons from unphased injection into channel guided laser wakefield accelerators.* Phys. Rev. E, 71:026404, 2005.

[39] A. F. Lifschitz, J. Faure, V. Malka, and P. Mora. *GeV wakefield acceleration of low energy electron bunches using petawatt lasers.* Phys. Plasma, 12:093104, 2005.

[40] S. Yu. Kalmykov, L. M. Gorbunov, P. Mora, and G. Shvets. *Injection, trapping, and acceleration of electrons in a three-dimensional nonlinear laser wakefield.* Phys. Plasmas, 13:113102, 2006.

[41] T. Esirkepov, S. V. Bulanov, M. Yamagiwa, and T. Tajima. *Electron, positron, and photon wakefield acceleration: trapping, wake overtaking, and ponderomotive acceleration.* Phys. Rev. Lett., 96:014803, 2006.

[42] A. G. Khachatryan, M. J. H. Luttikhof, F. A. van Goor, and K. J. Boller. *Effect of the ponderomotive scattering and injection position on electron-bunch injection into a laser wakefield.* App. Phys. B, 86:41, 2007.

[43] E. Esarey, P. Sprangle, J. Krall, and A. Ting. *Overview of plasma-based accelerator concept.* IEEE Trans. Plasm. Science, 24:252, 1996.

[44] A. J. W. Reitsma. Electron bunch quality in laser wakefield acceleration. PhD thesis, Technische Universiteit Eindhoven, The Netherlands, 2002.

[45] E. Esarey, P. Sprangle, J. Krall, and A. Ting. *Self focusing and guiding of short laser pulses in ionizing gases and plasmas.* IEEE J. Quantum Electron., 33:1879, 1997.

[46] P. Gibbon. Short pulse laser interaction with matter: an introduction. Imperial College Press, Shelton Street, London WC2H 9HE, 2005.

[47] P. Monot, T. Auguste, P. Gibbon, F. Jakober, G. Mainfray, A. Dulieu, M. Louis-Jacquet, G. Malka, and J. L. Miguel. *Experimental demonstration of relativistic self-channeling of a multiterawatt laser pulse in an underdense plasma.* Phys. Rev. Lett., 74:2953, 1995.

[48] L. M. Chen, H. Kotaki, K. Nakajima, J. Koga, S. V. Bulanov, T. Tajima, Y. Q. Gu, H. S. Peng, X. X. Wang, T. S. Wen, H. J. Liu, C. Y. Jiao, C. G. Zhang, J. F. Hua, W. M. An, C. X. Tang, and Y. z. Lin. *Self-guiding of 100 TW femtosecond laser pulses in centimeter-scale underdense plasma.* Phys. Plasmas, 14:040703, 2007.

[49] A. Butler, D. J. Spence, and S. M. Hooker. *Guiding of high intesity laser pulse with a hydrogen filled capillary discharge waveguide.* Phys. Rev. Lett., 89:185003, 2002.

[50] D. J. Spence, A. Butler, and S. M. Hooker. *Gas filled capillary discharge waveguides.* J. Opt. Soc. Am. B., 20:138, 2003.

[51] P. Volfbeyn, E. Esarey, and W. P. Leemans. *Guiding of laser pulses in plasma channels created by the ignitor-heater technique.* Phys. Plasmas, 6:2269, 1999.

[52] C. G. Durfee and H. M. Milchberg. *Light pipe for high intensity laser pulses.* Phys. Rev. Lett., 71:2409, 1993.

[53] C. G. Durfee III, J. Lynch, and H. M. Milchberg. *Mode properties of a plasma waveguide for intense laser pulse.* Opt. Lett., 19:1937, 1994.

[54] S. P. Nikitin, I. Alexeev, J. Fan, and M. H. Milchberg. *High efficiency coupling and guiding of intense femtosecond laser pulses in preformed plasma channels in an elongated gas jet.* Phys. Rev. E., 59, 1999.

[55] T. Hosokai, M. Kando, H. Dewa, H. Kotaki, S. Kondo, Nakajima K. Hasegawa, N., and K. Horioka. *Optical guidance of terawatt laser pulses by the implosion phase of a fast Z-pinch discharge in a gas filled capillary.* Opt. Lett., 25:10, 2000.

[56] J. Faure, V. Malka, J.-R. Marquès, P.-G. David, F. Amiranoff, K. Ta. Phuoc, and A. Rousse. *Effects of pulse duration on self-focusing of ultra-short lasers in underdense plasmas.* Phys. Plasmas, 9:756, 2002.

[57] A. J. Gonsalves, T. P. Rowlands-Rees, B. H. P. Broks, J. J. A. M. van der Mullen, and S. M. Hooker. *Transverse interferometry of a hydrogen filled capillary discharge waveguide.* Phys. Rev. Lett., 98:025002, 2007.

[58] P. Sprangle, E. Esarey, and A. Ting. *Nonlinear theory of intense laser-plasma interactions.* Phys. Rev. Lett., 64:2011, 1990.

[59] P. Sprangle, E. Esarey, and A. Ting. *Nonlinear interaction of intense laser pulse in plasmas.* Phys. Rev. A., 41:4463, 1990.

[60] A. G. Khachatryan. *Excitation of nonlinear two-dimensional wake waves in radially nonuniform plasma.* Phys. Rev. E., 60:6210, 1999.

[61] N. E. Andreev, L. M. Gorbunov, V. I. Kirsanov, K. Nakajima, and A. Ogata. *Structure of the wake field in plasma channels.* Phys. Plasmas, 4:1145, 1997.

[62] S. V. Bulanov, F. Pegoraro, A. M. Pukhov, and A. S. Sakharov. *Trasnverse-wake wave breaking.* Phys. Rev. Lett., 78:4205, 1997.

[63] E. Esarey, R. F. Hubbard, W. P. Leemans, A. Ting, and P. Sprangle. *Electron injection into plasma wake fields by colliding laser pulses.* Phys. Rev. Lett., 79:2682, 1997.

[64] H. Kotaki, S. Masuda, M. Kando, J. K. Koga, and K. Nakajima. *Head-on injection of a high quality electron beam by the interaction of two laser pulses.* Phys. Plasmas, 11:3296, 2004.

[65] C. I. Moore, A. Ting, S. J. McNaught, J. Qiu, H. R. Burris, and P. Sprangle. *A laser-accelerator injector based on laser ionization and ponderomotive acceleration of electrons.* Phys. Rev. Lett., 82:1688, 1999.

[66] S. Bulanov, N. Naumova, F. Pegoraro, and J Sakai. *Particle injection into the wave acceleration phase due to nonlinear wake wave breaking.* Phys. Rev. E, 58, 1998.

[67] R. G. Hemker, N. M. Hafz, and M Uesaka. *Computer simulations of a single-laser double-gas-jet wakefield accelerator concept.* Phys. Rev. ST Accel. Beams, 5:041301, 2002.

[68] P. Tomassini, M. Galimberti, A. Giulietti, D. Giulietti, L. A. Gizzi, and L. Labate. *Production of high quality electron beams in numerical experiments of laser wakefield acceleration with longitudinal wave breaking.* Phys. Rev. ST Accel. Beams, 6:121301, 2003.

[69] W. H. Urbanus, W. Van Dijk, S. B. Van Der Geer, G. J. H. Brussaard, and M. J. Van Der Wiel. *Front-to-end simulations of the design of a laser wakefield accelerator with external injection.* J. Appl. Phys., 99:114501, 2006.

[70] M. J. H. Luttikhof, A. G. Khachatryan, F. A. van Goor, and K. J. Boller. *The effect of vacuum-plasma transition and an injection angle on electron bunch injection into a laser wakefield.* Phys. Plasmas, 14:083101, 2007.

[71] W. Lu, M. Tzoufras, C. Joshi, F. S. Tsung, W. B. Mori, J. Vieira, R. A. Fonseca, and L. O. Silva. *Generating mulit-GeV electron bunches using single stage laser wakefield acceleration in a 3D nonlinear regime.* Phys. Rev. ST. Accel. Beams, 10:061301, 2007.

[72] http://www.pulsar.nl/gpt.

[73] A. G. Khachatryan, A. Irman, F. A. van Goor, and K. J. Boller. *Femtosecond electron-bunch dynamics in laser wakefield and vacuum.* Phys. Rev. ST. Accel. Beams, 10:121301, 2007.

[74] R. Assmann and K. Yokoya. *Transverse beam dynamics in plasma-based linacs.* Nucl. Instrum. Methods Phys. Res. A., 410:544, 1998.

[75] S. Cheshkov, T. Tajima, W. Horton, and K. Yokoya. *Particle dynamics in mutistage wakefield collider.* Phys. Rev. ST. Accel. Beams, 3:071301, 2000.

[76] C. Chiu, S. Cheshkov, and T. Tajima. *High energy laser wakefield collider with synchronous acceleration.* Phys. Rev. ST. Accel. Beams, 3:101301, 2000.

[77] V. Malka, A. Lifschitz, J. Faure, and Y. Glinec. *Staged concept of laser plasma acceleration toward multi-GeV electron beams.* Phys. Rev. ST. Accel. Beams, 9:091301, 2006.

[78] G. Pöplau, U. Van Rienen, S. B. Van Der Geer, and M. J. De Loos. *Multigrid algorithms for the fast calculation of space-charge effects in accelerator design.* IEEE Trans. Magnetics, 40:714, 2004.

[79] S. B. Van Der Geer, O. J. Luiten, M. J. De Loos, G. Pöplau, and U. Van Rienen. *3D space charge model for GPT simulations of high brightness electron bunches.* Institute of Physics Conference Series, 175:101, 2005.

[80] K. Floettman. *Some basic features of the beam emittance.* Phys. Rev. ST. Accel. Beams, 6:034202, 2003.

[81] E. Esarey, B. A. Shadwick, P. Catravas, and W. P. Leemans. *Synchrotron radiation from electron beams in plasma-focusing channels.* Phys. Rev. E, 65:056505, 2002.

[82] P. Michel, C. B. Schroeder, B. A. Shadwick, E. Esarey, and W. P. Leemans. *Radiative damping and electron beam dynamics in plasma-based accelerators.* Phys. Rev. E, 74:026501, 2006.

[83] C. DesRosiers, V. Moskvin, A. F. Bielajew, and L. Papiez. *150-200 MeV electron beams in radiation therapy.* Phys. Med. Biol., 45:1781, 2000.

[84] R. F. X. A. M. Mols. Drive laser and electron dynamics of a linac with photo cathode. PhD thesis, Universiteit Twente, The Netherlands, 1994.

[85] D. A. Jaroszynski, R. Bingham, E. Brunetti, B. Ersfeld, J. Gallacher, S. B. Van Der Geer, R. Issac, S. P. Jamison, D. Jones, M. J. De Loos, A. Lyachev, V. Pavlov, A. Reitsma, Y. Saveliev, G. Vieux, and S. M. Wiggins. *Radiation sources based on laser-plasma interactions.* Phil. Trans. R. Soc. A, 364:689, 2006.

[86] F. B. Kiewiet. Generation of ultra-short, high brightness relativistic electron bunches. PhD thesis, Technische Universiteit Eindhoven, The Netherlands, 2003.

[87] J. H. Billen and L. M. Young. Poisson superfish manual, No. LA-UR-96-1834. Los Alamos National Laboratory, revised July 15, 2002.

[88] T. Wangler. RF linear accelerators. John Wiley and Sons, Inc., 1997.

[89] O. J. Luiten, S. B. Van Der Geer, M. J. De Loos, F. B. Kiewiet, and M. J. Van Der Wiel. *How to realize uniform three-dimensional ellipsoidal electron bunches.* Phys. Rev. Lett., 93:094802, 2004.

[90] L. Serafini, R. Zhang, and C. Pellegrini. *Generation of sub-picosecond electron bunches from RF photoinjectors.* Nucl. Instrum. Methods Phys. Res. A., 387:305, 1997.

[91] M. J. De Loos, S. B. Van Der Geer, Y. M. Saveliev, V. M. Pavlov, A. J. W. Reitsma, S. M. Wiggins, J. Rodier, T. Garvey, and D. A. Jaroszynski. *Radial bunch compression: path-length compensation in an RF photoinjector with a curved cathode.* Phys. Rev. ST. Accel. Beams, 9:084201, 2006.

[92] Z. M. Yusof, M. E. Conde, and Gai. W. *Schottky-enabled photoemission in a rf accelerator photoinjector: possible generation of ultralow transverse thermal-emittance electron beam.* Phys. Rev. Lett., 93:114801, 2004.

[93] W.S. Graves, L.F. DiMauro, R. Heese, E.D. Johnson, J. Rose, J. Rudati, T. Shaftan, and B. Sheehy. *Measurement of thermal emittance for a copper photocathode.* Proceedings of the 2001 Particle Accelerator Conference, page 2227, 2001.

[94] J. B. Rosenzweig. Fundamentals of beam physics. Oxford University Press, Great Clarendon Street, Oxford OX2 6DP, 2002.

[95] P. Piot. *State-of-the-art electron bunch compression.* Proceedings of LINAC, Lübeck, Germany, page 528, 2004.

[96] M. Uesaka, K. Tauchi, T. Kozawa, T. Kobayashi, T. Ueda, and K. Miya. *Generation of a subpicosecond relativistic electron single bunch at the S-band linear accelerator.* Phys. Rev. E., 50:3068, 1994.

[97] J. F. Wishart, A. R. Cook, and J. R. Miller. *The LEAF picosecond pulse radiolysis facility at Brookhaven National Laboratory.* Rev. Scientific Insturm., 75:4359, 2004.

[98] W. Decking, G. Hoffstaetter, and T. Limberg. *Bunch compressor for the TESLA linear collider.* TESLA report-2000-40, 2000.

[99] http://www.comsol.com.

[100] K. L. Brown, F. Rothacker, D. C. Carey, and Ch. Iselin. Transport: A computer program for designing charged particle beam transport systems, CERN Report 80-04, 1980.

[101] T. Katsouleas, S. Wilks, P. Chen, J. M. Dawson, and J. J. Su. *Beam loading in plasma accelerators.* Part. Accel., 22:81, 1987.

[102] S. Wilks, T. Katsouleas, J. M. Dawson, P. Chen, and J. J. Su. *Beam loading in plasma waves.* IEEE Trans. Plasma Sci., 15:210, 1987.

[103] T. C. Chiou and T. Katsouleas. *High beam quality and efficiency in plasma-based accelerators.* Phys. Rev. Lett., 81:3411, 1998.

[104] R. Brogle, P. Muggli, P. Davis, G. Hairapetian, and C. Joshi. *Studies of linear and nonlinear photoelectric emission for advanced accelerator applications.* Proceedings of the 1995 Particle Accelerator Conference, 2:1039, 1995.

[105] J. P. Chambaret, C. Le Blanc, G. Chériaux, P. Curley, G. Darpentigny, P. Rousseau, G. Harmoniaux, A. Antonetti, and F. Salin. *Generation of 25-TW, 32-fs pulses at 10 Hz.* Opt. Lett., 21:1921, 1996.

[106] H. Wang, S. Backus, Z. Chang, R. Wagner, K. Kim, X. Wang, D. Umstadter, T. Lei, M. Murnane, and H. Kapteyn. *Generation of 10-W average power, 40-TW peak-power, 24-fs pulses from a Ti:sapphire amplifier system.* J. Opt. Soc. Am. B., 16:1790, 1999.

[107] O. Svelto. Principles of lasers. Springer Science+Business Media Inc., Spring Street, New York, NY 10013, 1998.

[108] G. Cheriaux, P. Rousseau, F. Salin, J. P. Chambaret, B. Walker, and L. F. Dimauro. *Aberration-free stretcher design for ultrashort pulse amplification.* Opt. Lett., 21:414, 1996.

[109] L. M. Frantz and J. S. Nodvik. *Theory of pulse propagation in a laser amplifier.* J. Appl. Phys., 34:2346, 1963.

[110] http://www.zemax.com.

[111] R Trebino. Frequency-resolved optical gating: the measurement of ultrashort laser pulses. Kluwer Academic Publishers Group, P.O.Box 322, 3300 AH Dordrecht, The Netherlands, 2000.

[112] G. J. Ernst, W. J. Witteman, J. W. J. Verschuur, R. F. X. A. M. Mols, B. M. van Oerle, A. F. Bouman, J. I. M. Botman, H. L. Hagedoorn, J. L. Delhez, and W. J. G. M. Kleeven. *The TEU-FEL project.* Infrared Phys. Technol., 36:81, 1994.

[113] J. W. J. Verschuur, R. Analbers, P. J. M. van de Slot, G. J. Ernst, and W. J. Witteman. *Compact beam transport system for a 6 MeV electron beam to a race-track-microtron accelerator.* Nucl. Instrum. Methods Phys. Res. A., 427:68, 1999.

[114] M. Berz, B Erdélyi, and K Makino. *Fringe field effects in small rings of large acceptance.* Phys. Rev. ST. Accel. Beams, 3:124001, 2000.

[115] A. F. Nieuwenhuis. TEUFEL laboratory logbook, 1995.

[116] P. S. Antsiferov, M. R. Akdim, and H. T. van Dam. *Direct measurement of the matched spot size in a slow capillary discharge optical waveguide.* Rev. Sci. Instrum., 78:123107, 2007.

[117] B. H. P. Broks, W. van Dijk, and J. J. A. M. van der Mullen. *Parameter study of a pulsed capillary discharge waveguide.* J. Phys. D: Appl. Phys., 39:2377, 2006.

[118] N. Bloembergen. *The influence of electron plasma formation on superbroadening in light filaments.* Opt. Commun., 8:285, 1973.

[119] S. C. Rae and K. Burnett. *Simulations of plasma-induced spectral broadening.* Phys. Rev. A, 46:1084, 1992.

[120] Wm. M Wood, C. W. Siders, and M. C. Downer. *Measurement of femtosecond ionization dynamics of atmospheric density gases by spectral blueshifting.* Phys. Rev. Lett., 67:3523, 1991.

[121] T. P. Rowlands-Rees, C. Kamperidis, S. Kneip, A. J. Gonsalves, S. P. D. Mangles, J. G. Gallacher, E. Brunetti, T. Ibbotson, C. D. Murphy, P. S. Foster, M. J. V. Streeter, F. Budde, P. A. Norreys, D. Jaroszynski, K. Krushelnick, Z. Najmudin, and S. M. Hooker. *Laser-driven acceleration of electrons in a partially ionized plasma channel.* Phys. Rev. Lett., 100:105005, 2008.

[122] N. A. Bobrova, A. A. Esaulov, J. I. Sakai, P. V. Sasorov, D. J. Spence, A. Butler, S. M. Hooker, and S. V. Bulanov. *Simulations of a hydrogen-filled capillary discharge waveguide.* Phys. Rev. E, 65:016407, 2001.

[123] B. H. P. Broks, W. van Dijk, J. J. A. M. van der Mullen, A. J. Gonsalves, T. P. Rowlands-Rees, and S.M. Hooker. *Modeling of a square pulsed capillary discharge waveguide for interferometry measurements.* Phys. Plasmas, 14:023501, 2007.

[124] K. Nakamura, B. Nagler, Cs. Toóth, C. G. R. Geddes, C. B. Schroeder, E Esarey, W. P. Leemans, A. J. Gonsalves, and S. M. Hooker. *GeV electron beams from a centimeter-scale channel guided laser wakefield accelerator.* Phys. Plasmas, 14:056708, 2007.

[125] S. Karsch, J. Osterhoff, A. Popp, T. P. Rowlands-Rees, Zs. Major, M. Fuchs, B. Marx, R. Hörlein, K. Schmid, L. Veisz, S. Becker, U. Schramm, B. Hidding, G. Pretzler, D. Habs, F. Grüner, F. Krausz, and S. M. Hooker. *GeV-scale electron acceleration in a gas-filled capilary discharge waveguide.* New Journal of Physics, 9:415, 2007.

[126] M. Bruken, H. Genz, P Göttlicher, C. Hessler, M. Hüning, H. Loos, A. Richter, H. Schlarb, P. Schmüser, S. Simrock, D. Suetterlin, M. Tonutti, and D. Türke. Electro-optic sampling at the TESLA test accelerator: experimental setup and first results, TESLA Report 2003-11, 2003.

[127] S. Masuda, E. Miura, K. Koyama, and S. Kato. *Absolute calibration of an electron spectrometer using high energy electrons produced by the laser-plasma interaction.* Rev. Sci. Instrum., 79:083301, 2008.

[128] X. Yan, A. MacLeod, W. Gillespie, G. Berden, G. Knippels, A. van der Meer, and W. Seidel. *Subpicosecond electro-optic measurement of relativistic electron pulses.* Phys. Rev. Lett., 85:3404, 2000.

[129] G. Berden, S. P. Jamison, A. M. MacLeod, W. A. Gillespie, B. Redlich, and A. F. G. van der Meer. *Electro-Optic Technique with Improved Time Resolution for Real-Time, Nondestructive, Single-Shot Measurements of Femtosecond Electron Bunch Profiles.* Phys. Rev. Lett., 93:114802, 2004.

Samenvatting

Dit proefschrift beschrijft de modelering en het ontwerp van een experimentele opstelling die als doel heeft om voor de eerste keer laser wakefield versnelling met externe injectie van een electronenbundel te demonstreren. Ons complete simulatiemodel van de gehele laser wakefield versneller voorspelt dat zo'n versneller op een gecontroleerde manier relativistische electronenbundels van hoge kwaliteit en extreme korte duur kan genereren in zeer korte versnellers. Dit soort bundels zal in de toekomst grensverleggend onderzoek van de relativistische interactie van licht en materie mogelijk maken.

Het onderwerp dat in dit proefschrift centraal staat is het zogenaamde injectieprobleem. Om een kwalitatief hoge kwaliteit electronen bundel te verkrijgen met laser wakefield versnellers is het noodzakelijk om een bundel electronen te injecteren in de plasmagolf met zowel in plaats als in tijd zeer hoge precisie. De nauwkeurigheid waarmee dit moet gebeuren moet een fractie van de plasma golflengte zijn welke in de orde van slechts enkele tientallen micrometers is. Dit vereist extreem kleine afmetingen van de bundel in zowel longitudinale als transversale richtingen en een controleerbare injectieprecisie op een schaal van respectievelijk femtoseconden en micrometers. Deze kleine afmetingen kunnen onmogelijk met de huidige technologie gerealiseerd worden en alternatieve injectiemethodes moeten worden gevonden.

Om het injectieprobleem op te lossen is door één van onze groepsmedewerkers een nieuwe methode voorgesteld om een electronen puls met grote en realiseerbare afmetingen in het laser wakefield te injecteren [21-23]. De methode is geïmplementeerd in de ontwerpcriteria van de experimentele opstelling die in dit proefschrift beschreven wordt. In deze benadering wordt een electronenbundel, geproduceerd m.b.v. een conventionele lineaire versneller, geïnjecteerd in een plasmakanaal juist voor de aankomst van een laserpuls met hoge intensiteit. In het kanaal wordt de electronenpuls vervolgens ingehaald door de laserpuls. Hierna zal het gegenereerde laser wakefield, dat de laserpuls volgt, de electronenbundel invangen, comprimeren en versnellen naar ultra-relativistische energieën. Theoretisch wordt verwacht dat dit zal resulteren in electronenbundels met nog niet eerder vertoonde, zeer kleine afmetingen: micrometer doorsnedes en femtoseconde tijdsduren, gecombineerd met een lage spreiding in energie.

Dit proefschrift beschrijft de essentiële experimentele stappen die moeten worden genomen om te komen tot laser wakefield versnelling met externe bundelinjectie.

Stap 1: Begin-tot-eind modelering en ontwerp van het experiment
Een zorgvuldig ontwerp van het complete systeem is uitermate belangrijk vanwege het zeer grote aantal parameters dat een rol speelt. Om het risico van mislukken van het experiment, dat gemakkelijk kan plaatsvinden indien het begrip van de invloed van de experimentele parameters te gering is, zo klein mogelijk te maken, hebben we een allesomvattende simulatie van de complete laser wakefield versneller uitgevoerd. Het model bevat alle noodzakelijke stappen, inclusief de generatie van een electronenpuls d.m.v. een foto cathode, propagatie en voorversnelling van de bundel in een rf-lineaire versneller (linac) en compressie in de tijd en focusering van de bundel d.m.v. magnetische velden. Tenslotte beschrijft het model de injectie, het invangen en het versnellen van de electronen in een wakefield dat gegenereerd wordt d.m.v. een multi-TW laserpuls die geleid wordt in een plasmakanaal op een analoge manier als in een optische glasvezel. Na zorvuldige analyse en optimaliseringen hebben we gekozen voor de meest veelbelovende en in de praktijk realiseerbare parameters.

De optimalisering werd uitgevoerd rekeninghoudend met de eis dat de laserpuls en zijn wakefield de electronenbundel moeten inhalen gedurende een kleine fractie van de lengte van de plasmaversneller. Dit bleek noodzakelijk te zijn ten einde een lage relatieve energiespreiding na de versnelling te verkrijgen. Om gebruik te kunnen maken van bestaande technologie, die lengtes van plasmakanalen van typisch 5 cm lengte mogelijk maakt, is de duur en de kinetische energie van de electronenbundel zo gekozen dat de compressie naar het gebied in het plasma waarin zich een maximaal versnellend wakefield bevindt, plaatsvindt over een afstand van ongeveer 1.8 cm. Ons laser wakefield versneller model voorspelt een maximale energie van ongeveer 750 MeV met een relatieve energiespreiding van ongeveer 1 % na versnelling in een 5 cm lang plasmakanaal. Opgemerkt kan worden dat de verkregen energie vergelijkbaar is met die die ook gegenereerd kan worden met een conventionele versneller, echter één met vrij grote afmetingen. Met de hier gepresenteerde opstelling is het mogelijk om dezelfde energie te verkrijgen met een versneller met afmetingen van slechts enkele centimeters.

Stap 2: Constructie van de experimentele opstelling
Gebaseerd op de geoptimaliseerde parameters verkregen met ons model hebben we een experimentele opstelling gebouwd ten einde onze benadering te demonstreren. Te onderscheiden zijn de belangrijkste onderdelen, nl. het multi-TW laser systeem, het plasmakanaal gebaseerd op een ontlading in een capillair, een fotocathode rf geëxciteerde lineaire versneller en een electronenbundel transportsysteem. Verder hebben we een timing- en synchronisatie systeem ontwikkeld dat het mogelijk maakt om de genoemde elementen synchroon te laten werken.

Het eerste onderdeel is een lasersysteem waarin gebruikgemaakt wordt van - "chirped pulse" versterking. De laser maakt gebruik van Ti:Sa kristallen als het versterkende medium en produceert momenteel een puls met energie van ongeveer 475 mJ bij een tijdsduur van 40 fs, hetgeen correspondeert met een piekvermogen van 12 TW. De laserbundel wordt gefocuseerd op de ingang van het plasmakanaal waarbij we een spotdiameter hebben gemeten van 40 μm en 35 μm in respec-

tievelijk de transversale x- en y-richting. In het focus schatten we een piekintensiteit van 5×10^{17} W/cm^2. Wanneer we de laserparameters, met name de pulsenergie, waarover we op dit moment beschikken, vergelijken met die die we in het model beschreven in hoofdstuk 4 hebben gebruikt, is de huidige beschikbare laserenergie een factor 2.1 lager. We hebben er echter voor gekozen om eerst bij deze lage energie te gaan werken met als doel het demonstratie experiment versneld uit te kunnen voeren en om in een later stadium de resultaten te verfijnen bij een hoger piekvermogen van de laserpuls. We hebben ons model gebruikt om de invloed van onze experimenteel beschikbare laser parameters (laser energie, pulsduur en piek intensiteit) op de generatie van het wakefield en het versnellingsproces te onderzoeken. We hebben gevonden dat de minimaal vereiste energie van de electronen waarbij ze kunnen worden ingevangen op de as van het wakefield ongeveer 1.9 MeV bedraagt. Dit is ongeveer een factor 4 hoger dan de invang-drempel die we berekend hebben in hoofdstuk 4. Deze energie is ruim binnen de energieën die geleverd kunnen worden door onze rf-linac, met echter als consequentie dat de invang efficiëntie beperkt blijft tot ~7 % (0.35 pC) in plaats van ~48 % (2.4 pC) bij vol laser vermogen. Een tweede gevolg is dat de uiteindelijke energie van de electronenbundel na laser wakefield versnelling af zal nemen tengevolge van de lagere sterkte van het gegenereerde wakefield. We hebben berekend dat er sprake zal zijn van een afname met een factor 3.6. Na versnelling bij een lengte van 5 cm zal de bundelenergie ongeveer 200 MeV met een relatieve spreiding van ongeveer 2% bedragen.

Om te kunnen bepalen of de uiteindelijke bundelparameters, met name de lagere lading van de electronenpuls, aanvaardbaar zijn voor het demonstratieexperiment, hebben we ons detectiesysteem geanalyseerd. Om de versnelde bundel te kunnen detecteren wordt er een fosfor scherm (Kodak Lanex) geïnstalleerd op een afstand van 1.4 m achter het plasmakanaal op de plaats van de electron spectrometer. Als het scherm door electronen geraakt wordt, wordt het geëmitteerde licht m.b.v. een CCD camera gedetecteerd. Ons model, beschreven in hoofdstuk 3, voorspelt dat t.g.v. de propagatie in vacuum na de laser wakefield versnelling, de radius van de verwachte electronenbundel met een lading van 0.35 pC groeit naar ongeveer 3.5 mm, hetgeen zal resulteren in een aantal van 6Œ104 electronen/mm2 op het fosfor scherm. Masuda et al. [127] rapporteerde dat een fosfor scherm (Kodak Lanex) minimaal 104 electronen/mm2 kan detecteren. We concluderen daarom dat onze 0.35 pC bundel kan worden gedetecteerd met ons detectiesysteem.

Recente berekeningen laten zien dat het geplande demonstratie experiment voor laser wakefield versnelling met externe bundel injectie inderdaad kan worden uitgevoerd met de op dit moment beschikbare laserparameters. In een stadium na het demonstratie experiment verwachten we de uiteindelijke bundeleigenschappen (bundel energie, invang efficïentie en energiespreiding) te kunnen verbeteren door de output energie van onze laser en daarmee de sterkte van het gegenereerde wakefield te verhogen. Voor deze laatste modificatie aan de laser is er een extra pomplaser beschikbaar.

Als het volgende essentiële element hebben we een zorgvuldig ontworpen bundeltransport systeem geconstrueerd dat de belangrijke functie van zowel tijds- als

ruimtelijke compressie uitoefent. Metingen aan de magnetische velden van de individuele magnetische elementen lieten zien dat de gemeten waarden van de parameters in goede overeenstemming zijn met die van het ontwerp. Dit is een indicatie dat de tijds-compressie en ruimtelijke focuserings eigenschappen van de gerealiseerde bundel transmissie lijn vergelijkbaar zijn met die die gebruikt worden in het numerieke model. Beperkt door de warmte dissipatie in de spoelen van de magneten en de maximale stroom die door de voedingen kunnen worden geleverd concluderen wij dat de bundellijn elctronen bundels kan transporteren met een maximale kinetische energie tot ongeveer 4 MeV.

Het kleinste element, het plasmakanaal, wordt gevormd in een alumina capillair gevuld met waterstofgas dat volledig geïoniseerd wordt door een pulsvormige ontlading. De vuldruk, die de plasma dichtheid op de as bepaalt, wordt zodanig gekozen dat een resonant wakefield wordt geëxciteerd door de laserpuls. Gebaseerd op de duur van de stroompuls hebben we berekend dat een vuldruk van ongeveer 46 mbar nodig is. Verder is de keuze van de radius van het capillair (~153 μm) gebaseerd op de eis van optimaal transport van de laserpuls door het plasmakanaal bij een gegeven vuldruk, d.w.z. de radius van het kanaal is zodanig dat deze overeenstemt ("matched") met die van de laserpuls aan de ingang van het capillair.

We hebben tenslotte de laserpuls gesynchroniseerd met de geïnjecteerde electronenbundel en het plasmakanaal d.m.v. een aantal synchronisatiesystemen die werken bij verschillende tijdsintervallen variërend van seconden tot picoseconden. Een onnauwkeurigheid van ongeveer 12.5 ns werd gemeten in de tijdsperiode tussen de start van de ontladingsstroom in het plasmakanaal en de aankomst van de laserpuls bij de ingang van het plasmakanaal. Deze jitter is veel kleiner dan de duur van het tijdsvenster (ongeveer 100 ns) waarin goed transport van de laserpuls in het kanaal werd waargenomen. Verder hebben we een tijdsjitter van niet meer dan 3 ps gemeten tussen de fase van het rf-veld van de linac en de aankomsttijd van de laserpuls bij de cathode in de linac. Gebaseerd op onze berekeningen zal dit leiden tot een schot-tot-schot fluctuatie van minder dan 1% na het laser wakefield versnellingsproces. Het is mogelijk om deze jitter te verbeteren tot kleiner dan 1 ps door modificatie van het sysnchronisatiesysteem.

Stap 3: Essentiële tests van de experimentele opstelling
Nadat de individuele elementen, zoals de TW laser, de rf-linac, het electronenbundel transportatiesysteem en het plasmakanaal afzonderlijk zijn getest, hebben we twee essentiële experimenten aan de complete opstelling uitgevoerd. Het eerste experiment was de generatie van de electronenbundel en voorversnelling in de linac gevolgd door de propagatie van de bundel door de transportlijn naar de ingang van het capillair. Gebaseerd op de resultaten van dit experiment hebben we de energie van de bundel en zijn schot-tot-schot fluctuatie bepaald wat resulteerde in waardes die geheel binnen het geplande bereik liggen. Ten tweede hebben we transport experimenten van laserpulsen met hoge intensiteiten door het plasmakanaal uitgevoerd. Gebaseerd op de analyses van de ruimtelijke, temporale en spectrale eigenschappen van de getransporteerde laser puls hebben we zoals verwacht succesvol transport binnen een optimaal tijdsvenster na de ontsteking van de ontlading waar-

genomen. Deze experimenten hebben laten zien dat onze experimentele opstelling werkt en gereed is voor het laser wakefield versneller experiment dat uitgevoerd zal worden in loop van het jaar 2009.

Acknowledgments

I would like express my sincere thanks to everyone who have contributed directly or indirectly to the achievements of this work. It is obvious that such results can only be obtained in teamwork and with a lot of feedback of colleagues and friends.

First of all, I would like to express my sincere gratitude to my promotor Prof. Dr. Klaus Boller for giving an opportunity to work in this fascinating project and for his guidance during the entire PhD research. I really appreciate the encouragement he has given to me which has brought me up to this point and for that I owe him many thanks.

I am specially grateful to Dr. Fred van Goor for his guidance, fruitful discussions and helpful assistance during the course of this work. The conference trip to Azores was always unforgettable. I also would like to thank him for the Dutch summary of this thesis. I would like to express my sincere thanks to Dr. Arsen Khachatryan for numerous discussions regarding the theoretical part of this thesis. Arsen, thanks a lot to you, you have always been willing to answer any questions that I have asked.

My sincere thanks go to Prof. Dr. Vinod Subramaniam, Prof. Dr. Harold Zandvliet and Prof. Dr. Wim van der Zande for their willingness to be members of my graduation committee.

I am grateful to Jeroen who introduced me to the linear accelerator and assisted me to run the machine. Thanks a lot to Bert, you have helped me with the development of the plasma channel. This must have taken a lot of your precisions time.

I owe many thanks to Gerard and Jacob for their useful and helpful assistance particularly during the construction phase of the setup. I am grateful to Ab for his kindness and assistance to solve many problems regarding to the linac. I owe many thanks to Donna who helped me in checking the English of my thesis.

I would like to express my special thanks to all of my colleagues both past and present members of the Laser Physics and Nonlinear Optics group: Liviu, Balaji, Isabel, Lars, Anton, Dennis, Denny, Peter, Petra, Ian, Malvin, Dimitri, Thijs, Marten, Martijn T., Hein, Ronald, Roel, Johan, Martijn, Simone, Fred, Chris, Ruud, Jelle, Bas-Jan, Robert, Mark, Willem, Rolf, Thomas, Peter, Piet. Especially to Rolf, Thijs, Mark, Ronald, Johan, Martijn T., our trip to Rome, Italy in 2006 was really fun and memorable. I am so fortunate to know you guys.

I am grateful to all my Indonesia's friends in Enschede. You have made me feel like home during my stay in The Netherlands. My special thanks go to: David and Vince, Sena and Fitri, Budi and Vita, Ariando and Liza, Eko and Susan, Ella and Dedy, Danang and Munky. *Terima kasih banyak*!.

I am most indebted to my parents, mama, papa, bundo and ayah in Padang, for

their prayer and invaluable support for me to finish my study. Also for my brother and sister, many thanks for your support.

Finally, I would to express my deepest gratitude to my beloved wife Meli and my son Adriaan to whom this thesis is dedicated.

Enschede, March 2009